Fachhochschule
Münster University of
Applied Sciences

Development of Solid Acid Fuel Cell Electrolytes operating at intermediate temperature (110-250 ºC)

Masterarbeit

vorgelegt von
Zeynep KANLIDERE
aus Ankara

Fachhochschule Münster
University of Applied Sciences
Fachbereich Chemieingenieurwesen

December, 2009

Practical Work of the Research performed at:
Arbeit durchgeführt bei:

Faculty of Science and Technology
Membrane Technology Group
Inorganic Membrane Part
University of Twente
Enschede
Netherlands

Supervisor: Prof. Dr.-Ing. Peter Dettmann
Referent

Second Examiner: Prof. Dr.-Ing. Norbert Ebeling
Korreferent

This Master Thesis was presented to the Department of Chemical Engineering on:
Dem Prüfungsausschuss des Fachbereichs Chemieingenieur vorgelegt am:

Declaration:

I hereby declare that this Master Thesis was carried out independently and only by use of the aids that are stated.

Erklärung:

Hiermit wird versichert, dass diese Arbeit selbstständig angefertigt wurde und die benutzten Hilfsmittel angegeben worden sind.

Signature/Unterschrift

ACKNOWLEDGEMENTS

The master work for this thesis was carried out in the Inorganic Membranes Part of Membrane Technology Group at University of Twente, Netherlands. This thesis has been submitted to University of Applied Sciences Münster, Chemical Engineering Department.

First of all, I would like to thank my professor and supervisor **Prof. Dr.-Ing Peter Dettmann** in whose seminars I learnt the basic rules for how to write a scientific paper, and who was willing to supervise my external thesis. I also wish to give a great thank to him for his valuable advices and guidance not only for master thesis but also for all my project works of my study that I performed in the Laboratory of Environmental Technology, in Fachhochschule Münster. Also I would like to thank him for the excellent working condition in his modern laboratory.

Secondly, I would like to thank to **Prof. Dr. H.J.M Bouwmeester** for giving me the opportunity to work at the University of Twente on this topic for my master thesis and for his valuable advices during our scientific discussions. A special thank goes to **MSc. Weihua Zhou** for his great helps whenever I asked during my work at University of Twente. I specially thank him for his infinite patience. Of course I must thank to the University of Twente and specifically Inorganic Membrane Group that had provided me the opportunity to meet and work with so many exceptional people from all over the world.

A special thank I want to give to the Second Examiner of my master thesis to **Prof. Dr.-Ing. Norbert Ebeling** for his helps for the defence of the thesis and for his advices during my study at Fachhochschule Münster. I am also grateful to **Dipl.-Ing. Helmut Schweers** for his encouragement and supports not only during my master thesis but also for his helps during my two years study programme at Fachhochschule Münster.

Personally, I would not forget to thank to my parents **Malik Kanlidere** and **Sidika Kanlidere** and my brother **Oguzkagan Kanlidere** who have always supported me in what I have been doing. They made this work possible.

ABSTRACT

Fuel cells convert chemical energy directly into electrical energy cleanly and efficiently. An integral part of a fuel cell is the electrolyte that conducts ions. Major developments in the fuel cell technology are based on polymer electrolytes. Current technology for the polymer electrolytes is limited by its inability to operate at temperatures above 100 ºC, which is undesirable for applications. This thesis deals with an alternative electrolyte that operates at intermediate temperatures (110-250 ºC) and based on non-polymer, inorganic *solid acid* compounds.

Solid acids are chemicals between normal salts and normal acids. At room temperature, they have ordered structure, however, upon heating they undergo solid-state phase transition to highly disordered structure in which the proton conductivity increases by several orders of magnitude and takes on values of ~10^{-2} $\Omega^{-1}cm^{-1}$. Because of their high proton conductivity at high temperatures (>100 ºC) they are referred as "superprotonic" solid acids.

In this work, the synthesis and characterization of $MH(PO_3H)$- type solid acids (where M= Cs^+ and K^+) have been investigated. It has been found that, potassium dihydrogen phosphite, $KH(PO_3H)$, and cesium dihydrogen phosphite, $CsH(PO_3H)$, has monoclinic ordered structure at room temperature. Upon heating $KH(PO_3H)$ and $CsH(PO_3H)$ undergo superprotonic phase transition at 125 ºC and 142 ºC, respectively, and the proton conductivity increases value of $4.5 \cdot 10^{-3}$ at 143 °C for $KH(PO_3H)$ and $3 \cdot 10^{-3}$ at 160°C for $CsH(PO_3H)$.

Secondly, the effect of cation substituted solid acids have been developed by doping different amounts of K^+ into $CsH(PO_3H)$ and the result formula was $K_xCs_{(1-x)}H(PO_3H)$ where x = 0.1, 0.2, 0.3, 0.4, 0.5, 0.6, 0.7, 0.8, 0.9, 0.95. Superprotonic phase transition temperatures and protonic conductivities have been investigated for the mixed system. Cs^+ rich compounds have not affected the transition temperature while K^+ rich compounds have shifted transition temperature to very low around 100 ºC. $K_{0.95}Cs_{0.05}H(PO_3H)$ has a superprotonic phase transition at 100 ºC and its superprotonic conductivity is starting from $3.2 \cdot 10^{-3}$ $\Omega^{-1}cm^{-1}$ at 113 °C and reaches values of 10^{-2} $\Omega^{-1}cm^{-1}$ at 147 °C.

CONTENTS

LIST OF TABLES

LIST OF FIGURES

BACKGROUND and OBJECTIVES

1.1 Background

Fuel cells are today's highly efficient sustainable sources of energy and electricity. Current fuel cell technologies have proven their ability to generate electricity from hydrogen with zero emission and high efficiency [1].

A variety of fuel cells have been developed over the years; the basic design is comprised of two electrodes (an anode and a cathode) separated by a proton conducting electrolyte. This electrolyte can be referred as membrane. The electrolyte being used varies the type of fuel cells. Currently major developments in fuel cell technology are based on *polymer electrolytes*.

As an example of polymer electrolytes, Nafion®, which have been the industry benchmark, is commercially used and produced by insertion of sulphonic acid into a solid polymer membrane. Nafion® is a good proton conductor, very popular and useful at low temperatures (<100 °C) as proton conducting polymer membrane [2]. The proton transfer mechanism for polymer electrolyte is usually described as a diffusion mechanism (e.g. through water solvent)[3].

Beside advantages of polymeric solid electrolytes, however, it has also some disadvantages such as;

- Nafion® is very expensive so the cost of the Nafion® based fuel cells is high,
- Polymer electrolyte membrane fuel cells (PEMFCs) are not able to operate at high temperature above 100 °C since the water content disappears above this temperature. Nafion® dehydrates at the temperature around 100 ^{o}C
- The high methanol permeability through the membrane results in catalyst poisoning and reduces cell potential.

The operating temperature of a fuel cell is an important characteristic. Since polymer electrolyte membrane fuel cells are limited with the operation temperatures less than 100 °C, and fuel cells with higher operating temperatures (600-1000 °C) suffer from stability problem, many researchers throughout the world are searching for fuel cell electrolytes operating at intermediate temperatures (150-250 °C) .

In the year of 2001, a company from California Institute Technology in Pasadena developed a new type of electrolyte for fuel cells called as "*Solid Acid Fuel Cells*" [4]. Solid acids are described as chemical intermediates between salts and acids. They are typically composed of cations and oxyanion groups. Solid acids have conductive properties at intermediate temperatures 150-250 °C.

The uniqueness of the solid acids is that, in contrast with proton conducting polymer electrolytes, the protons themselves are the mobile species, i.e., no water molecules are required to enable transport [5]. Solid acids are able to carry the hydrogen ions (protons) from one side to another by an atomic hopping process, in which the proton sticks to oxygen atoms of oxyanion group, until it reaches to the other neighboring oxyanion group in the chain [6]. The proton transfer from one oxyanion group to the next one occurs on a much slower time scale.

Cesium phosphate CsH_2PO_4 is a good example of solid acids. At room temperature it has an ordered structure, however upon heating through 141 °C it undergoes disordered structure. This change from order to disorder is accompanied by an increase in the conductivity by 2-3 orders of magnitude and often referred to as a "superprotonic" transition [7].

Proton-conducting solid acids have been known for about 25 years but had not been considered for fuel cell applications till 2001. A long time it was assumed that solid acids used as electrolyte would dissolve in water. But they have been demonstrated at high temperatures, when water transforms into vapors, there's no danger for the solid acid fuel cells, SAFC [8].

1.2 Objectives

The goal of this work is to develop solid acid electrolytes that work within an intermediate temperature range (~ between 110 °C and 250 °C). The objectives and structure of this study are given in the following section of this chapter.

In this work, the below given tasks are achieved to approach the main objective.

- To synthesize polycrystalline solid acids of cesium dihydrogen phosphite $CsH(PO_3H)$ and potassium dihydrogen phosphite $KH(PO_3H)$.
- To synthesize polycrystalline solid acids of mixed cation systems by replacing some cesium atoms of $CsH(PO_3H)$ with potassium atoms, K, to obtain general formula $K_xCs_{(1-x)}H(PO_3H)$ (where x= 0-1).

- To characterize the crystal structure of solid-acids by X-ray powder diffraction (XRD) methods.
- To analyze the thermal properties (such as phase transition temperature and melting point temperature) of the synthesized solid acids by Differential Scanning Calorimetry (DSC) and Thermal Gravimetry (TG).
- To analyze the proton conductivity of the solid acids by Electrochemical Impedance Spectrometer and to evaluate the effect of cation substitution on the superprotonic conductivity in mixed cation systems.
- To prepare composite membranes from porous anodic alumina membranes (AAM) filled with the solid acid proton conductor $KH(PO_3H)$.

- To characterize the filled AAM membranes by Scanning Electron Microscope before and after filling with $KH(PO_3H)$.
- To characterize the filled AAM membranes, AAM/$KH(PO_3H)$, by X-ray diffractometer (XRD).
- To analyze the thermal properties such as superprotonic phase transition temperatures and melting points of filled AAM membranes, AAM/$KH(PO_3H)$, by Differential Scanning Calorimetry (DSC).

1.3 Structure of Thesis

This thesis is organized in 7 chapters.

Chapter 1 gives a background and objectives of the research,

Chapter 2 gives a brief introduction to fuel cells; by explaining components of fuel cells, classification of fuel cells, properties of electrolytes and a brief introduction to solid acid electrolytes,

Chapter 3 contains theoretical aspects of solid acid electrolytes, bonding structure of solid acids, order-disorder transition phenomenon in solid acids,

Chapter 4 discusses the proton transport mechanism in solid acids and provides detailed information on the reasons for the superprotonic phase transition. This chapter also describes methods to prepare anodic alumina -solid acid composite membranes,

Chapter 5 gives experimental outlines, the methods employed and the principles of characterization techniques used for preparation and characterization of the solid acid electrolytes,

Chapter 6 presents experimental results and interpretation of the data obtained,

Chapter 7 gives conclusions and recommendations for future research.

INTRODUCTION

2.1 Introduction to Fuel Cells

The first technology behind fuel cells was demonstrated by a Welsh scientist, Sir William Grove (often referred to as the "Father of the Fuel Cell"), as early as 1839. He discovered that it may be possible to generate electricity by reversing the electrolysis of water. Fuel cells remained in obscurity until 1950s when the U.S space programs chose fuel cells instead of expensive solar energy or risky nuclear energy, and fuel cells are still interest to NASA.

Fuel cells are today attractive alternatives to combustion engines for electrical power generation, because of their high efficiencies and their potential to reduce the environmental impact. On the other hand they are expensive to make and to maintain. Unlike a battery cell, a fuel cell never "goes dead" and never needs recharging. It will continue to produce power as long as it has a constant supply of fuel and oxygen. However, like a battery cell, a fuel cell converts chemical potential energy into electricity, so a fuel cell is an electrochemical device.

A fuel cell generates electric power by oxidation of the fuel which is supplied to it. Like a combustion engine, a fuel cell uses some sort of chemical fuel as its energy source. Fuel cell is an electrochemical cell composed of two electrodes, where oxidation occurs at one electrode and reduction at the other. At one of the electrodes, called anode, oxidation occurs. Here the electrons are released as a result of the reaction. The other electrode is called cathode where reduction reaction occurs. The electrons released in the anodic reaction are consumed in the cathode reaction. These reactions occur as long as fuel is fed to the electrochemical cell[2].

In Fig. 2.1, a schematic diagram of a fuel cell is given. The following steps occur [2],

(1) A fuel such as hydrogen is fed into the anode compartment,

(2) An oxidant, such as oxygen is fed into the cathode compartment,

(3) At the anode the hydrogen atoms are split in protons and electrons by using a catalyst in accord with the reaction;

$$2H_2 \rightarrow 4H^+ + 4e^- \qquad \textbf{(2-1)}$$

(4) The protons produced in (3) pass through the electrolyte between the anode and the cathode, from anode to the cathode,

(5) The electrons produced in (3) are forced through an electric circuit and form an electrical voltage between the anode and the cathode,

(6) The oxygen fed to cathode as oxidant and the protons coming from anode reacts at the cathode to produce water.

$$O_2 + 4H^+ + 4e^- \rightarrow 2H_2O \qquad \textbf{(2-2)}$$

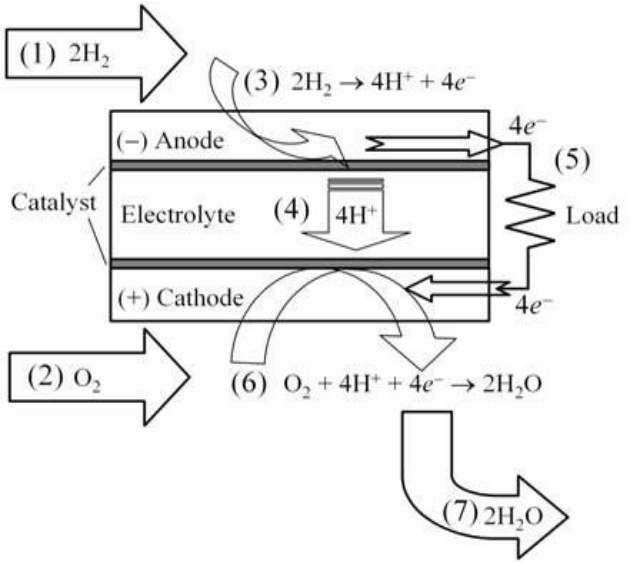

Figure 2.1 Schematic diagram of basic H_2/O_2 fuel cell [2]

The main components of a fuel cell are an ion conducting electrolyte, a cathode, and an anode. These three components together, are often referred to as the membrane-electrode assembly (MEA) [2].
In Table 2.1, a description of the essential components for the operation of a fuel cell and examples of each are given.

Table 2.1 The basic components of a fuel cell [2]

Component	Description	Example
Fuel	Source of chemical energy	H_2, methanol, ethanol, methane,
Oxidant	Used of oxidize fuel	O_2, air
Anode	Porous electron conducting negative electrode	Carbon paper, Ni
Cathode	Porous electron conducting positive electrode	Carbon paper
Electro catalyst	catalyzes electrochemical reactions at anode and cathode	Pt, Pd, Ni
Electrolyte	ion conducting, electron insulating membrane, separating fuel and oxidant	Nafion, ZrO_2, CsH_2PO_4

Fuel cells are classified due to the kind of electrolyte that they are composed of. Therefore it is important to explain more about electrolytes.

2.1.1 Electrolyte

An electrochemical fuel cell produces an electric current as a result of chemical reactions. The ions taking part in these reactions are passing through the electrolyte which is sandwiched between the anode and cathode. So, an ***electrolyte*** may be defined as substance that contains free mobile ions and current is carried by movement of ions. Most of the electrolytes of fuel cells known as ionic solutions, but solid electrolytes are also possible.

Electrolytes separate the fuel (H_2) from the oxidant (O_2). In this way the direct chemical combustion is prevented. The electrolyte between the anode and cathode behaves as a barrier to gas diffusion, but let ions to migrate across it. Ions can be produced in the anode or cathode by half cell reactions. Those ions produced in anode or cathode can pass the electrolyte. In case of the example, in Fig. 2.1, protons are produced in the anode, and the electrolyte is able to conduct protons; then electrons are consumed in the cathode. The thermodynamic driving force behind fuel cells are chemical reactions that performed by fuel [2].

Proton conducting electrolyte [2]

Anode: $H_2 \rightarrow 2H^+ + 2e^-$ **(2-3)**

Cathode: $\frac{1}{2}O_2 + 2H^+ + 2e^- \rightarrow H_2O$ **(2-4)**

Overall: $H_2 + \frac{1}{2}O_2 \rightarrow H_2O$ **(2-5)**

O^{2-} ion conducting electrolyte [2]

Anode: $H_2 + O^{2-} \rightarrow H_2O + 2e^-$ **(2-6)**

Cathode: $\frac{1}{2}O_2 + 2e^- \rightarrow O^{2-}$ **(2-7)**

2.1.1.1 Factors Effecting Electrolyte Selection for Fuel Cells

Some factors effecting to select the electrolyte are its ionic conductivity, stability and its cost.

- The most important property of an electrolyte is its ionic conductivity. The electrolyte used in a fuel cell should have high proton conductivity around 10^{-3}-10^{-2} Ω^{-1} cm^{-1}.
- The electrolyte has to offer a convenient environment for chemical reaction to take place. Under harsh conditions such as temperature increases and pressure changes the electrolyte has to have chemical and physical stability. Due to the physical contact, portability, pH and flow rate amongst other factors, which the electrolyte has to endure with tough mechanical properties.
- Cost is often a decisive factor when large-scale production for commercialization is considered.

2.1.2 Types of Fuel Cells

As it is mentioned before fuel cells are classified according to the kind of electrolyte that they are composed of. Electrolytes in which protons, hydronium ions, hydroxide ions, oxide ions, and carbonate ions are mobile are the basis for the many categories of fuel cells under development today [2]. There are several types of fuel cells, each of it with its own advantages, limitations, and potential applications. Most common types of fuel cells and their electrolytes are listed in Table 2.2.

Table 2.2 Types of fuel cells [2]

Fuel Cell Type	Electrolyte	Mobile Ion	Operating Temperature(°C)	Fuels

PEMFC Polymer Electrolyte Membrane FC	Sulfonated polymer (Nafion®)	H_3O^+	70-110 °C	H_2, CH_3OH
AFC Alkaline FC	(Na,K)OH	OH^-	100-250 °C	H_2
PAFC Phosphoric Acid FC	H_3PO_4	H^+	150-220 °C	H_2
MCFC Molten Carbonate FC	$(Na,K)_2CO_3$	$(CO_3)^{-2}$	500-700 °C	Hydrocarbons, CO
SOFC Solid Oxide FC	$(Zr,Y)O_{2-\zeta}$	O^{-2}	500-700 °C	Hydrocarbons, CO
SAFC* Solid Acid FC	Solid acid compounds (CsH_2PO_4, KH_2PO_4, $CsHSO_4$…)	H^+	150-250 °C	H_2, CH_3OH

**Solid acid fuel cells are not commercially developed yet, therefore it is not included in the original table of the reference .*

2.1.2.1 Polymer Electrolyte Fuel Cells

Progress in fuel cells based upon polymer electrolytes has been possibly the most popular one over the last decade. The most widely implemented polymer electrolyte in fuel cells is called Nafion®. Polymeric membranes, such as Nafion® are composed of a hydrophobic perfluorinated polymer backbone with covalently bonded hydrophilic sulfonic acid functional groups. Upon hydration of these polymers, protons are transported through the polymer matrix via a vehicle transport mechanism, in which H_3O^+ ions are the carriers [2].

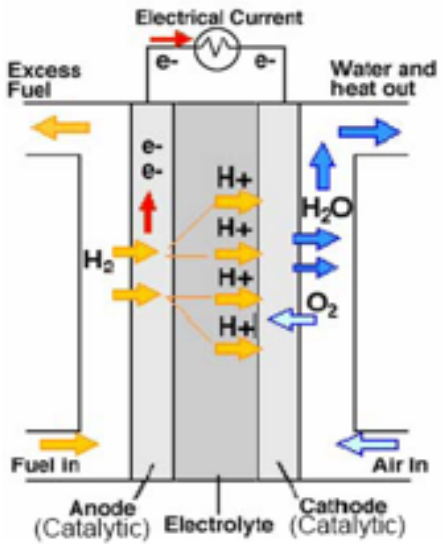

Figure 2.2 Polymer electrolyte membrane fuel cell (PEM) [9]

Polymer Electrolyte Membrane Fuel Cells (PEMFCs) need only hydrogen, oxygen from the air, and water to operate and do not require corrosive fluids like some fuel cells. Due to the inherent need for water in polymer electrolytes, they might, in fact, be more correctly termed as "polymer-water composite electrolytes". The polymer membrane allows hydronium ions to pass through it when wet. Hydrogen fuel is supplied as hydrogen gas or is reformed from methanol, ethanol, natural gas or liquefied petroleum gas and then fed into the fuel cell. The power range of existing PEMFCs is about 50 W to 250 kW [1].

Due to membrane limitations, polymer electrolyte membrane fuel cells operate at relatively low temperatures, around (70-110 °C). Low-temperature operation allows them to start quickly (less warm-up time) and results in less wear on system components, resulting in better durability. However, it requires that a noble-metal catalyst (typically platinum) be used to separate the hydrogen's electrons and protons, adding to system cost. The platinum catalyst is also extremely sensitive to CO poisoning, making it necessary to employ an additional reactor to reduce CO in the fuel gas if the hydrogen is derived from an alcohol or hydrocarbon fuel. This also adds cost. Developers are currently exploring platinum/ruthenium catalysts that are more resistant to CO. Because of these problems, another approach has been through the replacement of water by an acid within a basic polymer matrix, such as phosphoric acid (H_3PO_4) into polybenzimidazole (PBI). This phosphoric acid fuel cells (PAFCs) operating temperatures are in the range of 150-220 °C. Existing PAFCs have outputs of up to 11MW[1,10].

2.1.2.2 Solid Oxide Electrolyte Fuel Cells

Solid oxide electrolytes use non-porous ceramic compound as the electrolyte. Today's demonstrations SOFCs utilize yttria stabilized zirconia (YSZ) containing typically 8 mol% Y, as the electrolyte; a ceramic metal composite (cermet) comprised of Ni+YSZ as the anode, and other electronically conducting ceramics at the cathode [2].

Solid oxide fuel cells operate at very high temperatures around 500-700 °C [2]. High temperature operation removes the need for precious-metal catalyst, thereby reducing cost. It also allows SOFCs to reform fuels internally, which enables the use of a variety of fuels and reduces the cost associated with adding a reformer to the system [10].

In summary, solid oxide electrolytes opposite to polymer electrolytes are operating at high temperatures. At these temperatures, expensive processing techniques and thermal-mechanical toughness of materials still remain technical challenges to overcome, providing an impetus for research to develop intermediate-temperature solid electrolytes [11].

2.1.2.3 Alkaline Electrolyte Fuel Cells

In principle they are very similar to polymer electrolytes but differ in the medium employed and the product of oxygen reduction. Alkaline fuel cells (AFCs) use aqueous solution of alkaline potassium hydroxide contained within an inert matrix as the electrolyte. A variety of non-precious metals are used as a catalyst at the anode and as cathode. AFCs operate at temperatures between 100 °C and 250 °C. A typical fuel cell stack has an output in the range from 300 W to 5 kW. They are widely used by NASA to produce electrical energy and drinking water [10].

2.1.2.4 Molten Carbonate Electrolyte Fuel Cells

MCFCs are high-temperature fuel cells that use an electrolyte composed of a molten carbonate salt mixture suspended in a porous, chemically inert ceramic lithium aluminum oxide ($LiAlO_2$) matrix. Because they operate at extremely high temperatures in the range of 700-900 °C, non-precious metals can be used as catalysts at the anode and cathode, reducing costs [10].

2.2 Solid Acid Electrolyte Fuel Cells

This section is meant to serve as a brief introduction to solid acid materials and to set the stage for the remainder of this thesis.

In every handbook about fuel cells, the reader finds five classic types of fuel cells which were also given Table 2.2. This study deals with a new fuel cell based on an inorganic solid acid electrolyte. Solid acid fuel cells are alternatives to conventional fuel cells. Solid-acid fuel cells (SAFCs) use an anhydrous, non-polymeric proton conducting electrolyte that can operate at slightly elevated temperatures. Unlike other classic fuel cells, SAFCs operate at intermediate temperatures (150-250 ºC), using a truly solid acid electrolyte. For solid acid electrolyte, the mobile ions are protons H^+. Therefore, the ionic conductivity is referred to as protonic conductivity for solid acid electrolytes. Such compounds offer the possibility of proton transport under anhydrous conditions. Distinct from polymer electrolytes no water molecules are required for proton transport [2]. In proton transport of the solid acids, the protons hop through a dry crystal lattice.

Solid acids are chemical intermediates between normal salts and normal acids. Physically, the materials are similar to salts. Solid acid proton conducting compounds are comprised of oxyanions, for example SO_4^{-2}, SeO_4^{-2}, PO_4^{-3}, AsO_4^{-3} or even PO_3H^{-2}, which are linked together via O-H···O hydrogen bonds. The hydrogen bonding structure is highly ordered at room temperature however upon heating through 100-140 °C, some solid acids undergo a solid-state phase transition at which ion conductivity increases by 2-3 orders of magnitude. Therefore, these solid acids are referred to as "*superprotonic*" conductors.

Solid acid electrolytes exhibit the following properties:

- Solid proton conductors,
- Based on “tetrahedral oxy-anion” groups,
- Exhibit anhydrous proton transport,
- Ionic conductors above a transition temperature usually above 100°C,
- Conductivities in the range between 10^{-3} to 10^{-2} $\Omega^{-1}cm^{-1}$ at intermediate temperatures (150-250 ºC),
- Insulators at room temperature,
- Structural disorder at high temperatures,
- Direct H^+ transport,
- Humidity insensitive,
- Water soluble (disadvantage)

Solid acids were known to exhibit high proton conductivity since several years, but were not considered for fuel cell applications. The important reason for this is that most of the solid acids are soluble in water. It was thought that H_2O generated at the cathode of the fuel cell would dissolve away the solid acid when employed as an electrolyte and this is useless for the fuel cells. However, this problem is avoided by operating above the boiling point of water (100 ºC) [11].

2.2.1 History of Solid Acid Fuel Cells

The first example of a solid acid fuel cell was demonstrated in 2001 by Haile *et al.* in Calif-Superprotonic, Inc., Pasadena using the electrolyte $CsHSO_4$ [4]. This was able to operate at 150-160 ºC in a H_2/O_2 configuration with an open circuit voltage of 1.1V. Unfortunately, especially in the presence of fuel cell catalyst, sulfate based acid compounds react with H_2 in the anode chamber. The reaction by-product, H_2S (or H_2Se in case of selenate based acid compounds), is a fuel cell poison and therefore these electrolytes are not suitable for long-term operation.

More recently the same research group have extended the solid acid demonstration with a CsH_2PO_4 electrolyte that undergoes a true, polymorphic superprotonic transition [12]. They developed a fuel cell made of a CsH_2PO_4 electrolyte membrane about 25-36 μm thick, on porous stainless steel gas-diffusion electrodes, operated at ~240 °C with humidified H_2 supplied to the anode and humidified O_2 supplied to the cathode. Power was obtained as high as 415 mW/cm^2 [12].

A number of different solid acid compounds with such behavior as CsH_2PO_4 have been discovered. In this study $CsH(PO_3H)$ and $KH(PO_3H)$ solid acid structures have been investigated.

STRUCTURE OF SOLID ACID ELECTROLYTES

In this chapter structure of solid-acids are described.

(1) Atomic Bonding Structure

(2) Order-Disorder Structure

3.1 Structure of Solid Acids

Solid acids have a salt-like structure, and are chemicals between acids and salts. As example, if a normal acid such as phosphoric acid (H_3PO_4) partially reacts with a normal salt such as cesium carbonate (Cs_2CO_3), the new product is a solid acid, cesium dihydrogen phosphate.

$$½\,Cs_2CO_3(salt) + H_3PO_4(acid) + H_2O \rightarrow CsH_2PO_4(solid\ acid) \quad \textbf{(3-1)}$$

or, if sulphuric acid (H_3PO_4) partially reacts with cesium sulfate (Cs_2SO_4), the new product is a solid acid, cesium hydrogen sulfate.

$$½\,Cs_2SO_4(salt) + ½\,H_2SO_4(acid) + H_2O \rightarrow CsHSO_4(solid\ acid) \quad \textbf{(3-2)}$$

The general composition of solid acids is MH_nXO_4 (M=alkali metal, K, Rb, Cs, NH_4; X= S, Se, P, As). All are formed of (1) oxyanion tetrahedral groups XO_4 (X = S, Se, P, As) that are linked together hydrogen bonds (2) cations.

All possible solid acids' tetrahedral oxy-anions and cations are listed in Table 3.1

Table 3.1 Cations and tetrahedral oxy-anions which are structure of solid acid [11]

Cations		Oxyanions	
M^+	Li^+, K^+, Na^+, Tl^+, Rb^+, NH_4^+, VO^+, Cs^+	XO_4^{-2}	SO_4^{-2}, SeO_4^{-2}, CrO_4^{-2} TeO_4^{-2}, MoO_4^{-2}, WO_4^{-2}
M^{+2}	Be^{+2}, Mg^{+2}, Ca^{+2} Sr^{+2}, Pb^{+2}, Ba^{+2}	XO_4^{-3}	PO_4^{-3}, AsO_4^{-3}, VO_4^{-3} NbO_4^{-3}, MnO_4^{-3}, SbO_4^{-3}
		XO_4^{-4}	SiO_4^{-4}, GeO_4^{-4}

The structure of solid acids is comprised of hydrogen-bonded tetrahedral oxy-anions charge balanced by a host lattice of cations. In Fig. 3.1 structure of a solid acid with formula MH_nXO_4 (M=alkali metal, K, Rb, Cs, NH_4; X= S, Se, P, As) is shown. The figure shows the room temperature structure with zigzag pattern of the hydrogen bonds between XO_4 tetrahedral oxyanions. Yellow dashed lines in the figure indicate the hydrogen bonds.

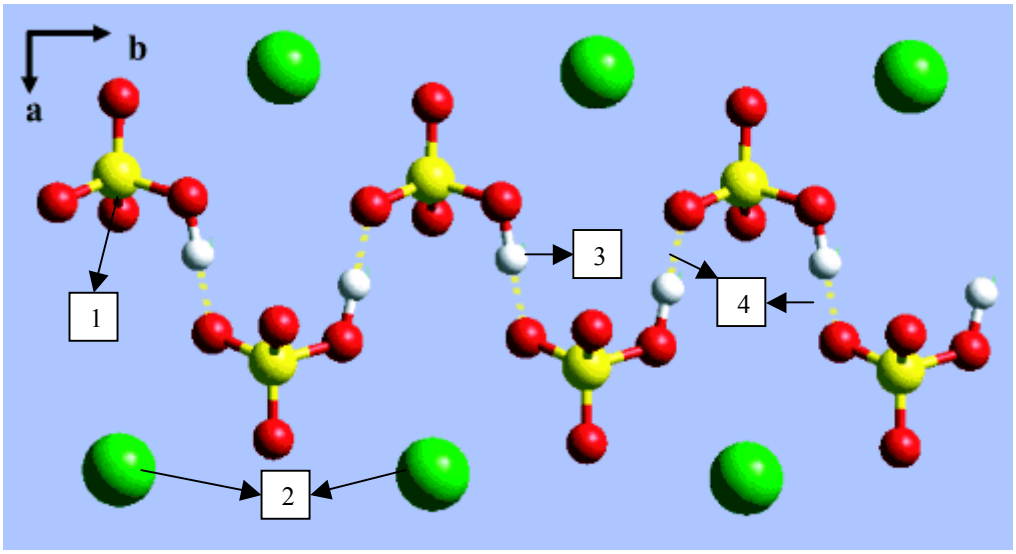

Figure 3.1 Room temperature ordered structure of solid acid with formula MH_2XO_4 (1)tetrahedral oxy anion, XO_4=SO_4, PO_4 (2) cation, M= K^+, Rb^+, Cs^+, (3)Hydrogen atoms (4) Hydrogen bonds

Particularly, in this work $MH(PO_3H)$ (where M=Cs and K) types of solid acids were investigated. These compounds contain the tetrahedral group PO_3H. The overall chemical and structural similarity of $MH(PO_3H)$ and MH_nXO_4 (e.g. $CsHPO_4$), both containing tetrahedral anions linked by hydrogen bonds to form infinite chains.

The structure of all solid acids at room temperatures is characterized by highly ordered hydrogen bond network [Fig. 3.1]. However, upon heating through 100-140 $^{\circ}$C it undergoes a phase transition to a disordered hydrogen bond network. Hydrogen bonds play a significant role in determining the structure and properties of solid acids. Therefore, hydrogen bonds need to be described in detail to properly explain the protonic conduction in solid acids.

3.1.1 Atomic Bonding

Solids are held together by cohesive forces. These cohesive forces between atoms are termed as atomic bonds. Furthermore there are four types of atomic bonds in the structure of solid acids.

(1) Ionic bonds;

(2) Covalent bonds;

(3) Metallic bonds;

(4) Hydrogen bonds

Ionic bonds result from the electrostatic interaction between the positively charged and negatively charged ions (in the case of solid acids the ionic bond is between cations and tetrahedral oxy-anions). Other electrostatic forces, such as Van der Waals interaction play a minor role. The Van der Waals interaction is caused by induces polarization of the electronic charge distribution of an atom by a neighboring atom [11, 13].

3.1.2 Hydrogen Bonding

Hydrogen bond is a special type of interaction between molecules: it forms whenever a hydrogen atom, bound to a strongly electronegative (able to attract electrons) atom, at the same time interacts with another strongly electronegative atom having a lone pair of electrons, like oxygen, nitrogen or fluorine. Usually, one bond will be stronger, written A—H, and is called the normal A—H bond while the weaker bond is commonly represented as a dotted line between the hydrogen atom and the other electronegative atom written H···B, is termed the hydrogen bond. The A and B atoms are termed the donor and acceptor atoms, respectively[11, 14].

The hydrogen atom can form only one covalent bond because it contains only a single 1s electron. Therefore, the attraction observed between hydrogen-bonded atoms must be due largely to ionic forces. In the case of solid acids, hydrogen bonds occur between two oxygen atoms. Amongst these two oxygen atoms, one of the oxygen is labeled as the proton donor oxygen atom (O_d), in which the proton lies within the electron density of the oxygen atom and bond most closely resembles a covalent bond, and the other oxygen is labeled as the proton acceptor oxygen atom (O_a), which is hydrogen-bonded to O_d via largely ionic forces[11,14,15]

Two types of H bonded complexes may be formed;

(1) "Intermolecular H-bonds"; involving two or more separate molecules, intermolecular hydrogen bonds are formed between two independent molecules A—H and B [14].

(2) "Intramolecular H-bonds", involving donor and acceptor sites within the same molecule that means where molecular groups A—H and B are both parts of a same molecule [14].

These two types of H-bonds are different. An intra-molecular H-bond involves a single molecule, whereas an intermolecular H-bond involves two molecules that become independent upon disruption of the H-bonds [14].

3.1.2.1 Intra-Hydrogen Bonds

Hydrogen bond strengths run in the range of 2 to 15 kcal/mol, which is significantly greater than other intermolecular forces (e.g., van der Waals forces with energies in the range of 0.1 to 2 kcal/mol for smaller molecules), but much less than intra-molecular covalent bonds (30 to 230 kcal/mol) [13].

This bond energy is not only due to electrostatic interaction between electronegative atoms and hydrogen but also due to covalent bonding between the lone pair electron of B acceptor and A-B bond. If the distance between hydrogen and acceptor (B) decreases, amount of covalency increases and so the hydrogen bond strength increases. Due to donor-acceptor and donor-hydrogen lengths, the hydrogen bond strength is labeled as strong, medium or weak. In case of solid acids, hydrogen bonds between oxygen atoms can be characterized according to their strength, which is related to the donor oxygen to hydrogen distance (d_{Od-H}), and the donor to acceptor oxygen distance ($d_{Od...Oa}$) [11, 15].

Table 3.2 Correlation between hydrogen bond types and bond character [11, 15]

Bond Strength	d_{Od-H} / Å	$d_{Od...Oa}$ / Å	Character
Strong	1.3 to 1.0	2.4 to 2.6	covalent
Medium	1.02 to 0.97	2.6 to 2.7	polar covalent
Weak	Below 1.1	2.7 to 3	ionic

Depending on the local symmetry of oxygen atoms participating in the hydrogen bond, the hydrogen bonds between oxygen atoms can be further classified as symmetric or asymmetric. For an O-H···O bond, the type of bond can be symmetric or asymmetric. If the proton is exactly between the two oxygen atoms, then it is symmetric bond. If the proton is slightly closer to one of the oxygens then it is referred to as asymmetric bond [11, 15].

Table 3.3 is a schematic representation of the hydrogen bond potential energies E(r) (or potentials) as a function of interatomic distance between two oxygen atoms for strong, medium, and weak symmetric and asymmetric bonds.

The symmetric and asymmetric strong bonds: the hydrogen bond distance ($d_{Od...Oa}$) is less than 2.4 Å. Hydrogen bond is in a single-well between the oxygen atoms. There is no distinction between the donor and acceptor oxygen atoms, hydrogen resides in equal distance to both of the oxygen atoms.

The medium bonds: the hydrogen bond distance ($d_{Od...Oa}$) is ~2.6 Å. Hydrogen atom can be closed to both oxygen atoms, and sit in double-well potential.

The weak hydrogen bonds: the hydrogen bond distances ($d_{Od...Oa}$) is greater than 2.9 Å. Symmetric weak hydrogen bonds are not generally observed. In asymmetric weak hydrogen bonds, the proton is closed to the donor oxygen in a single-well potential.

Table 3.3 Weak, strong and medium hydrogen bonds with order-disorder [11]

Bond Type	Symmetric	Asymmetric
Strong	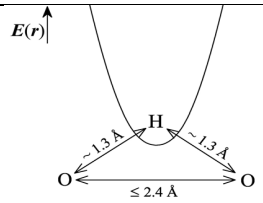	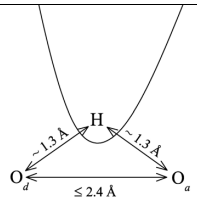
Medium	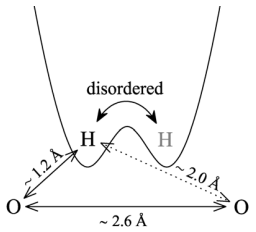	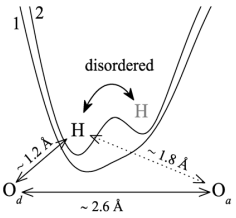
Weak	Not generally observed	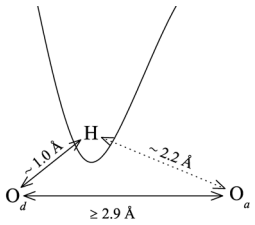

3.1.2.2 Inter-Hydrogen Bonds

Depending on the hydrogen bond density, the distribution of hydrogen bond can be zero, one, two or three dimensional network. The type of hydrogen bond network depends on the ratio of hydrogen to tetrahedral oxy-anions (H/XO_4). The $CsHSO_4$ solid acid has one hydrogen atom per XO_4 and tends to exhibit a one-dimensional network in the form of chains.

Table 3.4 The type of hydrogen bond network [11]

Dimensionality	Networks	H/XO_4	Example
1-D	Chains 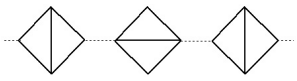	1	$CsHSO_4$

3.2 Order-Disorder Transitions of Solid Acids

At room temperature solid acids consist of linear zigzag chains of oxyanion molecules linked together by ordered hydrogen bonds. However, in the high temperature phase the ordered hydrogen bond network changes to dynamically disordered network of hydrogen bonds. The main driving force that leads to a disordered hydrogen bond network is believed to be the fast reorientation of the oxyanion units in solid acids [16]. In this section of the thesis, order-disorder phenomenon is expressed in detail.

Crystalline solids have a three dimensional periodicity in the arrangement of atoms. Perfect order is required that the position and the orientation of every atom be fixed in the lattice with respect to the position and orientation of every other atom or ion. However this perfect order is never realized in materials at any temperature other than 0 K. This is because of the thermal agitation in materials at non-zero temperatures which enables atoms or groups to diminish the order. An ordered state means a chosen order parameter is equal to or close to unity. In any order-disorder transition the material goes to disordered state and order parameter goes to zero [17].

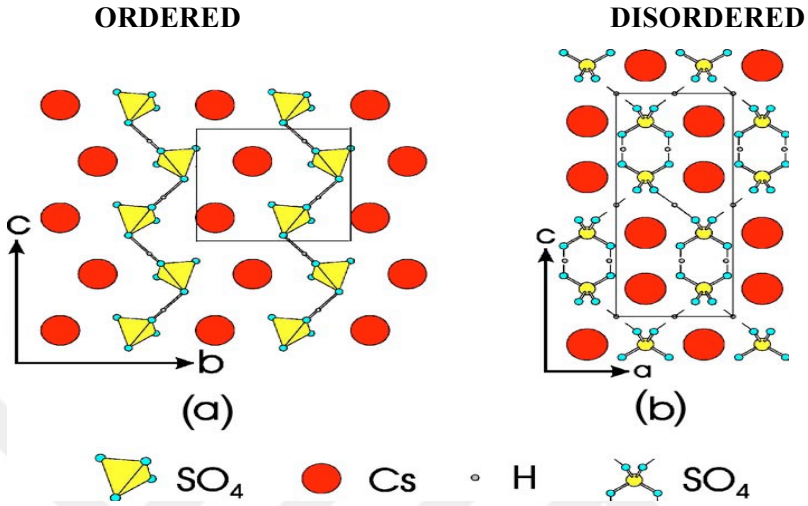

Figure 3.2 **Order-disorder structure of $CsHSO_4$** [11] (a) ordered structure at room temperature, monoclinic phase, (b) disordered structure at elevated temperatures, tetragonal phase

Order–disorder in solid acid structures is an important feature in determining the properties of these compounds. There are many types of order–disorder phenomenon observed in solids. The two main types of order–disorder phenomenon which describe the arrangement of atoms are;

(1) *Positional disorder*, in which atoms or ions occupy inappropriate sub-lattice positions are available for the atoms than are necessary [17].

(2) *Orientational disorder*, in which the ions or the basic units occupying the lattice sites contain more than one atom. In such a situation, more than one distinguishable orientation becomes possible for the ions in the lattice. It is possible that a low-temperature phase may have no disorder while the high-temperature phase which forms after a first-order transition may correspond to very high disorder [17]

Of these types of structural disorder, orientational disorder is important of understanding the properties of solid acid compounds. The orientational disorder exhibits in solid acids are as follows;

(1) Intra-hydrogen bond disorder,

(2) Inter-hydrogen bond disorder, and

(3) Oxy-anion disorder.

Intra-hydrogen bond disorder is responsible for ferroelectric transitions in solid acids, and *inter-hydrogen bond disorder* and *oxy-anion disorder*, being intimately related to one another, are responsible for superprotonic behavior [11].

3.2.1 Intra-Hydrogen Bond Disorder

Intra-hydrogen bond disorder occurs in medium strength symmetric and asymmetric hydrogen bonds. There are two well position separated by a barrier. At low temperatures, hydrogen resides in one of the well because there is no sufficient thermal energy for hydrogen to overcome the barrier. This structure is ordered. Upon heating, thermal oscillations are sufficient to overcome this barrier. This structure is disordered. This transition from order to disorder in solid acids leads to ferroelectric to paraelectric transitions [11].

3.2.2 Inter-Hydrogen Bond Disorder

Upon heating solid acids, the oxy-anions start to vibrate, while at same time breaking and reforming new hydrogen bonds. This is superprotonic phase transition. The inter-hydrogen bonds become disordered [11].

3.2.3 Oxy-anion Disorder

Oxy-anion disorder occurs when the oxygen atoms of structural tetrahedral oxy-anions partially occupy crystallographically equivalent positions. Due to the strong bonding between the oxygen atoms and the central tetrahedral atom, the overall tetrahedral structure is maintained, leading to the release of the tetrahedron between these crystallographically equivalent positions, and manifesting in several possible orientations of the tetrahedron [11].

PROPERTIES OF SOLID ACID ELECTROLYTES

The main properties of solid acids are;

(1) Protonic Conductivity (Superprotonic conductivity)

(2) Phase Transitions

4.1 Protonic Conductivity

Electrical conduction occurs by the long range migration of either electrons (electronic conduction) or ions (ionic conduction). In solid materials, one is usually interested in the specific conductivity, σ, which is the conductivity of a crystal of pellet that has a cell constant of unity, i.e. unit cross-sectional area and unit length. Commonly used units of specific conductivity are ohm^{-1} m^{-1}, and Sm^{-1} where 1 Siemens, $S \equiv ohm^{-1}$ [18]. Table 4.1 shows the difference between ionic conductivity and electronic conductivity.

Table 4.1 Typical values of electrical conductivity [18]

Type of Conduction	Material	σ (ohm $^{-1}$, cm^{-1})
Ionic Conduction	Ionic crystals	$< 10^{-18} – 10^{-4}$
	Solid electrolytes	$10^{-3} – 10^{-1}$
	Strong (liquid)electrolytes	$10^{-3} – 10^{-1}$
Electronic Conduction	Metals	$10^{1} – 10^{5}$
	Semiconductors	$10^{-5} – 10^{2}$
	Insulators	$< 10^{-12}$

Electrolytes in general possess high ionic conductivity. Therefore, the ionic conductivity and specifically protonic conductivity, is the principle material property of solid acids investigated here.

Proton conductivity is one of the key properties for separator materials for solid acid fuel cells. Protonic conduction can be considered as a particular case of ionic conduction. The presence of mobile species in a particular medium can give rise to a macroscopic concentration gradient obeying *Fick`s law*. The flux (the number of charged carriers passing through an area per time) of matter in a given x direction is given by [19];

$$J = -\frac{DdC}{dx} \qquad \textbf{(4-1)}$$ where,

C is the concentration of mobile species and D is the diffusion coefficient. The conductivity is given by [19];

$$\sigma = C\mu e^2 \qquad \textbf{(4-2)}$$

where, μ is the mobility and the e is the charge of mobile ions.

The Nernst-Einstein law which connects diffusion coefficient and conductivity is [19];

$$\sigma = \frac{DCe^2}{kT} \qquad \textbf{(4-3)}$$

where, k is Boltzmann`s constant and T is temperature.

Furthermore, the thermal activation of C and D must be taken into account, as follows [19];

$$C = C_0 \exp{-\frac{E_f}{2kT}} \qquad \textbf{(4-4)} \qquad\qquad D = f D_0 \exp{-\frac{E_m}{kT}} \qquad \textbf{(4-5)}$$

where, E_f corresponds to the enthalpy of formation of a defect pair. E_m is the enthalpy of defect migration, and f is the correlation factor. Its value varies between 0 and 1. f=1 when correlations are absent. Usually f is of order of 0.5-0.8 and plays a role determining the transport mechanism [19].

The conductivity can thus be written as,

$$\sigma = f\left(\frac{C_0 D_0 e^2}{kT}\right)\exp{-\frac{E_a}{kT}} \quad \text{where} \quad E_a = \frac{E_f}{2} + E_m \qquad \textbf{(4-6)}$$

The term $f\left(\frac{C_0 D_0 e^2}{kT}\right) = \sigma_0$ is frequently called pre-factor.

4.1.1 Superprotonic Conductivity

Inorganic solid acid compounds such as CsH_2PO_4 and $CsHSO_4$ have been known as superprotonic conductors, so these materials are expected as solid electrolyte in fuel cells operating at intermediate temperatures [5, 20].

The difference of solid acid proton conductors than other electrolyte solutions is that, electrolyte solutions have proton carriers which can rotate and diffuse but solid acids do not need any proton carrier. In case of solid acids, protons are migrating by their own movements [16].

Proton conductivity of solid acids in low temperatures is so low, because of highly ordered hydrogen bond structure of the crystal. As temperature increases solid acids undergo a phase transition and become superprotonic [Fig. 4.1].

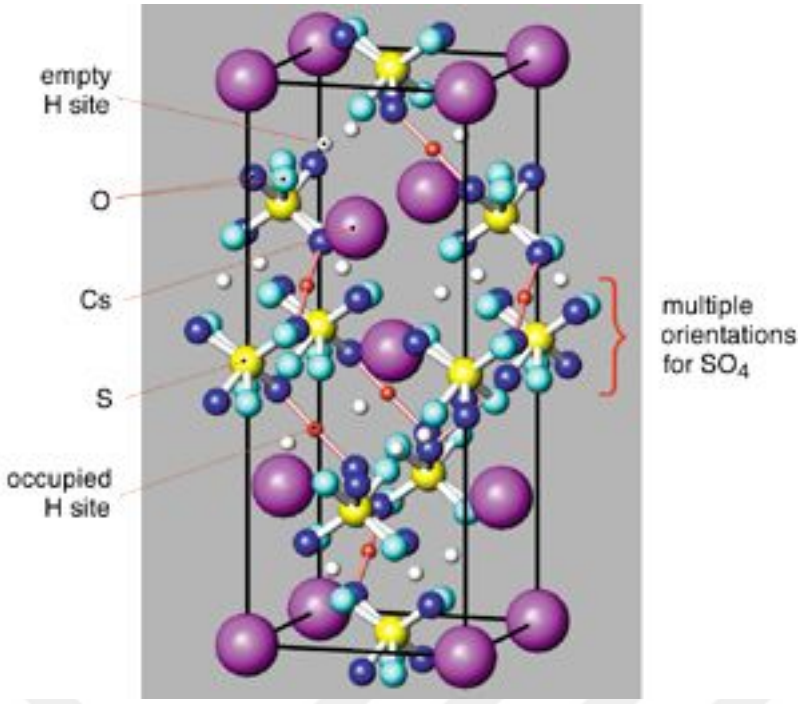

Figure 4.1 Disordered structure of $CsHSO_4$ [21]

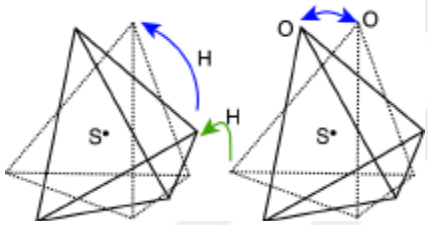

Figure 4.2 Reorientation of XO_4 group [21]

At high-temperatures, the XO_4 anion groups undergo rapid reorientation, on a time scale of about 10^{-11} seconds. The proton typically remains attached to one of the oxygen atoms of the XO_4 group until every so often a neighboring XO_4 group is in the proper orientation for proton transfer to occur [21].

There are five basic mechanisms for proton motion in solids:

(1) Atomic Diffusion

This type of proton motion is simply coupled proton-electron diffusion, which is common in materials such as metal hydrides, like Li_3AlH_6 and Na_3AlH_6. In such materials, the hydrogen can donate its electron density to the host matrix, accept electron density, or simply remain neutral [11, 15].

(2) Proton Displacement

This proton motion occurs when a proton "hops" along a hydrogen bond from one minima of a double-well potential to the other. This type of proton motion is quite common in solid acid compounds, and is responsible for ferroelectric behavior in solid acids, such as KH_2PO_4 [11, 15].

(3) Molecular reorientation

Also referred to as dipole reorientation, in this process a proton rides "piggy-back" a molecule undergoing a reorientation, rotation, or tumble. This motion was first proposed to describe proton transport in ice, but is also commonly observed in solid acid compounds, as well as liquid acids [11, 15].

(4) Vehicular mechanism; (proton-carried migration where proton attaches on a carrier molecule or ion)

In this mechanism, proton transport is associated with the diffusion of polyatomic species. In this type of proton motion, a proton rides on a mobile molecule, which may carry a positive charge (e.g. NH^{+4} , OH^{+3} , O_2H^{+5} , O_3H^{+7}), a negative charge (e.g. NH^{-2}, OH^{-}), or be neutral (e.g. NH_3, H_2O). The vehicle mechanism is, perhaps, the most common type of proton transport mechanism, and is exhibited by many fast-proton conductors, such as Nafion®, in which H_3O^+ ions are transported along sulfonic acid functional groups (SO^{3-}), within a polymer host matrix [11, 15].

(5) Grotthuss mechanism*;* (lone proton migration, proton jumps from a donor to a suitable acceptor molecule [19])

This mechanism is a cooperative process involving both a molecular (dipole) reorientation and proton-displacement. Superprotonic solid acids, such as $CsHSO_4$, conduct protons via this process. In these superprotonic solid acids, the oxyanion rearranges between crystallographically equivalent positions while carrying a proton with it, then the proton "hops" along a hydrogen bond to another oxyanion, followed by another oxyanion reorientation, and so on [11, 15] Superprotonic solid acids, such as $CsHSO_4$, conduct protons via *Grotthuss mechanism* process. The process of Grotthous results from (a) displacement of H^+ along a hydrogen bond and (b) transport of the H ion from this hydrogen bond to the following one [19].

The Grotthous conduction mechanism for superprotonic compounds has been explained by a two step process. The first step involves the displacement of a proton along the hydrogen bond between two neighboring XO_4 tetrahydrons and the second step consists of the reorientation of the XO_4 group by breaking O-H-O hydrogen bonds. The figure of proton transport mechanism is given below;

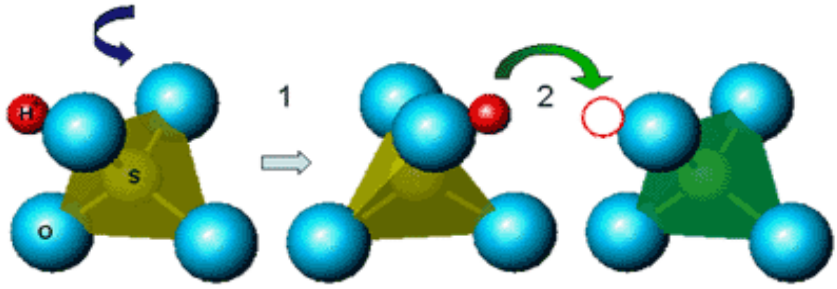

Figure 4.3 Proton transport mechanism in a disordered oxyanion [11]

(left) HSO_4^- tetrahedra undergoes rapid reorientations with the proton attached to a particular oxygen atom, (right) proton transfer from one tetrahedron to the next occurs on a much slower time scale

4.2 Phase Transition in Solid Acids

There are three different phase forms for solids, depending on temperature.

(1) Ferroelectric phase (phase III)

(2) Paraelectric phase (phase II)

(3) Superprotonic phase (phase I) [17].

Solid acids with general composition of MH_nXO_4 are prime example of a hydrogen-bonded crystalline system that undergoes a "superprotonic" phase transition. As an example, 3 phases of $CsHSO_4$ is like;

$$phaseIII \xrightarrow{330-370K} phaseII \xrightarrow{410-415K} phaseI$$ [4]

First of all, here, general description and thermodynamic of phase transition will be given, as well as a specific description of superprotonic phase transition.

A phase is a homogeneous solution of matter bounded by a surface so that it is mechanically separated from any other portion [11]. A phase transition is a transformation of matter after exposed a change in a thermodynamic function, such as temperature T, pressure P, volume V, or entropy S, from one phase to another phase that is noticeable from the first. During phase transition, the free energy of the system remains continuous, thermodynamic quantities undergo discontinuous changes [17].
Gibbs free energy is given by;

$$G = H - TS = E + PV - TS \quad \textbf{(4-7)}$$

Hence,

$$dG = dE + PdV + V\,dP - T\,dS - S\,dT \quad \textbf{(4-8)}$$

$$= V\,dP - S\,dT \quad \textbf{(4-9)}$$

The first and second derivatives of the free energy may be written as [17].

$$\left(\frac{\partial G}{\partial P}\right)_T = V \quad \textbf{(4-10)} \qquad \left(\frac{\partial G}{\partial T}\right)_P = -S \quad \textbf{(4-11)}$$

$$\left(\frac{\partial^2 G}{\partial P^2}\right)_T = \left(\frac{\partial V}{\partial P}\right)_T = -V\beta \quad \textbf{(4-12)} \qquad \left(\frac{\partial^2 G}{\partial P \partial T}\right) = \left(\frac{\partial V}{\partial T}\right)_P = V\alpha \quad \textbf{(4-13)}$$

$$\left(\frac{\partial G}{\partial T^2}\right)_P = -\left(\frac{\partial S}{\partial T}\right)_P = -\frac{Cp}{T} \quad \textbf{(4-14)}$$

Here Cp, α and β are the heat capacity, volume thermal expansivity, and compressibility respectively. We readily see that the transformations in which a discontinuous change occurs in volume and entropy (that is, when there is a latent heat of transformation) belong to first order, and those in which discontinuous change occurs in heat capacity, thermal expansivity, and compressibility belong to the second order [17].

For the purpose of this work phase transitions are identified by a discontinuous change in the extensive thermodynamic variables of a substance, such as volume V , entropy S, magnetization M, polarization P, while varying an intensive variable, such as pressure P, temperature T, magnetic field B, or electric field E. Specifically, for transitions in which there is a discontinuous change in the entropy through the phase transition while varying the temperature, there will also be a change in enthalpy ΔH or latent heat Q associated with the transition. This sort of phase transition is known as a first order phase transition. If the entropy is continuous, but its first derivative with respect to temperature, or heat

capacity Cp is discontinuous, then the phase transition is said to be of second order, and if the entropy and heat capacity are continuous, and the derivative of the heat capacity ∂Cp/∂T is discontinuous, the transition is third order, and so on [11, 15].

In this work, first order solid–solid phase transitions are of key interest. For these transitions the change in extensive thermodynamic variables such as volume, V, and magnetization, M, are negligible compared to the change in S [11, 15].

$$T = \frac{\partial E}{\partial S} \qquad \textbf{(4-15)}$$

When a solid undergoes a phase transition by absorbing thermal energy, the transformed phase will possess higher internal energy. In the high temperature phase, therefore, bonding between neighboring atoms or units would be weaker than in the low-temperature phase. These result a change in the nature of the first-nearest neighbors (primary coordination) or of the second-nearest neighbors (secondary coordination) [11].

Initial research into these compounds focused on the ferroelectric properties. Near room temperature these compounds have monoclinic symmetry where XO_4 groups are linked together by hydrogen bonds. These bonds formed between oxygen atoms of neighboring XO_4 (phosphate or sulfate) groups. The conductivities of most solid acids near room temperatures are on the order of 10^{-6} to 10^{-9}. Upon slight heating these compounds are known to undergo a "superpotonic" phase transition. At high temperatures $MH_n(XO_4)$ adopts a cubic structure, where the M atoms reside at the corners of the primitive unit cell and the PO_4 group is orientationally disordered about the center, taking on one of six possible orientations. On passing through the transition, the conductivity jumps by several orders of magnitude to a value of 10^{-3} to 10^{-2} Ω^{-1} cm^{-1}, and the material often become quite ductile. The transition temperatures typically lie between 50 and 150 °C, and the activation energy for transport in the high temperature phase is 0.3 to 0.45 eV. A key feature of the proton transport process is that, unlike polymeric systems, it does not require humid atmospheres [4]. Since then, there has been increasing interest in the high temperature properties of these compounds and their first-order phase transformations.

4.3 Literature Review

4.3.1 $CsHSO_4$ and CsH_2PO_4

In previous researches, cesium hydrogen sulfate $CsHSO_4$ and cesium dihydrogen phosphate CsH_2PO_4 have been widely studied and as known as superprotonic conductors at their high temperature phases [20, 22-24]. CsHSO4 is first investigated one amongst solid acids for fuel cell applications. Haile *et al.* have reported $CsHSO_4$ has superprotonic phase transition at 141 °C and the conductivity at 160 °C varies from 3.7 x 10^{-3} Ω^{-1} cm^{-1} to 2.8 x 10^{-3} Ω^{-1} cm^{-1} [4]. Unfortunately, compounds with sulfates and

selenates undergo a detrimental reaction with hydrogen as would be present in the fuel cell anode. Decompositon reaction for $CsHSO_4$ in a H_2 atmosphere at elevated temperatures is given below.

$$2CsHSO_4 + 4H_2 \rightarrow Cs_2SO_4 + 4H_2O + H_2S \qquad \textbf{(4-16)}$$

Since by-product of these reactions (H_2S and H_2Se) is very poisonal for fuel cells' catalyst, most of the studies have focused on CsH_2PO_4. CsH_2PO_4 has advantages beside $CsHSO_4$, since chemical instability observed in solid acids consist sulphates and selenates, the byproduct of the reaction product, H_2S or H_2Se, is an extreme poison for the fuel cell anode catalyst and, as a consequence, even a modest extent of reaction severely degrades the fuel cell power output. With this appreciation of the transport properties and thermodynamics of solid acids, only one candidate amongst known compounds remains a viable fuel cell electrolyte: CsH_2PO_4.

Rashkovich *et al.* reported CsH_2PO_4 exhibits high conductivity upon heating to temperatures above the superprotonic phase transitions at 230 °C with conductivity to be $2.3 \times 10^{-2}\ \Omega^{-1}cm^{-1}$ and decomposition begins at 300 °C [7]. Awakura *et al*. demonstrated that CsH_2PO_4 to be stable electrolyte for fuel cells in temperature range of 230 to 260 °C. Above 260 °C dehydration reaction to form solid $CsPO_3$ reported. Dehydration reaction is given below [22].

$$CsH_2PO_4(s) \rightarrow CsH_{2-2x}PO_{4-x}(s) + xH_2 0(g) \qquad \textbf{(4-17)}$$

Analogous compounds of RbH_2PO_4 and KH_2PO_4 all undergo a phase transition.

4.3.2 $CsH(PO_3H)$ and $KH(PO_3H)$

This work focused on another class of solid acid compound, $CsH(PO_3H)$ and $KH(PO_3H)$. This compound is lack of tetrahedral symmetry of XO_4 group.

Haile *et al.* investigated $CsH(PO_3H)$ and revealed that this material goes transition with an onset of 137 °C. High temperature X-Ray diffraction shows that high temperature phase is cubic likely CsCl structure. The high temperature conductivity at 160 °C is 5.5 x 10^{-3} Ω^{-1} cm^{-1} [25]. The conductivity of the phosphite (PO_3) is slightly lower than the other compounds. This may be a result of reduced number of sites of the tetrahedral group to which the migrating protons may attach.

Zhou *et al*. investigated superprotonic conductivity in $MH(PO_3H)$ ($M=Li^+$, Na^+, K^+, Na^+, Rb^+, Cs^+, NH_4^+). In their study except lithium dihydrogen phosphite which adopts orthorhombic structure the other phosphites have monoclinic structure at room temperature. The magnitude of the superprotonic conductivity of $KH(PO_3H)$ and $CsH(PO_3H)$ amounts to 4.2 *10^{-3} Ω^{-1} cm^{-1} (at 140 °C) and 3 *10^{-3} Ω^{-1} cm^{-1} (at 160 °C) respectively [5].

Compound	**Transition Temperature °C**	**Conductivity* Ω^{-1} cm^{-1}**	**Ref**
$CsHSO_4$	141	2.8 x 10^{-3}	[4]
CsH_2PO_4	230	2.3×10^{-2}	[7]
$CsH(PO_3H)$	137	4.6 x 10^{-3}	[25]

Table 4.2 Comparison of transport properties of solid acids
** The highest conductivity values that can be reached above transition temperature*

4.3.3 Anodic Alumina/Solid Acid Composite Membranes

Current researches are focused on developing alternative fuel cell membranes that are durable, higher in proton conductivity at higher temperatures. By taking into account the good thermal stability of alumina membranes in a rather wide range of temperatures, it is suggested the use of porous anodic alumina membranes as template for the fabrication, by filling the pores of alumina membranes with a protonic conductor, of inorganic membranes to use in fuel cell at temperatures higher than usual PEMFC. The operating temperature of membrane can be much higher than that used in this work if anodic alumina porous membranes are filled with a higher temperature proton conductor. Researchers proposed a pore-filling electrolyte membrane concept for hydrogen-oxygen fuel cell applications. These types of membranes are composed of two materials: a porous substrate and a solid acid that fills the pores [26-27].

The choice of porous anodic alumina membranes is due to its unique properties that are promising for fuel cell application:

(1) They have extremely ordered porous structure and they can be easily electrochemically grown in a rather wide range of thickness (from few micron to hundreds micron) and porosity (from 10 to 43%) with pores diameter ranging from 20 to 200 nm depending on anodizing parameters through a self-ordering process. Thus through an optimal filling it is easy to control the precise size of composite membrane (thickness and diameter) [26].
(2) The presence of the AAM support could also prevent powdering of the solid acid [26].
(3) The hydrophilicity of anodic alumina can also contribute to the proton transport at room temperature owing to the presence of water molecules inside the pores [26].

Composite membranes are fabricated by the impregnation of inorganic porous membranes with inorganic proton conductor. In this work, solid acid compound $KH(PO_3H)$, which is under going to superprotonic transition at 141 ºC is used as electrolyte for composite membranes.

EXPERIMENTAL

5.1 Synthesis and Preparation Techniques

5.1.1 Synthesis of Solid Acids

The solid acids analyzed in this study were synthesized by slow evaporation of an aqueous solution containing metal carbonates and the appropriate mineral acids.

$$M_2CO_3 \quad + \quad H_nXO_3 \quad + \quad H_2O \quad \xrightarrow{-H_2O} \quad \text{sing}le\,crystals \qquad \textbf{(5-1)}$$

(where M=Cs^+, K^+ and X = P for this study)

All crystals were grown at room temperature.

5.1.1.1 Synthesis of powders of $KH(PO_3H)$

Crystals of the potassium dihydrogen phosphites, $KH(PO_3H)$, were prepared by mixing the appropriate amounts of the potassium hydroxide KOH (Merck, 99.5%) and phosphorous acid H_3PO_3 (Aldrich, 99%) in an aqueous solution, followed by slow evaporation at room temperatures. The mole ratio of K: PO_3 was held at 1:1. Just enough water was added into KOH pellets to ensure complete dissolution. Aqueous solution of KOH was added in to aqueous solution of H_3PO_3 by means of a pipette. The solution was stirred and heated at 90 °C to induce H_2O slow evaporation and precipitation of the product. After the solutions were evaporated the crystals put into oven. All powders were dried in an oven in air at 105 °C during 20 h prior to experiments.

Solid acid synthesis recipe for 1g of $KH(PO_3H)$ is given below;

(1) Weigh out 0.449 g of potassium hydroxide pellets.

(2) Add distilled water to (1) while stirring, until complete dissolution.

(3) Weigh out 0.656g of phosphorous acid powder.

(4) Add distilled water to (3) while stirring, until complete dissolution.

(5) Slowly add (2) into (3).

(6) Stir (5) on a heater at 90 °C till all the water evaporate.

(7) Dry precipitate in an oven at 105 °C during 20 h prior to experiments.

$$KOH + H_3PO_3 \rightarrow KH(PO_3H) + H_2O \qquad \textbf{(5-2)}$$

5.1.1.2 Synthesis of powders of $CsH(PO_3H)$

Crystals of the cesium dihydrogen phosphites, $CsH(PO_3H)$, were prepared by mixing the appropriate amounts of the cesium carbonate Cs_2CO_3 (Aldrich, 98%) and phosphorous acid H_3PO_3 (Aldrich, 99%) in an aqueous solution, followed by slow evaporation at room temperatures. The mole ratio of Cs: PO_3 was held at 1:1. Just enough water was added into Cs_2CO_3 powders to ensure complete dissolution.

Aqueous solution of Cs_2CO_3 was added in to aqueous solution of H_3PO_3 by means of a pipette. The solution was stirred and heated at 90 °C to induce H_2O slow evaporation and precipitation of the product. After the solutions were evaporated the crystals put into oven. All powders were dried in an oven in air at 105 °C during 20 h prior to experiments.

Solid acid synthesis recipe for 1g of $CsH(PO_3H)$ is given below;

(1) Weigh out 0.815 g of cesium carbonate powder.
(2) Add just enough distilled water to (1) while stirring, until complete dissolution.
(3) Weigh out 0.41g of phosphorous acid powder.
(4) Add distilled water to (3) while stirring, until complete dissolution.
(5) Slowly add (2) into (3).
(6) Stir (5) on a heater at 90 °C till all the water evaporate.
(7) Dry precipitate in an oven at 105 °C during 20 h prior to experiments.

$$^{(1-x)}\!/_{2}\, Cs_2CO_3 + H_3PO_3 \rightarrow CsH(PO_3H) + H_2O \qquad \textbf{(5-3)}$$

5.1.1.3 Synthesis of powders of $K_xCs_{(1-x)}H(PO_3H)$

Crystals of the mixed cation system phosphites with formula $K_xCs_{(1-x)}H_2PO_3$ were prepared by mixing the appropriate amounts of the potassium hydroxide KOH (Merck, 99.5%), cesium carbonate Cs_2CO_3 (Aldrich, 98%) and phosphorous acid H_3PO_3 (Aldrich, 99%) in an aqueous solution, followed by slow evaporation at room temperatures. The mole ratio of (Cs + K):PO_3 was held at 1:1. Just enough water was added into KOH + Cs_2CO_3 mixture to ensure complete dissolution. Aqueous solution of KOH + Cs_2CO_3 was added in to aqueous solution of H_2PO_3 by means of a pipette. The solution was stirred and heated at 90 °C to induce H_2O slow evaporation and precipitation of the product. After the solutions were evaporated the crystals put into oven. All powders were dried in an oven in air at 105 °C during 20 h prior to experiments.

$$^{(1-x)}\!/_{2}\, Cs_2CO_3 + (x)KOH + H_3PO_3 + H_2O \rightarrow K_xCs_{(1-x)}H(PO_3H) \qquad \textbf{(5-4)}$$

5.1.2 Sample Preparation for Instrumental Analysis

5.1.2.1 Preparation of Pellets

Synthesized powders of solid acids were pressed into pellets in order to use for analysis with X-ray Powder Diffractometer, Impedance Spectroscopy and Infrared Spectroscopy.

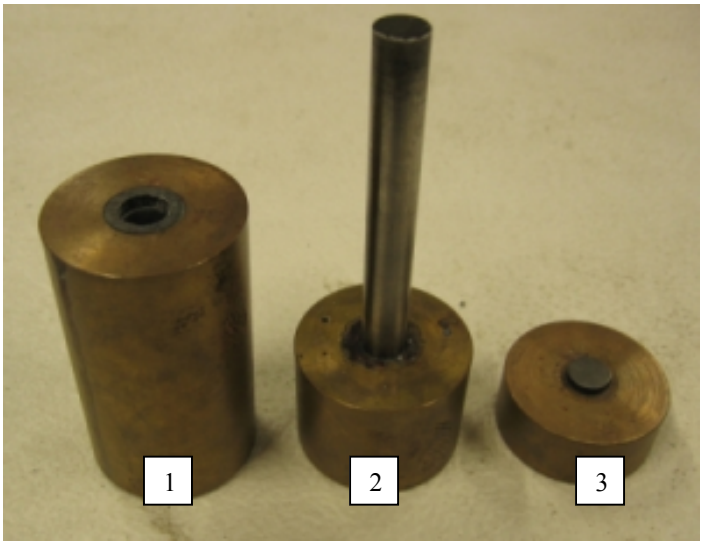

Figure 5.1 (1) punch, (2) die and (3) base for preparing pellets

Crystals are ground-up and pressed into pellets by applying pressure 400MPa.

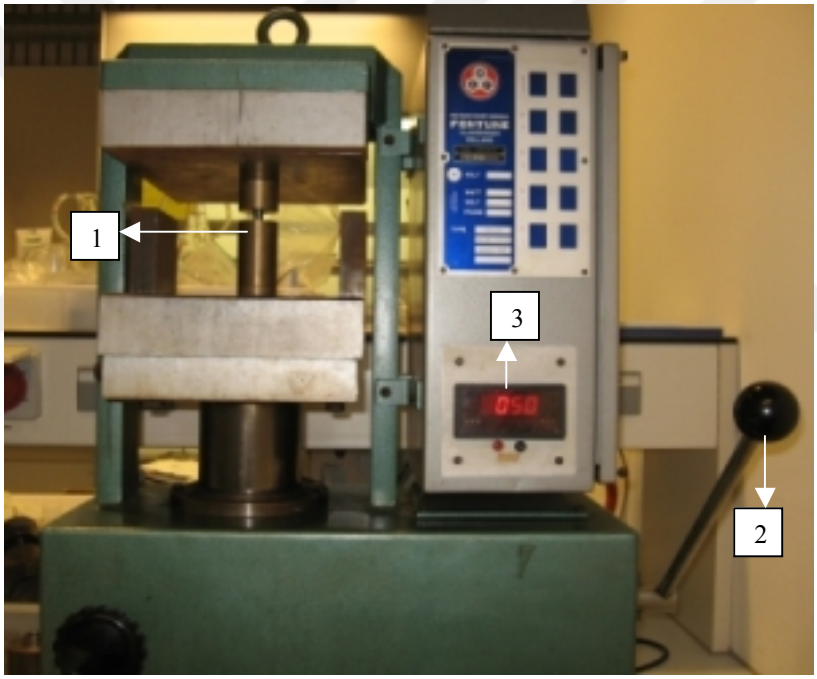

Figure 5.2 **Press used for preparing pellets**: (1) punch, die, base (2) handle (3) indicates the amount of force (units) required to press discs

5.1.2.2 Sputtering of Pellets

Pellets were sputtered with gold in order to use for analysis with Impedance spectroscopy.

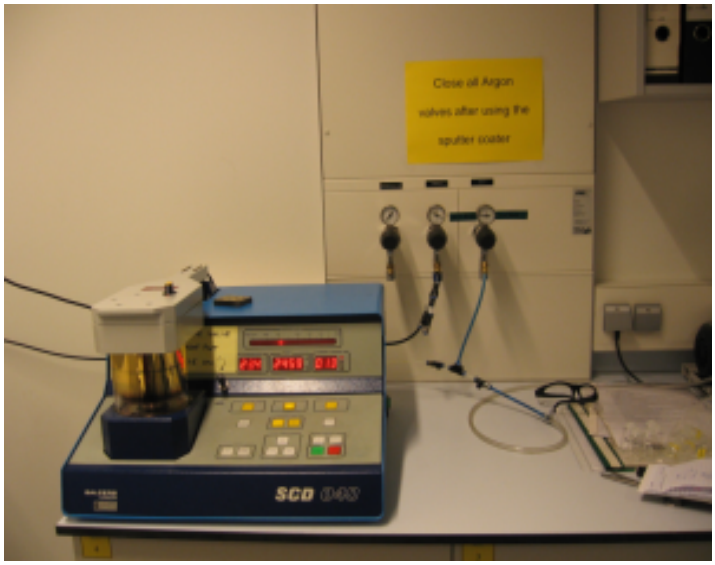

Figure 5.3 Sputtering Instrument

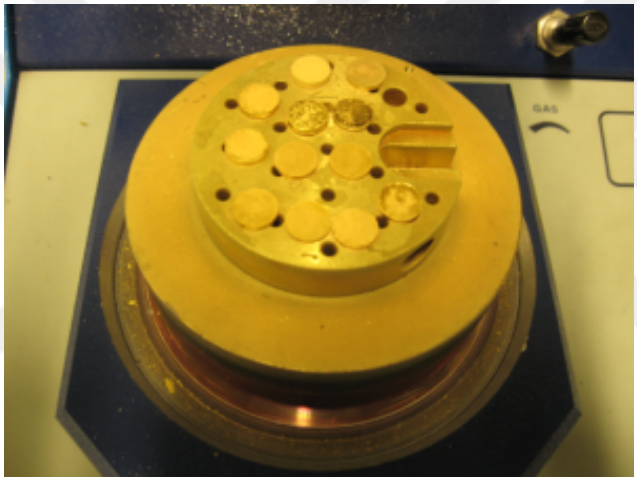

Figure 5.4 Pellets after sputtered with gold

5.2 Fabrication of Composite Membranes

In this part of study, commercially acquired porous anodic alumina membranes were filled with synthesized potassium diphosphite $KH(PO_3H)$. Commercial (Anodisc 13, Whatman, 0.2 μm) alumina membranes of thickness 50 μm was used. The pore filling of membranes was performed with $KH(PO_3H)$ protonic conductor which was synthesized from aqeous solution of KOH (Merck, 99.5%) and H_3PO_3 (Aldrich, 99%) as described in 5.1.1.1. Scanning Electron Microscopy analysis of alumina membranes before and after filling procedure was performed by using JEOL JSM-5600 LV Scanning Electron Microscope.

5.2.1 Filling Procedure

Alumina membranes were filled with $KH(PO_3H)$ salt by simple immersion of the sample in saturated $KH(PO_3H)$ aqueous solution for 15 min. The membrane was subsequently dried by dipping in acetone for 10s and exposure to air for 30s, for five times.

5.2.2 Preparation of Electrodes

Electrodes were prepared from carbon paper (Toray 10% polytetrafluoroethylene PTFE), covered with a mixture Pt black/C black (50% Pt on carbon black) stirred in n-butyl acetate for at least 1h [Fig 5.5]. Catalyst loading was 1 mg cm^{-2} of black platinum. The composite membranes of alumina/ $KH(PO_3H)$ were finally sandwiched between two carbon paper electrodes [Fig. 5.6].

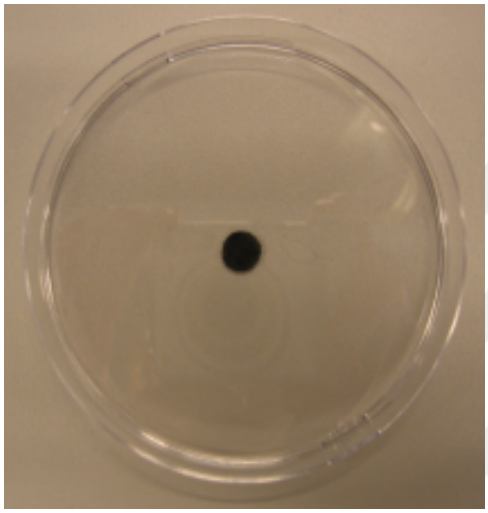

Figure 5.5 Electrodes for fuel cell prepared from carbon paper and covered with Pt black/C black

Figure 5.6 Membrane/Electrode Assembly

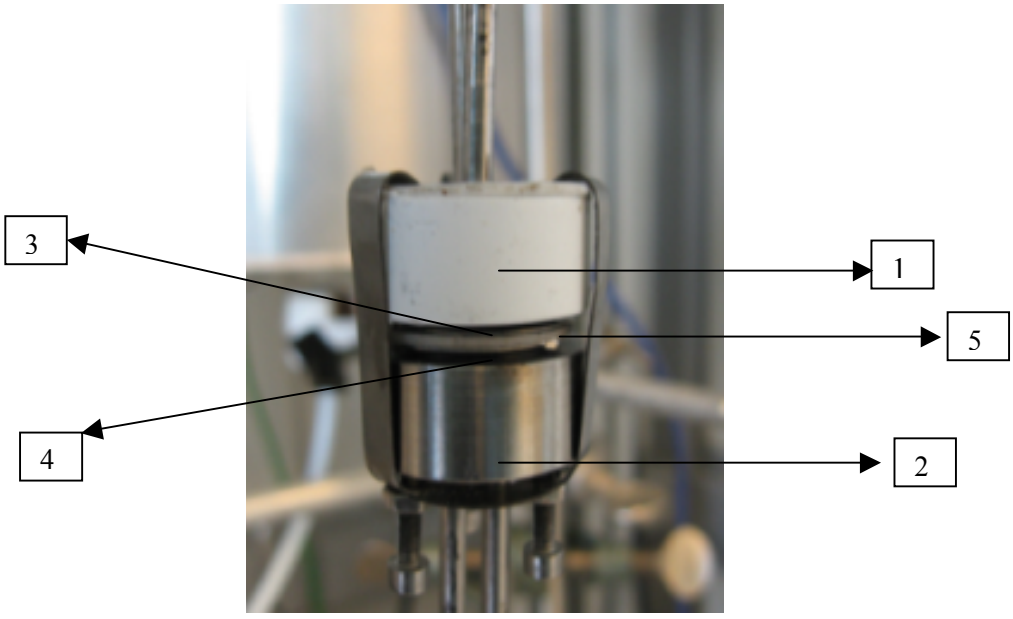

Figure 5.7 A fuel cell demonstration (1) and (2) stainless steel holder, (3) and (4)

electrodes, (5) electrolyte/membrane

5.3 Characterization Methods

The following methods were used:

- X-Ray Diffraction Analysis (XRD)
- Differential Scanning Calorimetry (DSC)
- Impedance Spectroscopy
- Infrared Spectroscopy
- Scanning Electron Microscopy (SEM)

5.3.1 X-Ray Powder Diffraction Analysis

X-ray diffraction is the most widely used and least ambiguous method for the precise determination of the positions of atoms in molecules and solids and much understanding of chemical bonding [28]. XRD is a rapid analytical technique primarily used for phase identification of a crystalline material and can provide information on unit cell dimensions. Powder X-ray diffraction is probably the most commonly employed technique in solid state inorganic chemistry and has many uses from analysis and assessing phase purity to determining structure.

X-rays are relatively short wavelength, high energy electromagnetic radiation. When viewed as a wave we think of it as a sinusoidal oscillating electric field with, at right angles, a similar varying magnetic field changing with time. The most common unit of measure for X-rays is the angstrom Å unit, defined as $1*10^{-10}$ m but the last IUPAC vention made the nanometer (10^{-9} m) a standard [29].

A typical X-ray diffractometer consist of an X-ray source, a goniometer and sample holder, and an X-ray detector. In X-ray powder diffractometer, X-rays are generated within a sealed tube that is under vacuum. A current is applied that heats a filament within the tube, the higher the current the greater the number of electrons emitted from the filament. When these electrons hit the target, X-rays are produced. The wavelength of these X-rays is characteristic of that target. These X-rays are collimated and directed onto the sample, which has been ground to a fine powder (typically to produce particle sizes of less than 10 μm). A detector detects the X-ray signal; the signal is then processed either by a microprocessor or electronically, converting the signal to a count rate. Changing the angle between the X-ray source, the sample, and the detector at a controlled rate between preset limits is an X-ray scan. When an X-ray beam hits a sample and is diffracted, we can measure the distances between the planes of the atoms mat constitute the sample by applying Bragg's Law [29].

Bragg noted that X-ray diffraction behaves like “reflection” from the planes of atoms within the crystal and that only at specific orientations of the crystal with respect to the source and detector are X-rays “reflected” from the planes. It is not like the reflection of light from a mirror, as this requires

that the angle of incidence equals the angle of reflection, and this is possible for angles. With X-ray diffraction, the reflection only occurs when the conditions for constructive interference are fulfilled.

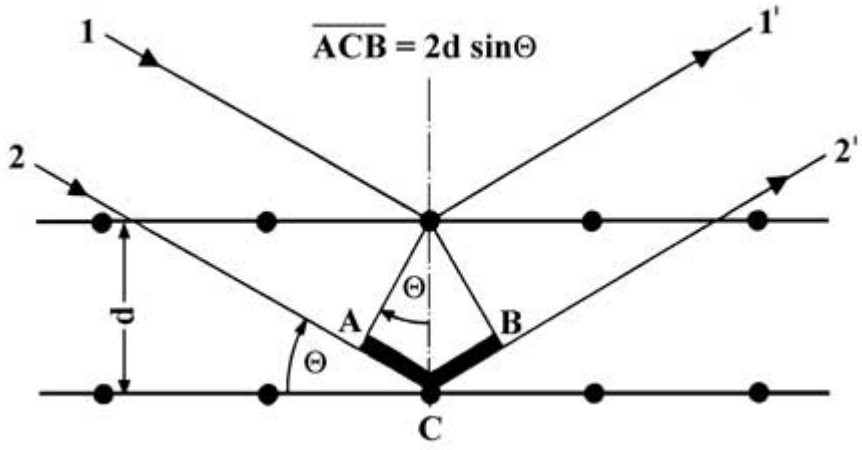

Figure 5.8 Bragg reflections from a set of crystal planes with a spacing d_{hkl}.

Fig 5.7 illustrates the Bragg condition for the reflection of X-rays by a crystal. The array of black points in the diagram represents a section through a crystal and the lines joining the dots mark a set of parallel planes with Miller indices *hkl* and interplanar spacing d_{hkl}.

A parallel beam of monochromatic X-rays 1-2 is incident to the planes at an angle Θ_{hkl}. The ray 2 is scattered by the atom at C. For the reflected beams to emerge as a single beam of reasonable intensity, they must reinforce, or arrive in phase with one another. This is known as constructive interference, and for constructive interference to take place, the path lengths of the interfering beams must differ by an integral number of wavelengths. If CA and CB are drawn at right angles to the beam, the difference in path length between the two beams is given by:

Difference in path length = CA + CB **(5-5)**

But,

$$CA=CB=d_{hkl}\sin\Theta_{hkl} \quad \textbf{(5-6)}$$

So,

$$\text{Difference in path length} = 2\, d_{hkl}\sin\Theta_{hkl} \quad \textbf{(5-7)}$$

This must be equal to an integral number, n, of wavelengths. If the wavelength of the X-rays is λ, then

$$n\lambda=2\, d_{hkl}\sin\Theta_{hkl} \quad \textbf{(5-8)}$$

This is known as Bragg equation, and it relates the spacing between the crystal planes, d_{hkl}, to the particular Bragg angle, Θ_{hkl} at which reflections from these planes are observed (mostly the subscript *hkl* is dropped from the Bragg angle Θ without any ambiguity as the angle is unique for each set of planes).

When n=1, the reflections are called first order, and when n=2 the reflections are second order and so on. However the Bragg equation for a second order reflection from a set of planes *hkl* is;

$$2\,\lambda=2\, d_{hkl}\sin\Theta_{hkl} \quad \textbf{(5-9)}$$

which can be rewritten as

$$\lambda = 2\frac{d_{hkl}}{2}\sin\theta \qquad \textbf{(5-10)}$$

Equation 6-10 represents a first order reflection from a set of planes with interplanar spacing $\frac{d_{hkl}}{2}$. The set of planes with interplanar spacing $\frac{d_{hkl}}{2}$ has Miller indices 2h2k2l. Therefore, the second order reflection from *hkl* is indistinguishable from first order reflection from 2h2k2l, and the Bragg equation may be written more simply as

$$n\lambda = 2d\sin\Theta \text{, where} \qquad \textbf{(5-11)}$$

d ; is the distance between adjacent planes of atoms (the d-spacing),

λ ; is the wavelength of the incident X-ray beam

Θ ; is the angle of diffraction

n ; is the integer n is the order of the diffracted beam

Since we know λ and we can measure Θ, we can calculate the d-spacing. The characteristic set of d-spacing generated in a typical X-ray scan provides a unique "fingerprint" of the mineral or minerals present in the sample. When properly interpreted, by comparison with standard reference patterns and measurements, this "fingerprint" allows for identification of the material.

Measurements were recorded at room temperature using Philips XRD PW1830 generator (50kV, 35mA). The diffraction data were analyzed using the software program X`PERT DATA COLLECTOR.

The following parameters are entered;

Starting 2-theta angle: 10
Step size: 0.02 degree
Count time per step: 0.2 second
Ending 2-theta angle: 80

5.3.2 Electrochemical Impedance Spectroscopy

5.3.2.1 Impedance definition: concept of complex impedance

Electrochemical impedance is usually measured by applying an AC potential to an electrochemical cell and measuring the current through the cell. If it is supposed that we apply a sinusoidal potential excitation, the current response to a sinusoidal potential will be a sinusoid at the same frequency but shifted in phase as seen in Fig. 5.8

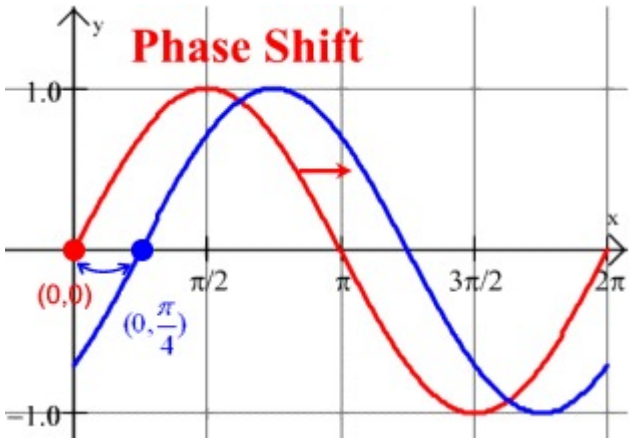

Figure 5.9 Phase shift

This sinusoidal excitation is produced by placing an ionic conducting material under an alternating electric field E, with an angular frequency of ω and amplitude, E_0, which can be described by the complex time (t) dependent wave function

$$E(t) = E_0 \cdot e^{i\omega t} \qquad \textbf{(5-12)}$$

The current response in the resistor, I_R, generated by this electric field, can be described by a similar time dependent wave function with a different amplitude, I_0, plus some phase shift Φ,

$$I(t) = I_0 \cdot e^{i(\omega t+\phi)} \qquad \textbf{(5-13)}$$

An expression analogous to Ohm's Law allows us to calculate the impedance of the system as:

$$Z = \frac{E(t)}{I(t)} = \frac{E_0 \cdot e^{i\omega t}}{I_0 \cdot e^{i(\omega t+\Phi)}} = Z_0 \frac{e^{i\omega t}}{e^{i(\omega t+\Phi)}} = Z_0 \cdot e^{-i\phi} = Zo(\cos\phi - i\sin\phi) \qquad \textbf{(5-14)}$$

where, Z is the complex impedance characterized by a real component Z' and an imaginary component Z''.

$$Z = Z' + Z'' \qquad \textbf{(5-15)}$$

It is convenient to define the reciprocal of impedance, or admittance Y , as

$$Y \equiv \frac{1}{Z} = Y' + iY'' \qquad \textbf{(5-16)}$$

Rewriting Ohm`s law using admittance

$$Y(\phi) = \frac{I(t)}{E(t)} = \frac{I_0 e^{i(\omega t+\phi)}}{E_0 e^{i\omega t}} = \frac{I_0}{E_0}(\cos\phi + i\sin\phi) \qquad \textbf{(5-17)}$$

When a material's current response is at frequency at which no phase shift occur $\phi = 0$,

then equation becomes

$$Y(0) = \frac{I_0}{E_0} = \frac{1}{R} \qquad \textbf{(5-18)}$$

5.3.2.2 Data Presentation

If the real part of Z is plotted on the X-axis and the imaginary part is plotted on the Y-axis of a chart, we get a "Nyquist Plot". Notice that in this plot the Y-axis is negative and that each point on the Nyquist Plot is the impedance at one frequency. When you look at any data point on the plot, you cannot tell what frequency was used to record that point.

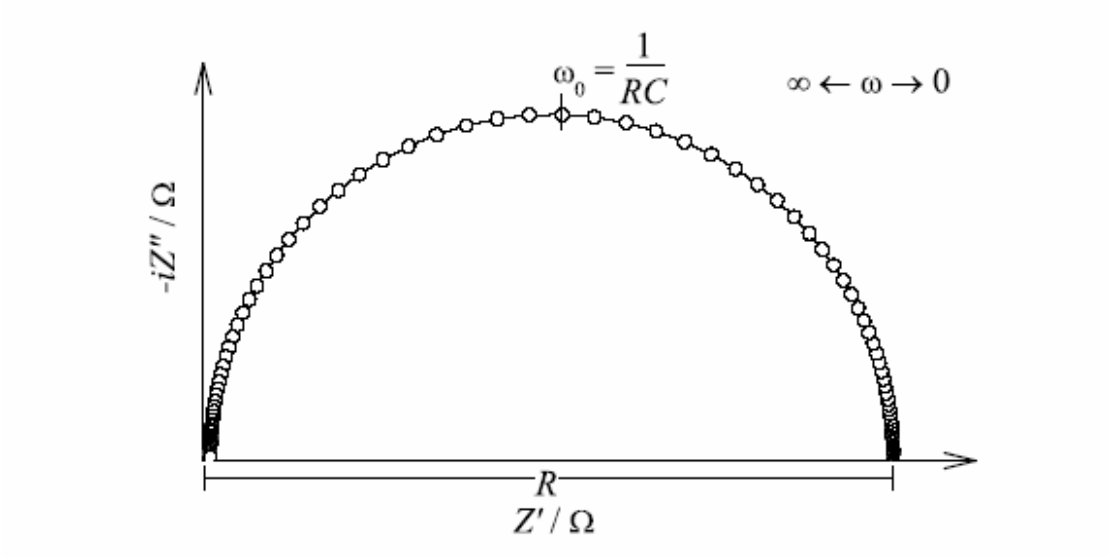

Figure 5.10 Nyquist Plot of the AC Impedance of a Material as a Function of frequency ω.

The Nyquist plot in Fig. 5.9 results from the electrical circuit of Fig. 5.10.

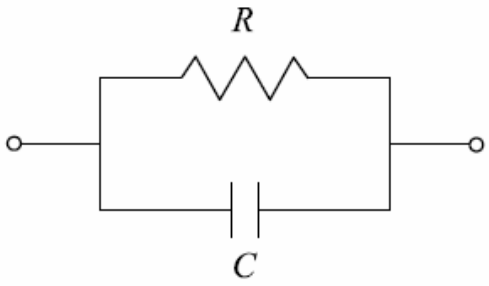

Figure 5.11 Circuit model used to describe ionic conduction in solid state materials.

One can simulate the impedance data if one knows the equivalent circuit before hand or one can fit the experimental impedance data to an equivalent circuit.

Another popular presentation method is the Bode Plot. The impedance is plotted with log frequency on the X-axis and both the absolute values of the impedance ($|Z|=Z_0$) and the phase-shift on the Y-axis. Unlike the Nyquist Plot, the Bode Plot does show frequency information.

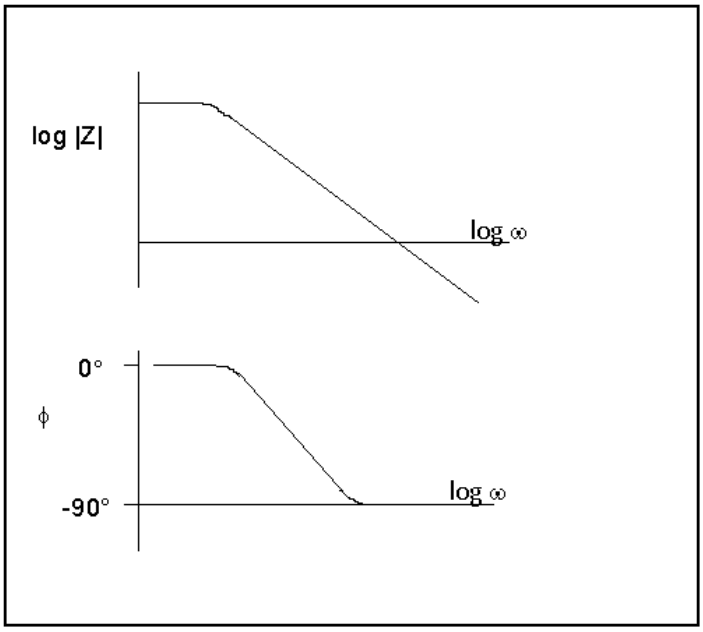

Figure 5.12 Bode Plot

In modern practice, the impedance is usually measured with lock-in amplifiers or frequency-response analyzers, which are faster and more convenient than impedance bridges. The job of theory is to interpret the equivalent resistance and capacitance values in terms of interfacial phenomena.

5.3.3 Differential Scanning Calorimetry

The operation of a Differential Scanning Calorimetry (DSC) is based on measurement of the thermal response of an unknown specimen as compared with a standard when both are heated uniformly at a constant rate. In DSC the difference in heat flow to the sample and a reference at the same temperature, is recorded as a function of temperature. The temperature of both sample and reference are increased at a constant rate. Since the DSC is at constant pressure, heat flow is equal to enthalpy changes:

$$\left(\frac{dq}{dt}\right)_p = \frac{dH}{dt} \qquad \textbf{(5-19)}$$

When a sample undergoes a physical transformation such as a phase transition, more or less heat will need to flow to it than to the reference to maintain both at the same temperature. If more or less heat must flow to the sample depends on the process is exothermic or endothermic. The heat flow difference between the sample and the reference is:

$$\Delta\frac{dH}{dt} = \left(\frac{dH}{dt}\right)_{sample} - \left(\frac{dH}{dt}\right)_{reference} \qquad \textbf{(5-20)}$$

and can be either positive or negative.

For example, as a solid sample melts to a liquid it will require more heat flowing to the sample to increase its temperature at the same rate as the reference. This is due to the absorption of heat by the sample as it undergoes the endothermic phase transition from solid to liquid. Hence Δdh/dt is positive.

Likewise, as the sample undergoes exothermic processes (such as crystallization) less heat is required to raise the sample temperature. . Hence Δdh/dt is negative. By observing the difference in heat flow between the sample and reference, differential scanning calorimeters are able to measure the amount of heat absorbed or released during such transitions.

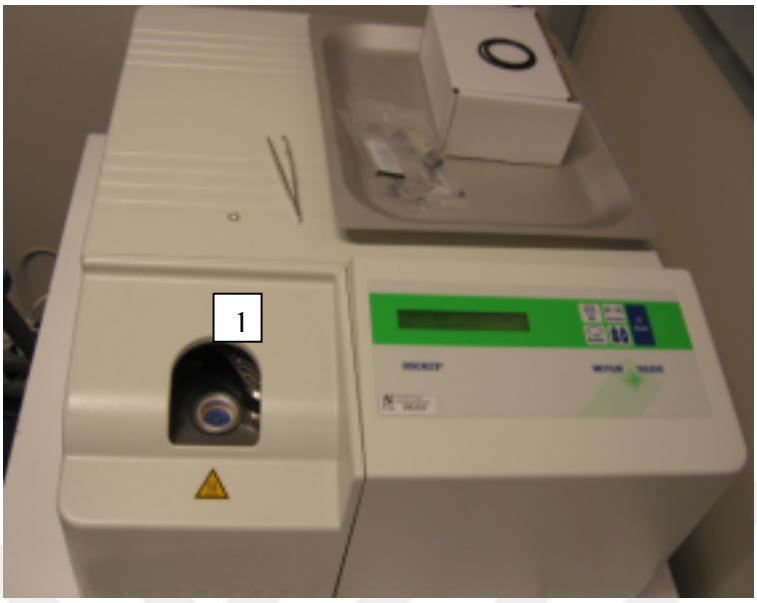

Figure 5.13 Differential Scanning Calorimeter (1) Sample Holder

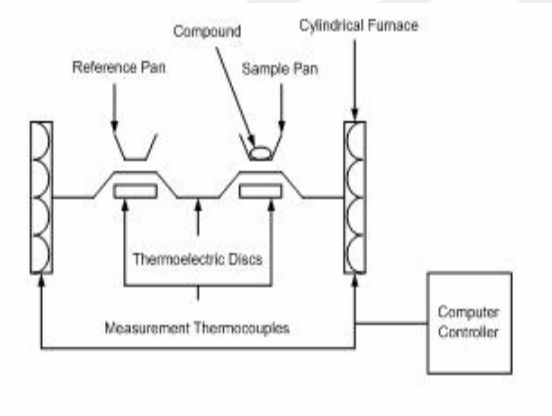

Figure 5.14 a Differential scanning calorimeter sample and reference holder

Figure 5.14 b Differential scanning calorimeter sample and reference holder

5.3.4 Infrared Spectroscopy

When a beam of electromagnetic radiation of intensity I_o is passed through a substance, it can either be absorbed or transmitted, depending upon its frequency and the structure of the molecule it encounters. Electromagnetic radiation is energy and hence when a molecule absorbs radiation it gains energy as it

undergoes a quantum transition from one energy state ($E_{initial}$) to another (E_{final}). The frequency of the absorbed radiation is related to the energy of the transition by Planck's law:

$$E_{final} - E_{initial} = E = h\nu = hc/\lambda \quad \textbf{(5-21)}$$

Thus, if an allowed infrared transition exists which is related to the frequency of the incident radiation by Planck's constant and then the radiation can be absorbed. Conversely, if the frequency does not satisfy the Planck expression, then the radiation will be transmitted.

There are in general several types of motion that molecule can possess namely translational, rotational and vibrational motion. Each of the vibrational motions of a molecule occurs with a certain frequency, which is characteristic of the molecule and of the particular vibration. The energy involved in a particular vibration is characterized by the frequency of the vibration, so that the higher the vibrational energy, the larger the frequency of the motion. According to the results of quantum mechanics, only certain vibrational energies are allowed to the molecule (the same may be said of rotational and translational energies), and thus only certain amplitudes are allowed. Associated with each of the vibrational motions of the molecule, there are series of energy levels (or vibrational energy states). The molecule may be made to go from one energy level to a higher one by absorption of a quantum of electromagnetic radiation, such that $E_{final} - E_{initial} = h\nu$. In undergoing such a transition, the molecule gains vibrational energy, and this is manifested in an increase in the amplitude of the vibration. The frequency of light required to cause a transition for a particular vibration is equal to the frequency of that vibration, so that we may measure the vibrational frequencies by measuring the frequencies of light which are absorbed by the molecule. Since vibrational motions in molecules often occur at frequencies of the order of about 10^{14} sec^{-1}, then light of wavelength = $c/\lambda = 3 \times 10^{-4}$ cm = 3 microns will be required to cause transitions. As it happens, light of this wavelength lies in the so-called infrared region of the spectrum. IR spectroscopy, then, deals with transitions between vibrational energy levels in molecules, and is therefore also called vibrational spectroscopy. An IR spectrum is generally displayed as a plot of the energy of the infrared radiation (expressed either in microns or wave numbers) versus the percent of light transmitted by the compound [30].

5.3.5 Scanning Electron Microscopy

The technique required the implementation of an electron microscope to study the surface and cross section of the composite membranes. The surface and cross-section of the composite membranes morphology were investigated by means of SEM. SEM images were obtained on a JEOL JSM-5600 LV SEM. The cross-sections of the composite membrane were obtained by breaking the membrane into small pieces.

RESULTS and DISCUSSIONS

In this chapter results of analysis are presented and discussed in detail. The first main objective of this work was to develop proton conducting electrolytes based upon solid acid compounds for fuel cells operating at intermediate temperature (110-250 ºC). Among these potential solid acid electrolytes, the main focus was on potassium dihydrogen phosphite, $KH(PO_3H)$, and cesium dihydrogen phosphite, $CsH(PO_3H)$.

Before considering all the results and discussions, it is necessary to first briefly reminding about structure and main role of $KH(PO_3H)$ and $CsH(PO_3H)$ solid acids.

$KH(PO_3H)$ contains independent K^+ cations and $HPHO_3^-$ anions. $CsH(PO_3H)$ contains independent Cs^+ cations and $HPHO_3^-$ anions. $KH(PO_3H)$ and $CsH(PO_3H)$ exists in three different forms depending on temperature: a ferroelectric phase, a paraelectric phase and a superprotonic phase [16]. At low temperatures, as room temperature, in their paraelectric phase $KH(PO_3H)$ and $CsH(PO_3H)$ possess a monoclinic structure [Fig. 6.1-6.2]. It has two different hydrogen bonds between HPO_3^{2-} tetrahedrons. As it is seen from Fig. 6.1 and 6.2, the hydrogen bonds along the b-axis form a zigzag chain with a short hydrogen bond, and those along the c-axis form a linear chain with longer hydrogen bond. This monoclinic structure is one dimensional (1-D) hydrogen bond network and highly ordered structure [16]. Due to ordered hydrogen bond network the proton conductivity of the paraelectric phase of $KH(PO_3H)$ and $CsH(PO_3H)$ is very low (around 10^{-6} $\Omega^{-1}cm^{-1}$) [5, 25]. As temperature increasing this ordered structure becomes disorder by deformations of hydrogen bonds. Therefore the crystal structure changes from monoclinic to cubic and conductivity reaches ~ 10^{-2}- 10^{-3} $\Omega^{-1}cm^{-1}$, which is closed to ionic liquids. The temperature where the conductivity jumps is called *superprotonic phase transition* temperature.

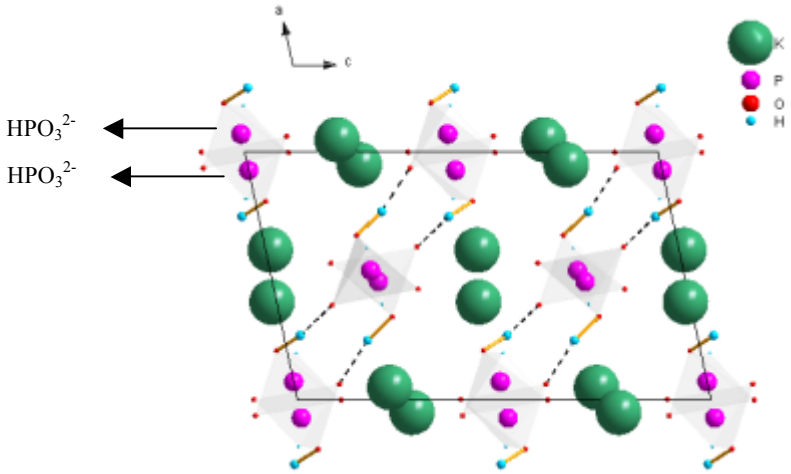

Figure 6.1 Monoclinic crystal structure of $KH(PO_3H)$

The dashed lines denote H···O bonds

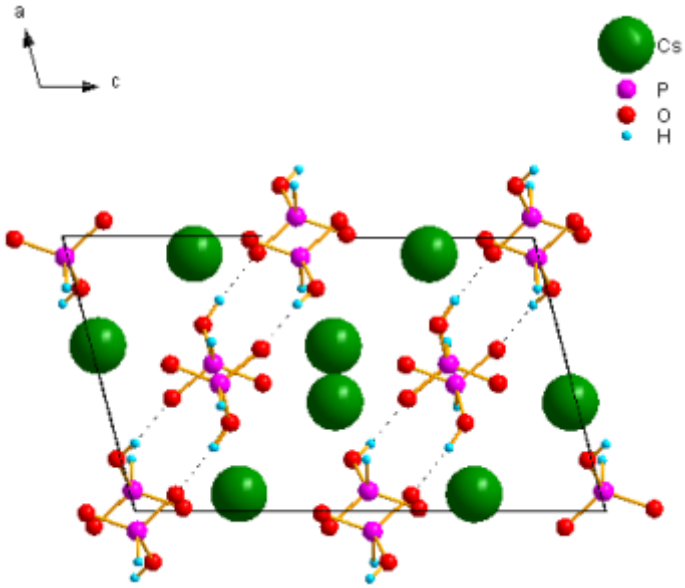

Figure 6.2 Monoclinic crystal structure of $CsH(PO_3H)$

The dashed lines denote H···O bonds

Therefore, first of all, in order to see the crystal structures of synthesized solid acids at room temperature X-ray diffraction analysis was performed on compounds. Afterwards to see the thermal behaviors and to find out the superprotonic temperature (T_{sp}) Differential Scanning Calorimeter (DSC) analysis was performed. An important property of solid acids, superprotonic conductivity, was investigated by A.C impedance spectroscopy.

Second main objective of the work was to develop mixed systems of potassium/cesium, K/Cs, phosphites. Different amount of cesium atoms in $CsH(PO_3H)$ was replaced with potassium atoms to get the mixed K/Cs phosphites with formula $K_xCs_{(1-x)}H(PO_3H)$. The goal of the study was to find out the effect of cation substitution on proton transport properties of solid acid electrolytes. Tests are performed with different fraction of doped K in the formula $K_xCs_{(1-x)}H(PO_3H)$ where x = 0.1, 0.2, 0.3, 0.4, 0.5, 0.6, 0.7, 0.8, 0.9. X-Ray diffraction analysis, thermal analysis and conductivity analysis were performed on mixed system compounds.

6.1 Results for $KH(PO_3H)$ and $CsH(PO_3H)$

6.1.1 Structures of $KH(PO_3H)$, $CsH(PO_3H)$ by XRD Analysis

$KH(PO_3H)$ was synthesized from two chemical compounds potassium hydroxide KOH and phosphorous acid H_3PO_3 with the mole ratio of K: PO_3 at 1:1 as described in Chapter 5. Secondly, $CsH(PO_3H)$ was synthesized from two chemical compounds cesium carbonate Cs_2CO_3 and phosphorous acid H_3PO_3 with the mole ratio of Cs: PO_3 at 1:1 as described in Chapter 5.

$CsH(PO_3H)$ has been proved to be very hygroscopic during tests which are performed under atmospheric conditions. That means it is attracting and adsorbing moisture from the air. $CsH(PO_3H)$ adsorbs water from the atmosphere at room temperature within 10 min of exposure. Further exposure to atmosphere, water droplets are formed on the surface. $KH(PO_3H)$ is not as hygroscopic as $CsH(PO_3H)$.

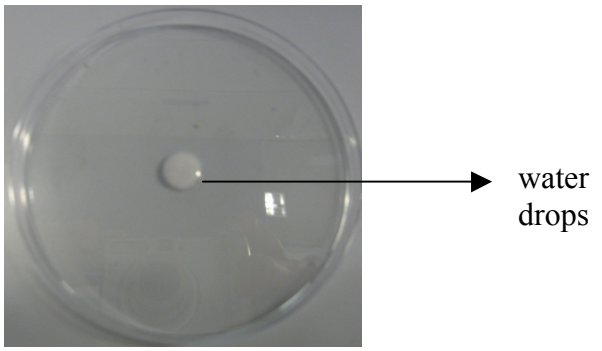

Figure 6.3 Water drops on $CsH(PO_3H)$ pellet after exposed to atmosphere

In order to find out crystal structure of synthesized solid acids at room temperature X-ray diffractometer is used. XRD patterns of pure $KH(PO_3H)$, $CsH(PO_3H)$, $NH_4H(PO_3H)$ polycrystals are shown in Fig. 6.4. X-ray diffraction data were recorded at room temperature using Philips XRD PW1830 generator (50kV, 35mA, $CuK\alpha_1$). Data were analyzed using the Philips X'Pert program.

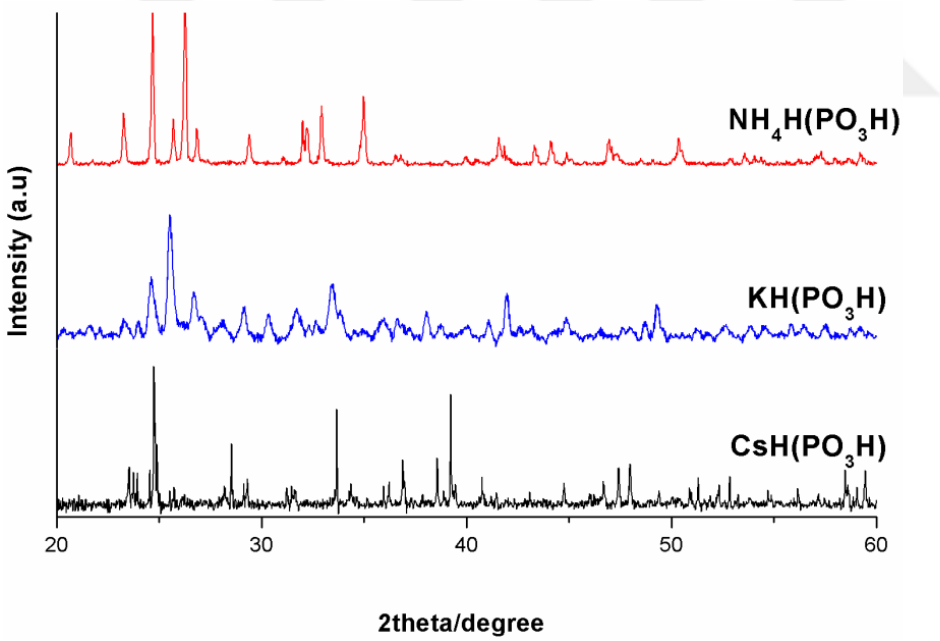

Figure 6.4 The XRD patterns of $KH(PO_3H)$, $CsH(PO_3H)$, $NH_4H(PO_3H)$
$NH_4H(PO_3H)$ is a solid acid. It was only given just to show most of solid acids have monoclinic structure at room temperature.

In this work, XRD patterns show that room temperature phase of $KH(PO_3H)$, $CsH(PO_3H)$ and $NH_4H(PO_3H)$ is monoclinic crystal structure [Fig. 6.4].

Monoclinic crystal structure of $KH(PO_3H)$ and $CsH(PO_3H)$ is already given in Fig. 6.1 and 6.2, respectively.

This work didn't compose the high temperature X-ray powder diffraction but Haile *et. al* showed in their studies that $CsH(PO_3H)$ undergoes a structural transformation at their high temperature structure between 110 and 160 °C to a cubic crystal structure [25].

In previous researches, room temperature XRD patterns of $KH(PO_3H)$, $CsH(PO_3H)$, $NH_4H(PO_3H)$ phosphites are indexed to a monoclinic unit cell [5]. W.Zhou *et. al.* performed conductivity measurements and thermal studies on $MH(PO_3H)$ where $M=Li^+$, Na^+, K^+, Cs^+, NH_4^+ [5]. In their study except lithium dihydrogen phosphite which adopts orthorhombic structure the other phosphites have monoclinic structure at room temperature. XRD patterns of $KH(PO_3H)$, $CsH(PO_3H)$ and $NH_4H(PO_3H)$ shows that samples are in monoclinic structure therefore it is obvious these compounds have ordered structure at room temperatures.

6.1.2 Phase Transition and Superprotonic Temperatures of the $CsH(PO_3H)$ and $KH(PO_3H)$ by Differential Scanning Calorimetry (DSC) Analysis

As it is mentioned before solid acids undergo phase transition upon heating and cooling. At low temperatures they have a paraelectric phase and at their high temperatures they have superprotonic phase. At superprotonic phase, protonic conductivity increases by several orders of magnitude, reaching values up to 10^{-2} and 10^{-3} $\Omega^{-1}cm^{-1}$. The goal of this work is to study the temperature that compounds undergo a superprotonic phase transition.

Thermal behavior of compounds with increasing temperature and then decreasing temperature was investigated by differential scanning calorimetry (DSC). The presence and characterization of phase transitions above room temperature were accomplished by these measurements. The response of compounds to heating and cooling was examined with a METTLER TOLEDO DSC823 Instrument in a flowing air atmosphere. The heating and cooling rates were 0.5 °C per minute.

The thermal behaviors of $CsH(PO_3H)$ and $KH(PO_3H)$ are shown in Fig. 6.5 and 6.6 respectively. The heating and cooling rates were 0.5 °C per minute. It is apparent that, upon heating, $CsH(PO_3H)$ undergoes a sharp transition, with an onset temperature at 142 ºC and is complete by 143 ºC to a new phase showing high proton conductivity measured by Haile *et al.* [25]. Phase transition enthalpy upon heating is 8.98 kJ/mol (42 J/g). $KH(PO_3H)$ undergoes a sharp transition with an onset temperature at 125 ºC and is complete by 129 ºC. Phase transition enthalpy upon heating is 4.44 kJ/mol (37 J/g). $CsH(PO_3H)$ has superprotonic transiton at higher temperature (142 ºC) than $KH(PO_3H)$ has (125 ºC).

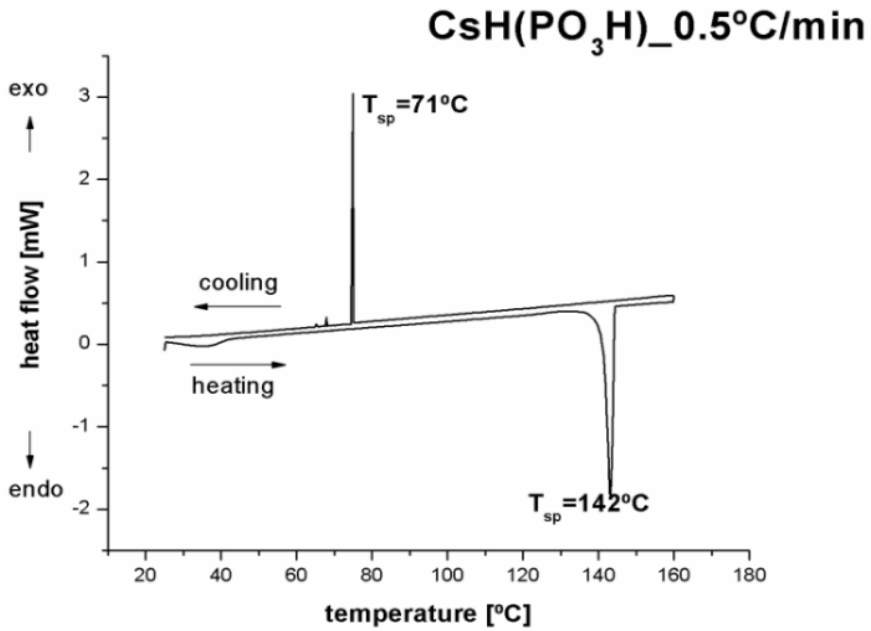

Figure 6.5 Thermal behavior of $CsH(PO_3H)$ for a heating/cooling cycle

Upon heating; T_{sp}=142 ºC, ΔH= 8.98 kJ/mol (42 J/g), Upon cooling; T_{sp}=71 ºC

T_{sp} is superprotonic phase transition temperature. Onset temperatures are accepted as transition temperature.

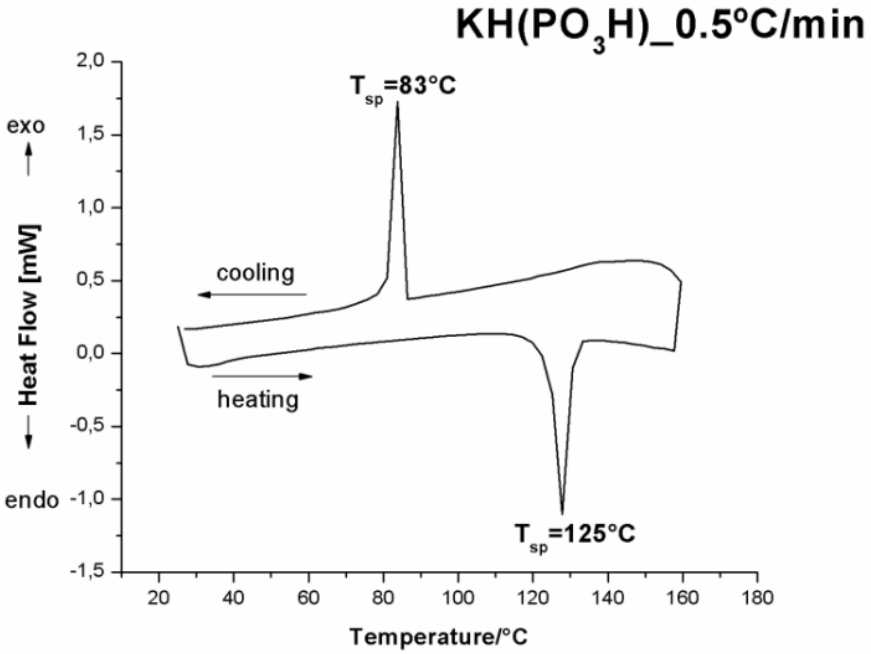

Figure 6.6 Thermal behavior of $KH(PO_3H)$ for a heating-cooling cycle

Upon heating; T_{sp}=125 ºC, ΔH= 4.44 kJ/mol (37 J/g), Upon cooling; T_{sp}=83 ºC

T_{sp} is superprotonic phase transition temperature. Onset temperatures are accepted as transition temperature.

6.1.3 Weight Losses of $CsH(PO_3H)$ and $KH(PO_3H)$ by Thermal Gravimetry Analysis

After analysis with differential scanning calorimeter (DSC), it was found that superprotonic temperature of $KH(PO_3H)$ and $CsH(PO_3H)$ is 125 ºC and 142 ºC respectively. DSC analysis also gives the melting temperature of the compounds. In order to distinguish peak of decomposition or peak of phase transition weight losses should be found by using Thermal Gravimetry (TG). TG results of $KH(PO_3H)$ and $CsH(PO_3H)$ are given in Fig. 6.7 and 6.8 respectively.

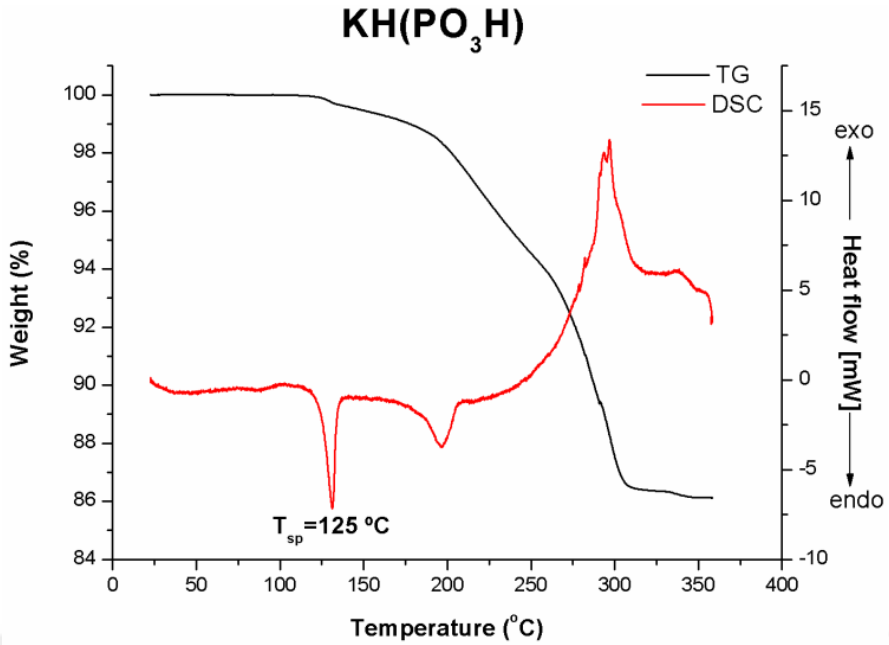

Figure 6.7 Weight loss of $KH(PO_3H)$ for heating cycle

Black curve is Thermal Gravimetry results, and red curve is Differential Scanning Calorimetry results.

As it is seen from Fig. 6.7, TG curve has no weight loss in the region that corresponds to peak of DSC at 125 ºC. So it means the peak that has been observed in DSC curve at 125 ºC is not a melting/decomposition region.

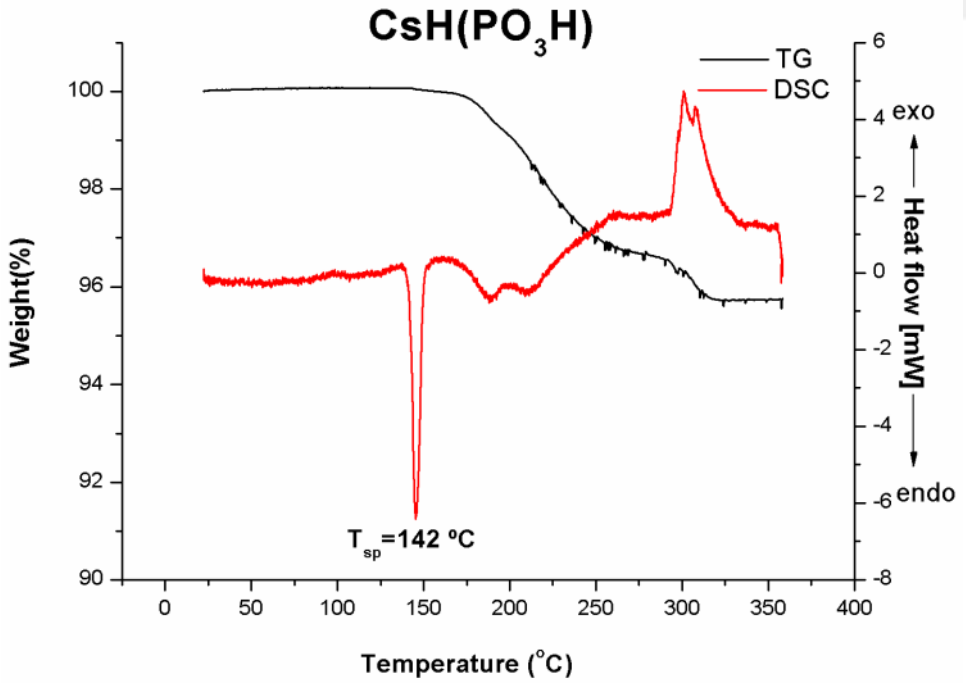

Figure 6.8 Weight loss of $CsH(PO_3H)$ for heating cycle

Black curve is Thermal Gravimetry results, and red curve is Differential Scanning Calorimetry results.

As it is seen from Fig. 6.8, TG curve has no weight loss in the region that corresponds to peak of DSC at 142 ºC. So it means the peak that has been observed in DSC curve at 142 ºC is not a melting/decomposition region.

Thermal decomposition of $KH(PO_3H)$ and $CsH(PO_3H)$ begins at temperatures beyond the superprotonic transition. A gradual weight loss event occurs for $KH(PO_3H)$ over the temperature range at 190-310 ºC and for $CsH(PO_3H)$ at 170-320 ºC.

The total weight loss of $KH(PO_3H)$ and $CsH(PO_3H)$ up to 350 ºC are 13.8 % and 4.3 %, respectively.

6.1.4 Conductivity Analysis of $CsH(PO_3H)$ and $KH(PO_3H)$ by Impedance Spectroscopy

After differential scanning calorimeter (DSC) results in chapter 6.1.2, superprotonic phase temperatures of $KH(PO_3H)$ and $CsH(PO_3H)$ were found at 125 ºC and 142 ºC, respectively. In this part superprotonic conductivities of the compounds are given.

The conductivity of the potential electrolytes was measured by A.C. impedance spectroscopy using an AUTOLAB Impedance Analyzer. Conductivity measurements were taken on 1 cm diameter pellets which were obtained by uni-axially pressing the sample. Measurements were made at a frequency of 1 MHz to 10 Hz under dry air.

As temperature is increasing for solid acids, at any temperature point conductivity is apparently increasing. This temperature where the conductivity is suddenly getting higher is called superprotonic temperature.

The dependences of the proton conductivity of the phosphites extracted from data of impedance measurements are presented in Fig. 6.9 and 6.10.

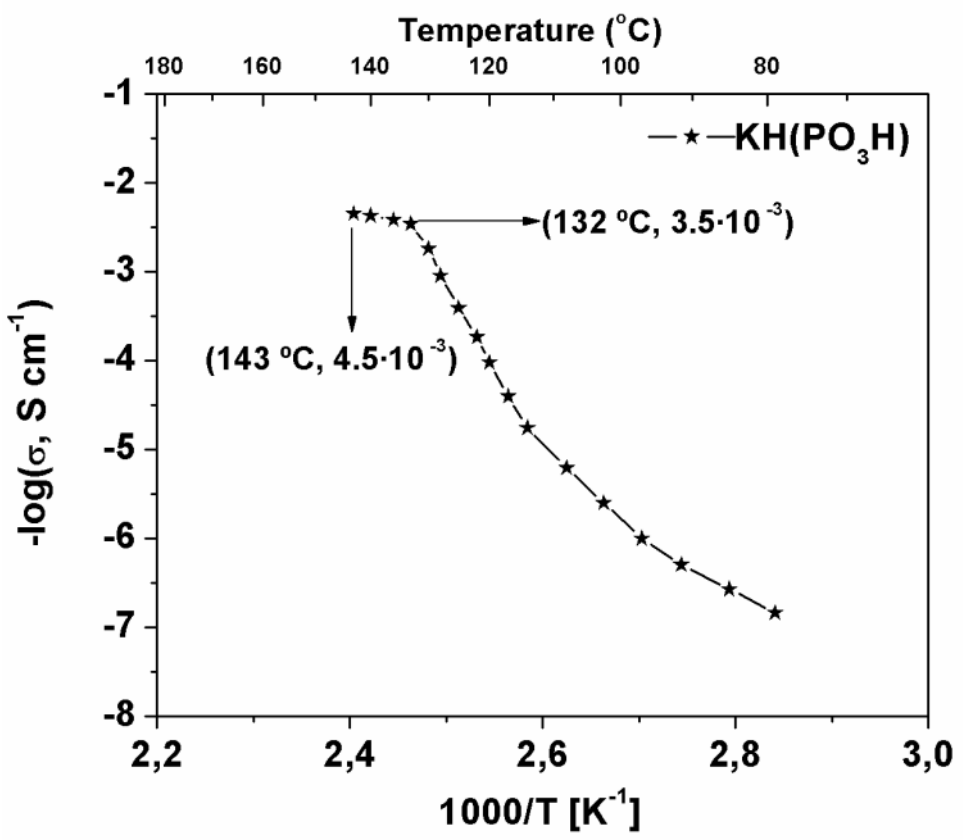

Figure 6.9 -log conductivity vs. temperature plot for $KH(PO_3H)$

As it is seen from the Fig. 6.9, upon heating for the first time the conductivity of $KH(PO_3H)$ increases from $1.4 \cdot 10^{-7}$ $\Omega^{-1}cm^{-1}$ at 80 °C to $3.5 \cdot 10^{-3}$ $\Omega^{-1}cm^{-1}$ at 132 °C. The proton conductivity reaches value of $4.5 \cdot 10^{-3}$ at 143 °C.

The superprotonic conductivity observed for $CsH(PO_3H)$ is from the Fig. 6.10, upon heating for the first time the conductivity of $CsH(PO_3H)$ increases from $1.9 \cdot 10^{-6}$ $\Omega^{-1}cm^{-1}$ at 80 °C to $2.2 \cdot 10^{-3}$ $\Omega^{-1}cm^{-1}$ at 150 °C, just above the superprotonic temperature. The proton conductivity reaches values of $3 \cdot 10^{-3}$ at 160 °C.

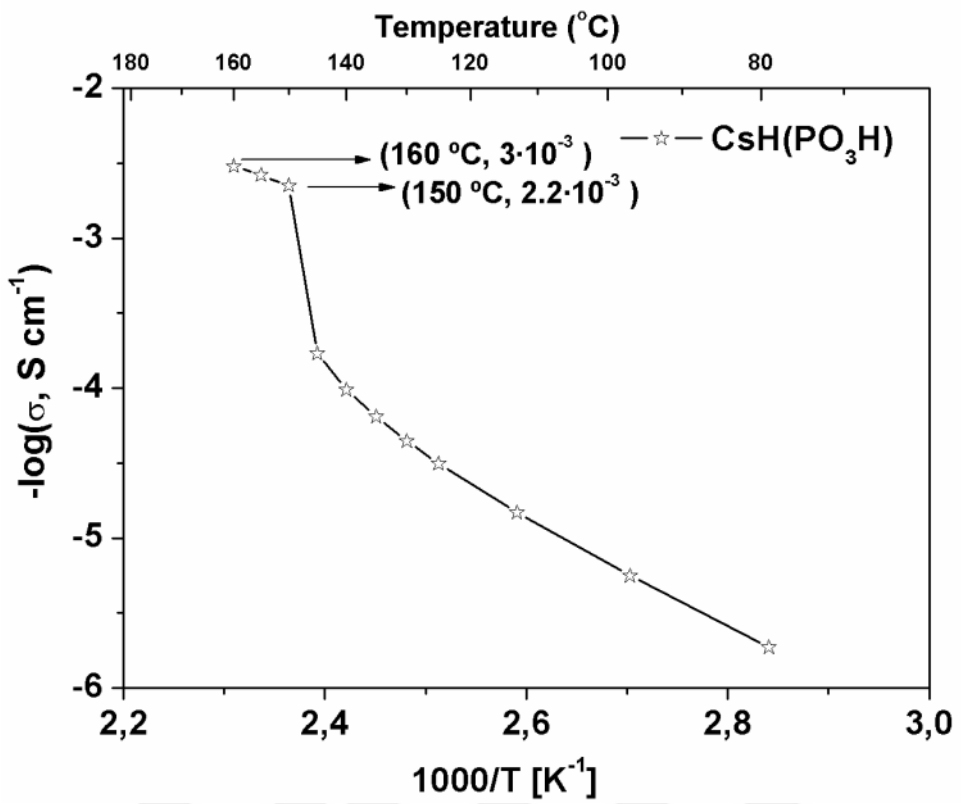

Figure 6.10 -log conductivity vs. temperature plot for $CsH(PO_3H)$

6.1.5 Infrared Spectroscopy of $KH(PO_3H)$

With XRD patterns it is known that $KH(PO_3H)$ has a monoclinic structure so that means it has highly ordered structure in its room temperature. Infrared spectroscopy is employed to determine the changes of hydrogen bond in the structure of the $KH(PO_3H)$ during operation under intermediate temperature conditions. IR spectra over the wave number range 4000-950cm^{-1}, with resolution 2 cm^{-1}, were recorded with the Bruker IFS-88.

After differential scanning calorimeter (DSC) results in chapter 6.1.2 it has found that $KH(PO_3H)$ has phase transition at 125 ºC . Before 125 ºC it has a monoclinic structure due to XRD patterns. In its monoclinic phase it has highly ordered crystal structure. After 125 ºC it has a cubic phase with disordered crystal structure. In order to see the hydrogen bond deformations in this disordered structure of $KH(PO_3H)$ infrared spectroscopy is used at three temperatures (room temperature, 100 ºC, 140 ºC).

Results are given in Fig. 6.11.

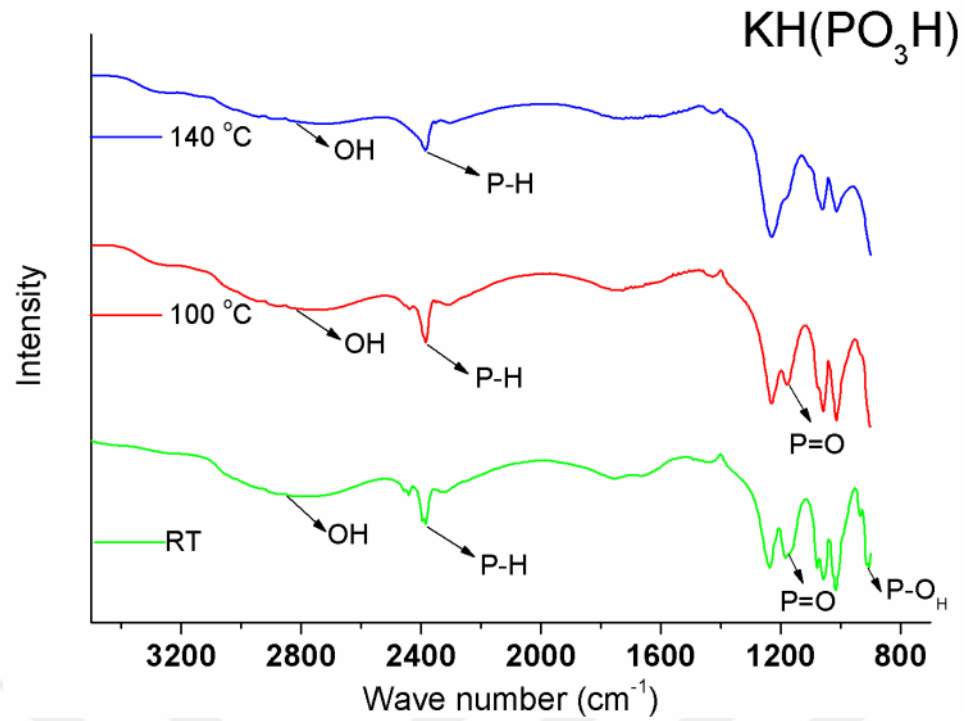

Figure 6.11 Infrared Spectrometer of $KH(PO_3H)$
at room temperature, at 100 ºC and at 140 ºC

As a remark, the crystal structure of $KH(PO_3H)$ is composed of potassium K^+ cations and phosphite HPO_3^{2-} anions. HPO_3^{2-} ions are linked by strong O-H···O hydrogen bonds into infinite chains of composition. The $P\text{-}O_H$ (proton donor) bond is the longest, followed by P-O···H (proton acceptor) bond and P=O bond without any contacts to protons is the shortest one.

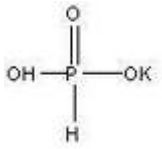

As it is seen from Fig. 6.11, at room temperature IR spectra, two kinds of P-O vibrations can be seen, at 910 cm^{-1} and at 1170 cm^{-1}. In addition, bands at 1650 and 1700 cm^{-1} are due to the vibrations of hydrogen bond [31].

However, as temperature increases up to 100 ºC, vibrations of hydrogen bonds and P=O reduce. While, peak for P-O bond increases clearly. As temperature reaches 140 ºC which is higher than the phase transition temperature (125 ºC), hydrogen bond and P=O vibrations almost disappear, and P-O bond is very strong. At high temperature condition, PO_3H groups perform very fast rotations, and therefore three oxygen atoms connecting to the center phosphorous atom becomes homogenized. Differences between P-O bonds and P=O bond is less. Therefore, learnt from IR spectra, P=O bond vibration disappears while vibrations of P-O bond increases with some wave number shift [31]. Due to very fast rotated PO_3H groups, inter molecular hydrogen bonds are broken, and therefore, from IR spectra hydrogen bond vibrations disappear.

6.2. Results for $K_xCs_{(1-x)}H(PO_3H)$

In section 6.1 of this chapter, superprotonic behaviors of $KH(PO_3H)$ and $CsH(PO_3H)$ were investigated. Here, the influence of mixing K^+ and Cs^+ cations in phosphite systems with formula was investigated. Polycrystals of $K_xCs_{(1-x)}H(PO_3H)$ were synthesized from aqueous solutions of Cs_2CO_3, KOH and H_3PO_3 in ratios x/(1-x) with x= 0 to 1 in 0.1 increments.

6. 2.1 Structures of $K_xCs_{(1-x)}H(PO_3H)$ by XRD Analysis

The room temperature XRD pattern of mixed cation system series with formula $K_xCs_{(1-x)}H(PO_3H)$ where x = 0.1, 0.2, 0.3, 0.4, 0.5, 0.6, 0.7, 0.8, 0.9 are shown in Fig. 6.12. All the measurements were performed under dry nitrogen condition because adsorbed moisture in crystal lattice will expand the distance between crystal plane so it will affect the value of theta degree due to hygroscopic character of the cesium phosphite compound. During XRD measurements, it was found that hydrogroscopic character increased with increasing Cs:K ratio.

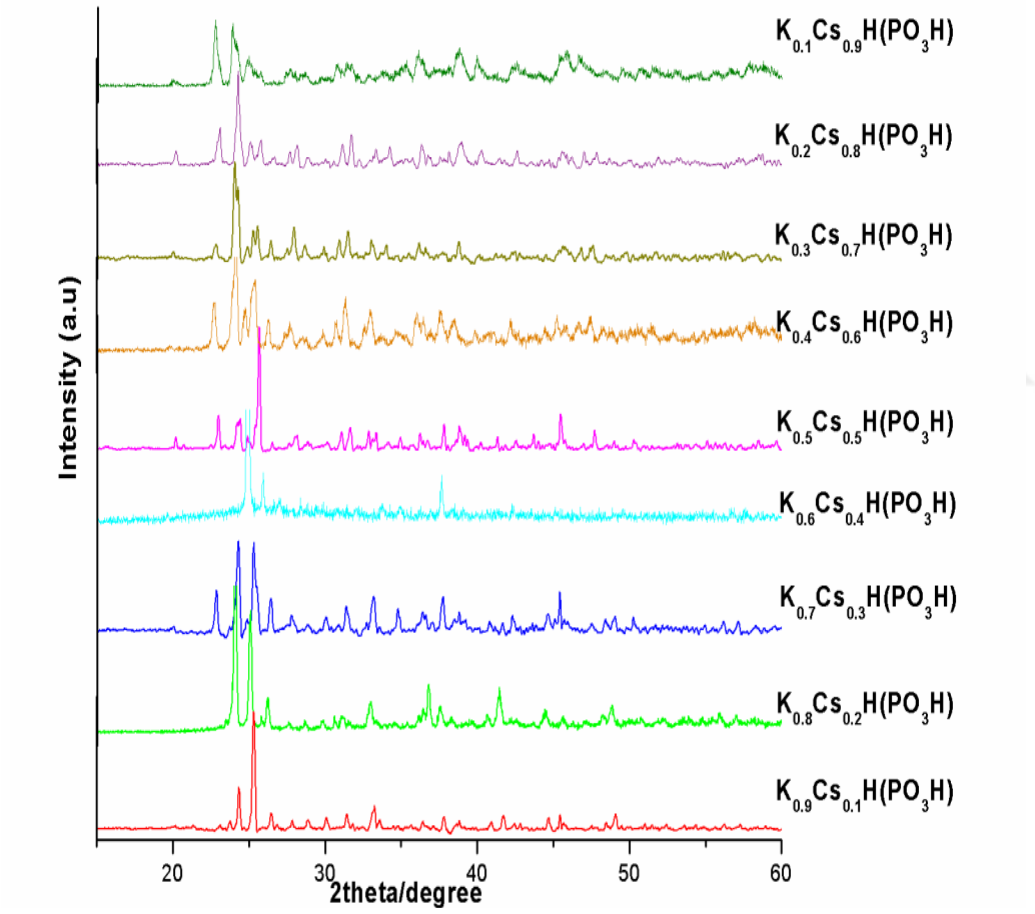

Figure 6.12 The XRD patterns of $K_xCs_{(1-x)}H(PO_3H)$ series where x = 0.1, 0.2, 0.3, 0.4, 0.5, 0.6, 0.7, 0.8, 0.9

Powder XRD patterns show that at room temperature all samples have same phase with monoclinic structure although there are some shifts. These shifts are due to difference of crystal plane distance between Cs^+ and K^+. As seen from the Table 6.1, ionic radius of Cs^+ is bigger than radius of K^+.

Table 6.1 Ionic radius of cations Na^+, K^+, Cs^+, NH_4^+

	Cs^+	Rb^+	NH_4^+	K^+
Radius Å	1.81	1.63	1.61	1.55

Therefore as Cs^+ fraction increases, structure changes can be seen. For example, in certain Cs^+ fraction range, peaks shift to lower 2 theta angles. It is because doped Cs^+ ions expand the crystal plane. If doping K into $CsH(PO_3H)$ similarly we can see that in certain range, peaks shift to bigger 2 theta angle. It is because K^+ reduces the distance of crystal plane.

In certain ratio range, as in $K_{0.7}Cs_{0.3}H(PO_3H)$ and $K_{0.4}Cs_{0.6}H(PO_3H)$, Cs^+ and K^+ dihydrogen phoshites can not form homogeneous compounds. Two- phase systems appear. Low intensity and lots of noise are due to high hygroscopicity and other reasons.

6.2.2 Phase Transition and Superprotonic Temperatures of the $K_xCs_{(1-x)}H(PO_3H)$ by Differential Scanning Calorimeter (DSC) Analysis

The effect of potassium atom substitution in the $CsH(PO_3H)$ compound on superprotonic phase temperature were investigated here. Replacing of some cesium atom of $CsH(PO_3H)$ with potassium was considered to have effects on the superprotonic transition temperature and so on conductivity. Thermal behaviors of mixed Cs/K phosphite systems $K_xCs_{(1-x)}H(PO_3H)$ are shown in Fig.6.13.

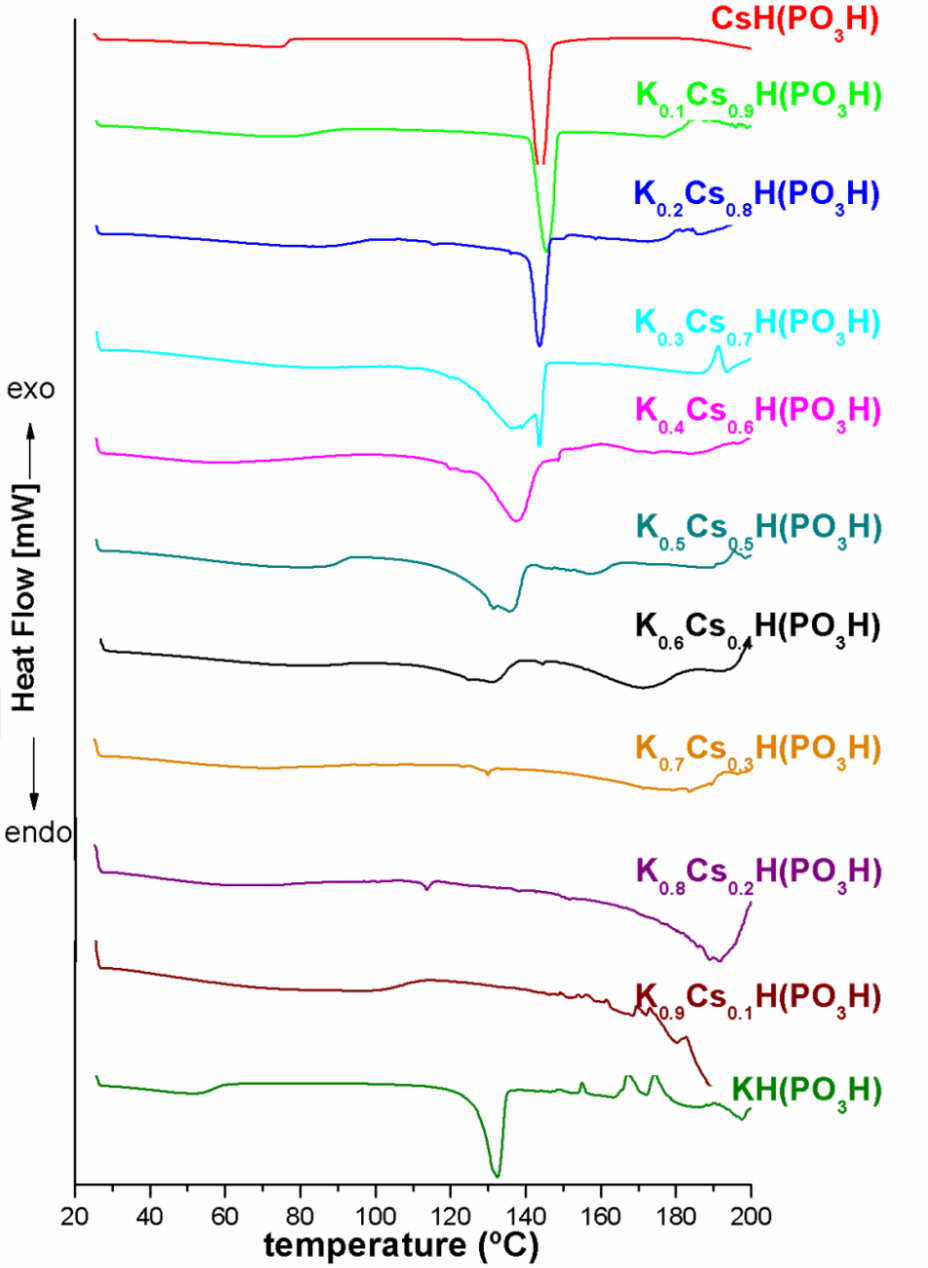

Figure 6.13 **Thermal behavior of $K_xCs_{(1-x)}H(PO_3H)$** where x=0.1- 0.9

Table 6.2 Superprotonic phase transition temperatures (T_{sp}) and transition enthalpies of K/Cs $H(PO_3H)$ mixed series

Compound	T_{sp} (°C) heating	ΔH (J/g) heating	T_c (°C) cooling
$\mathbf{Cs_{100\%}}H(PO_3H)$ (literature [25])	137	-58	60
$\mathbf{Cs_{100\%}}H(PO_3H)$	142	-42	71
$\mathbf{K_{10\%}Cs_{90\%}}H(PO_3H)$	142	-49	70
$\mathbf{K_{20\%}Cs_{80\%}}H(PO_3H)$	142	-52	75
$\mathbf{K_{30\%}Cs_{70\%}}H(PO_3H)$	131[a]	-9	117
$\mathbf{K_{40\%}Cs_{60\%}}H(PO_3H)$	122[b]	-7	111
$\mathbf{K_{50\%}Cs_{50\%}}H(PO_3H)$	120[c]	-7	120
$\mathbf{K_{60\%}\ Cs_{40\%}}H(PO_3H)$	119[d]	-7	120
$\mathbf{K_{70\%}Cs_{30\%}}H(PO_3H)$	no phase [*] transition	-	-
$\mathbf{K_{80\%}Cs_{20\%}}H(PO_3H)$	no phase [*] transition	-	-
$\mathbf{K_{90\%}Cs_{10\%}}H(PO_3H)$	no phase [*] transition	-	-
$\mathbf{K_{95\%}Cs_{5\%}H}(PO_3H)$	100	-31	53
$\mathbf{K_{100\%}}H(PO_3H)$	125	-37	83

a: There is a second peak at 142 °C, but it was proven by conductivity analysis that the first peak at 131 °C is phase transition temperature. Conductivity analysis is given in next section of this chapter in 6.4. The second peak can be melting/ decomposition temperature.

b, c, d: There are some other peaks can be melting/decomposition temperature

*: These compounds undergo no phase transition because it was proven by conductivity analysis that they are already at superprotonic phase.

If the amount of K^+ mixed into $CsH(PO_3H)$ is less than 20 mol%, they have same phase transition with $CsH(PO_3H)$ at 142 ºC, shown in Fig 6.13. (As it is seen from the Fig 6.13, $K_{0.1}Cs_{0.9}$ and $K_{0.2}Cs_{0.8}$ have one peak at 142 °C)

If still more amount of potassium is doped into $CsH(PO_3H)$ (30 mol% K^+-60 mol% K^+) phase transition is observed to systematically shifted to lower temperatures. The transition enthalpy is consistently lower for these compounds.

Also it is apparent that there are some more peaks other than phase transition peak. These other peaks are considered to be due to melting/decomposition temperatures. For $K_{0.3}Cs_{0.7}$ upon heating there are two peaks at 131 °C and 142 °C respectively. But after conductivity measurements with A.C

impedance spectroscopy it was found that the peak at 131 °C is the superprotonic phase temperature and the other one can be decomposition temperature.

With increase of doped potassium from 70 mol% to 90 mol% in to $CsH(PO_3H)$, phase transition was not observed as temperature up to 160 °C. However, there is abroad peak appeared after 160 °C at which sample is melting. Combining with the impedance results, these samples have been already at the superprotonic phases before heating began.

$KH(PO_3H)$ undergoes a phase transition at 125 °C. As K^+ fraction decrease to 90 mol % with increasing amount of doped Cs^+, a clear phase transition endothermic peak can not be found as in the case of $K_{0.9}Cs_{0.1}$ phosphites. This phenomenon continues to $K_{0.7}Cs_{0.3}$ and $K_{0.8}Cs_{0.2}$ phosphites. So it is concluded that between $K_{0.9}Cs_{0.1}H(PO_3H)$ and $K_{0.7}Cs_{0.3}H(PO_3H)$, superprotonic phase transition is disappeared. So as the second step, it was decided to synthesize and analyze the behavior of $K_{0.95}Cs_{0.05}H(PO_3H)$. It was performed 5%Cs 95%K and found that this compound has a phase transition at 100 °C also given in Fig 6.13.

As summary, DSC results can be assembled in 3 groups:

(1) The K^+ fraction less than 30 mol% was not significantly effect the superprotonic phase transition temperature.
(2) The K^+ fraction between 30 mol% - 70 mol% shifted the superprotonic phase transition temperature to lower temperatures.
(3) The K^+ fraction more than 70 mol%-90 mol% did not undergo a phase transition before its melting temperature at 160 °C.
(4) The K^+ fraction more than 90 mol% undergo a phase transition around 100 °C

6.2.3 Conductivity Analysis of $K_xCs_{(1-x)}H(PO_3H)$ by Impedance Spectroscopy

The conductivity of the potential electrolytes was measured by A.C. impedance spectroscopy using an AUTOLAB Impedance Analyzer. Conductivity measurements were taken on 1 cm diameter pellets which were obtained by uni-axially pressing the sample. Measurements were made at a frequency of 1 MHz to 10 Hz under dry air. The dependences of the proton conductivity of the phosphites extracted from data of impedance measurements are presented in Table 6.3 and Fig. 6.14.

Conductivity analyses were performed on these compounds:

(1)The K^+ fraction less than 30 mol% ($K_{0.1}Cs_{0.9}H(PO_3H)$ was analyzed)
(2)The K^+ fraction between 30 mol% - 70 mol% ($K_{0.4}Cs_{0.6}H(PO_3H)$ was analyzed)
(3)The K^+ fraction more than 70 mol%-90% ($K_{0.8}Cs_{0.2}H(PO_3H)$ and $K_{0.9}Cs_{0.1}H(PO_3H)$ were analyzed)
(4)The K^+ fraction more than 90 mol% ($K_{0.95}Cs_{0.05}H(PO_3H)$ was analyzed)

Table 6.3 Superprotonic phase transition temperatures (T_{sp}) and conductivities of K/Cs $H(PO_3H)$ mixed series

Compound	T_{sp} (°C) heating	Superprotonic Temperature Range (°C)	Conductivity Range σ (Ω^{-1} cm^{-1})
$CsH(PO_3H)$ (literature)	137 [25]	137-160	5.5×10^{-3}
$CsH(PO_3H)$	142	150-160	$2.2 \cdot 10^{-3} - 3 \cdot 10^{-3}$
$K_{0.1}Cs_{0.9}H(PO_3H)$	142	144-153	$3 \cdot 10^{-3} - 4 \cdot 10^{-3}$
$K_{0.4}Cs_{0.6}H(PO_3H)$	122	122-127	$2 \cdot 10^{-3} - 3 \cdot 10^{-3}$
$K_{0.8}Cs_{0.2}H(PO_3H)$	superprotonic*	superprotonic*	$8 \cdot 10^{-4} - 4 \cdot 10^{-3}$
$K_{0.9}Cs_{0.1}H(PO_3H)$	superprotonic*	superprotonic*	$5 \cdot 10^{-4} - 4 \cdot 10^{-3}$
$K_{0.95}Cs_{0.05}H(PO_3H)$	**100**	**113-147**	**$3.2 \cdot 10^{-3} - 10^{-2}$**
$KH(PO_3H)$	125	132-143	$3.5 \cdot 10^{-3} - 4.5 \cdot 10^{-3}$

** It was observed these compounds are already superprotonic, so they do not undergo a superprotonic phase transition.*

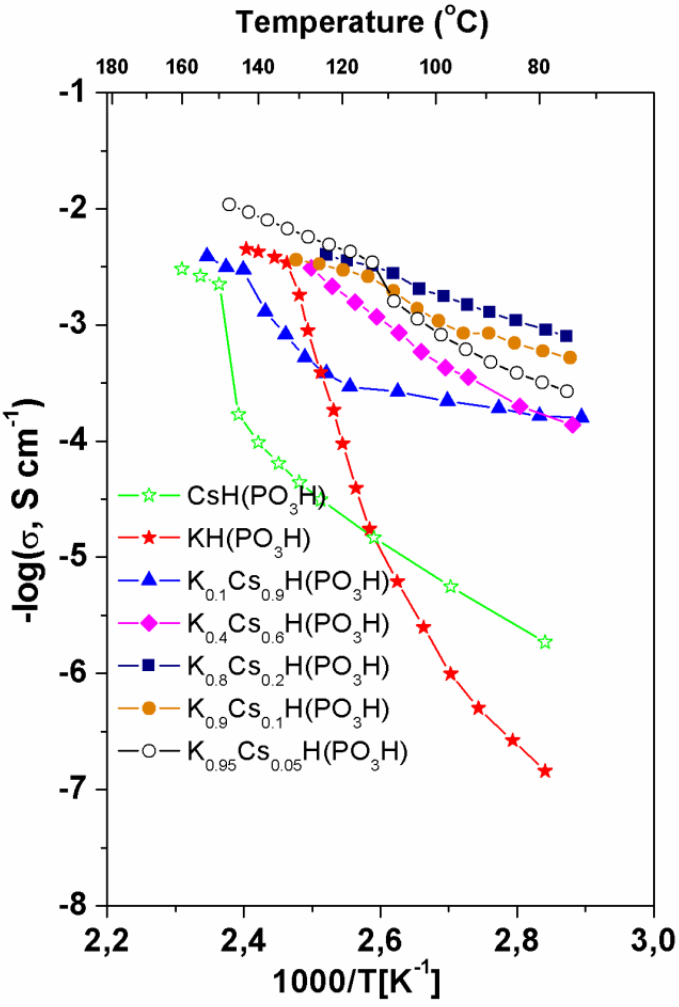

Figure 6.14 -log conductivity vs. temperature plot for $K_xCs_{(1-x)}H(PO_3H)$

The conductivities of $KH(PO_3H)$ and $CsH(PO_3H)$ have been already given in 6.1.4 and also here given in Table 6.3.

As it is seen from the Fig. 6.14, upon heating for the first time the conductivity of $K_{0.1}Cs_{0.9}H(PO_3H)$ increases from $1.6 \cdot 10^{-3}$ $\Omega^{-1}cm^{-1}$ at 72 °C to $3 \cdot 10^{-3}$ $\Omega^{-1}cm^{-1}$ at 144 °C. The proton conductivity reaches values of $4 \cdot 10^{-3}$ at 153 °C. Superprotonic conductivity range is between 144 and 153 °C.

Superprotonic conductivity range for $K_{0.4}Cs_{0.6}H(PO_3H)$ is very narrow between 122 and 127 °C as seen from Fig. 6.14. Upon heating for the first time the conductivity of $K_{0.4}Cs_{0.6}H(PO_3H)$ increases from $1.3 \cdot 10^{-3}$ $\Omega^{-1}cm^{-1}$ at 74 °C to $2 \cdot 10^{-3}$ $\Omega^{-1}cm^{-1}$ at 122 °C. Conductivity reaches only $3 \cdot 10^{-3}$ $\Omega^{-1}cm^{-1}$ at 127 °C.

As seen from Fig. 6.14 for $K_{0.8}Cs_{0.2}H(PO_3H)$ and $K_{0.9}Cs_{0.1}H(PO_3H)$ there are no jumping of the conductivity. It was already mentioned after DSC results that these compounds are already in superprotonic phase in nature. So no phase transition is observed for these compounds in temperature range of 80 – 130 °C.

For $Cs_{0.05}K_{0.95}H(PO_3H)$ there is a wide conductivity range. Upon heating the conductivity is $3 \cdot 10^{-4}$ $\Omega^{-1}cm^{-1}$ at 75 °C. Conductivity is $3.2 \cdot 10^{-3}$ $\Omega^{-1}cm^{-1}$ at 113 °C and reaches values of **10^{-2} $\Omega^{-1}cm^{-1}$ at 147 °C**. The magnitude of its conductivity is the highest one in mixed K-Cs phosphite system. The reason of this phenomena is that Cs^+ has bigger cation size than K^+ and if small amount of Cs is doped into $KH(PO_3H)$ the cation size is increasing and area is enlarging for movement of protons through the lattice.

6.3 Composite Membrane Formation

6.3.1 Anodic Alumina / $KH(PO_3H)$ Composite Membrane

Alumina membranes were filled with $KH(PO_3H)$ by ultrasonic bath of the sample in saturated $KH(PO_3H)$ aqueous solution. The membranes were dried by exposure to air.

6.3.1.1 Morphological Studies

The information about the morphology of potassium dihydrogen phosphite inside the pores of anodic alumina membranes have been obtained by SEM studies which were carried out on the surfaces and cross-sections of the samples.

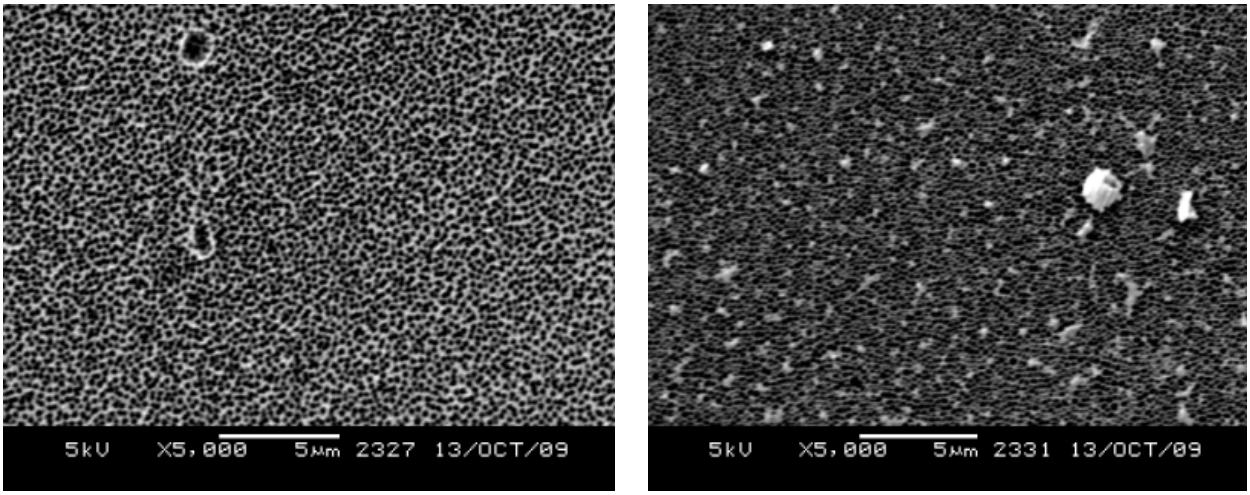

Figure 6.15 SEM morphology of anodic alumina membranes surfaces

before filling with protonic conductor $KH(PO_3H)$ and after filling with protonic conductor $KH(PO_3H)$

(a) before (b) after

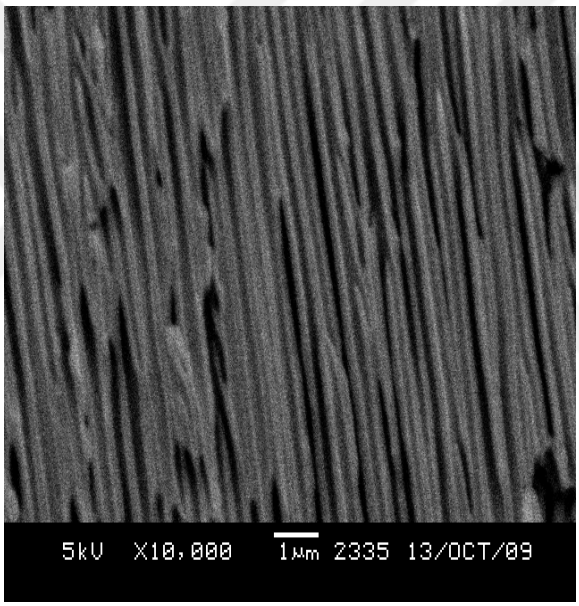

Figure 6.16 SEM morphology of anodic alumina membranes cross-sections

after filling with protonic conductor $KH(PO_3H)$

6.3.1.2 Structures of Anodic Alumina membrane/ $KH(PO_3H)$ Composite Membrane by XRD Analysis

In order to find out crystal structure of composite potassium dihydrogen phosphite/porous alumina at room temperature X-ray diffractometer is used. The X-ray pattern of pure $KH(PO_3H)$ was already proven as monoclinic at room temperature and was given in section 6.1 of this chapter. The X-ray patterns recorded for pure potassium dihydrogen phosphite and composite potassium dihydrogen phosphite/porous alumina were given in Fig. 6.17. $KH(PO_3H)$/AAM composites also exhibited monoclinic structure at room temperature.The $KH(PO_3H)$ showed the same crystalline structure after precipitation inside the alumina porous structure.

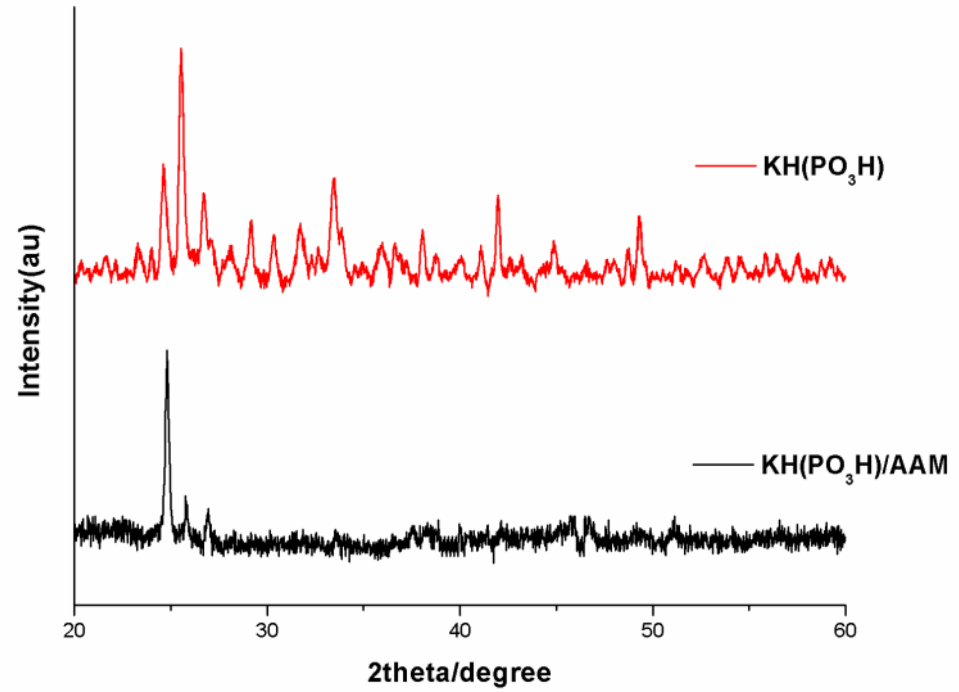

Figure 6.17 X-Ray Patterns of pure $KH(PO_3H)$ and $KH(PO_3H)$/AAM

6.3.1.3 Phase Transition and Superprotonic Temperatures of the Anodic Alumina membrane/ $KH(PO_3H)$ Composite Membrane by Differential Scanning Calorimeter (DSC) Analysis

The thermal behavior recorded for pure potassium dihydrogen phosphite and composite potassium dihydrogen phosphite/porous alumina were given in Fig. 6.18. $KH(PO_3H)$/AAM have a superprotonic phase transition with an onset temperature at 123 ºC.

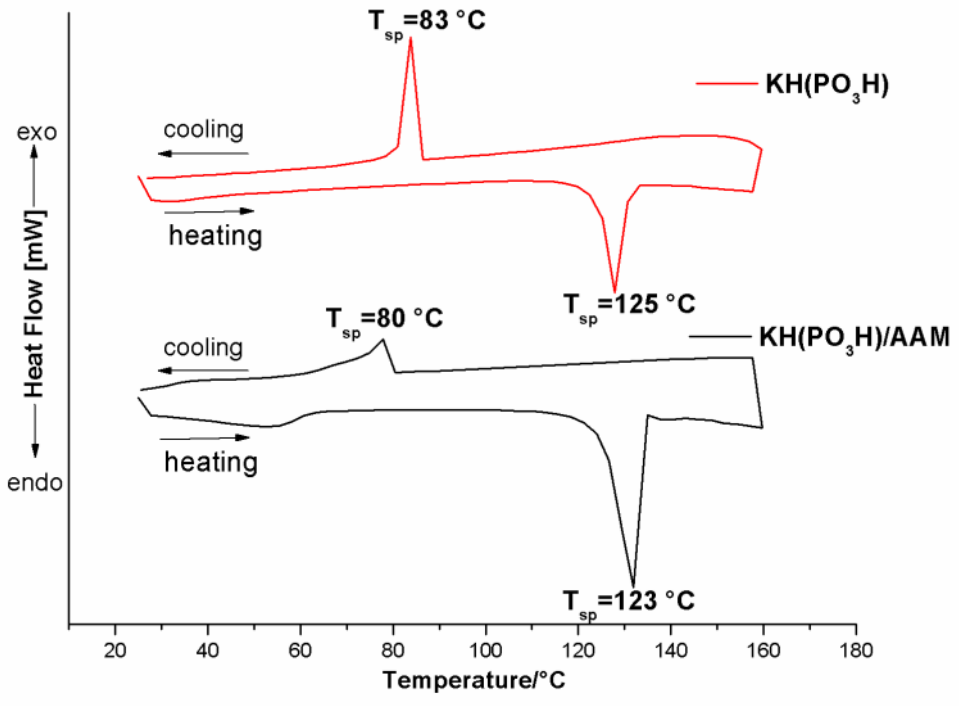

Figure 6.18 DSC curves of pure $KH(PO_3H)$ and $KH(PO_3H)$/AAM

CONCLUSIONS

In this work $CsH(PO_3H)$, $KH(PO_3H)$ and $K_xCs_{(1-x)}H(PO_3H)$ were synthesized and characterized as solid acid electrolytes.

The key results of this work are as follows.

1. $CsH(PO_3H)$ was proved to be very hygroscopic during tests which are performed under atmosphere condition. $KH(PO_3H)$ was not as hygroscopic as $CsH(PO_3H)$. In $K_xCs_{(1-x)}H(PO_3H)$ mixed systems hygroscopic character was increasing by increasing ratio of Cs:K.

2. X-ray diffraction analysis was performed at room temperatures on $KH(PO_3H)$, $CsH(PO_3H)$ and $K_xCs_{(1-x)}H(PO_3H)$ polycrystals. All the compounds exhibited highly ordered monoclinic phase at room temperature.

3. Thermal analysis was performed to confirm the presence of the superprotonic phase transition in the phosphites. $KH(PO_3H)$ and $CsH(PO_3H)$ exhibited superprotonic phase transition with an onset temperature at 125 °C and 142 ºC, respectively.

4. Thermal analysis for mixed systems of K/Cs phosphites showed that phase transition was changing due to the fractions of K^+ and Cs^+ between 100 -142 °C. Three types of behaviors were observed.

(a) K^+ fraction in $K_xCs_{(1-x)}H(PO_3H)$ less than 30 mol% was not significantly effect the superprotonic phase transition temperature, they have same phase transition with $CsH(PO_3H)$ at 142 ºC.

(b) The K^+ fractions between 30 mol% - 70 mol% shifted the superprotonic phase transition temperature to lower temperatures than 142 ºC.

(c) The K^+ fraction between 70 mol% - 90 mol% did not undergo a phase transition before its melting temperature at 160 °C. So it was concluded that between $K_{0.9}Cs_{0.1}H(PO_3H)$ and $K_{0.7}Cs_{0.3}H(PO_3H)$, superprotonic phase transition is disappeared.

5. $K_{0.95}Cs_{0.05}H(PO_3H)$ was synthesized as second step, and transition temperature was found at 100 ºC.

6. Protonic conductivities of the compounds were investigated upon heating. The conductivity of $KH(PO_3H)$ reached value of $4.5 \cdot 10^{-3}\ \Omega^{-1}cm^{-1}$ at 143 °C. The conductivity of $CsH(PO_3H)$ reached value of $3 \cdot 10^{-3}\ \Omega^{-1}cm^{-1}$ at 160 °C.

7. K^+ fraction in $K_xCs_{(1-x)}H(PO_3H)$ less than 30 mol% had a superptotonic conductivity range between $3 \cdot 10^{-3} - 4 \cdot 10^{-3}\ \Omega^{-1}\ cm^{-1}$ at the temperature range 144-153 °C.

The K^+ fractions between 30 mol% - 70 mol% in $K_xCs_{(1-x)}H(PO_3H)$ had very narrow superprotonic conductivity range.

The K^+ fraction between 70 mol% - 90 mol% was found that they were already superprotonic in nature.

8. $K_{0.95}Cs_{0.05}H(PO_3H)$ had a superprotonic conductivity range between 113-147 °C. The conductivity value could reached to 10^{-2} Ω^{-1} cm^{-1} at 147 °C.

FUTURE RESEARCHES

Further research can be studied for the anodic alumina /solid acid composite membranes. Thin film fuel cells can be fabricated and fuel cell performances can be investigated.

THERMAL RESULTS OF $K_xCs_{(1-x)}H(PO_3H)$ by DSC

A.1.1 Phase Transition of the solid solutions x=0.1 ($K_{\%10}Cs_{\%90}$) and x=0.2 ($K_{\%20}Cs_{\%80}$)

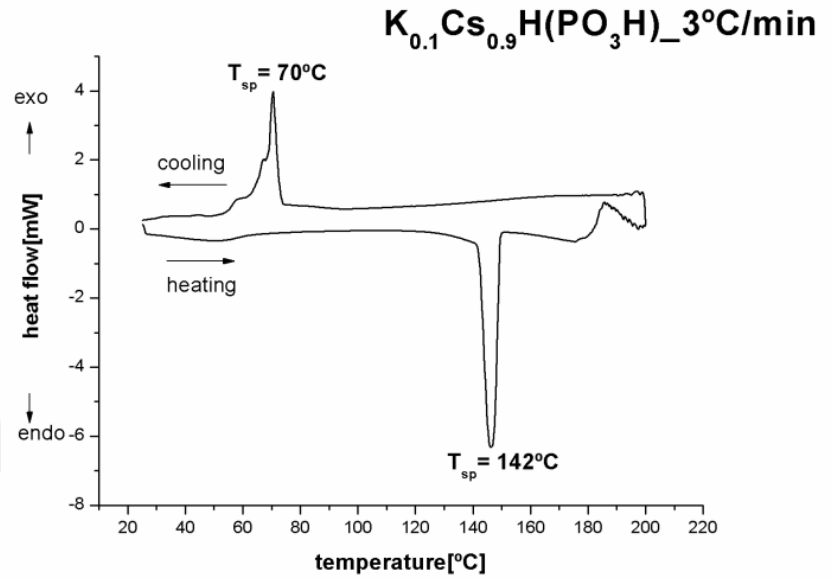

Figure A.1 Thermal behavior of $K_{0.1}Cs_{0.9}H(PO_3H)$ for a heating-cooling cycle
Upon heating; T_{sp}=142 ºC, ΔH= -49 J/g, Upon cooling; T_{sp}=70 ºC
T_{sp} is superprotonic phase transition temperature. Onset temperatures are accepted as transition temperature.

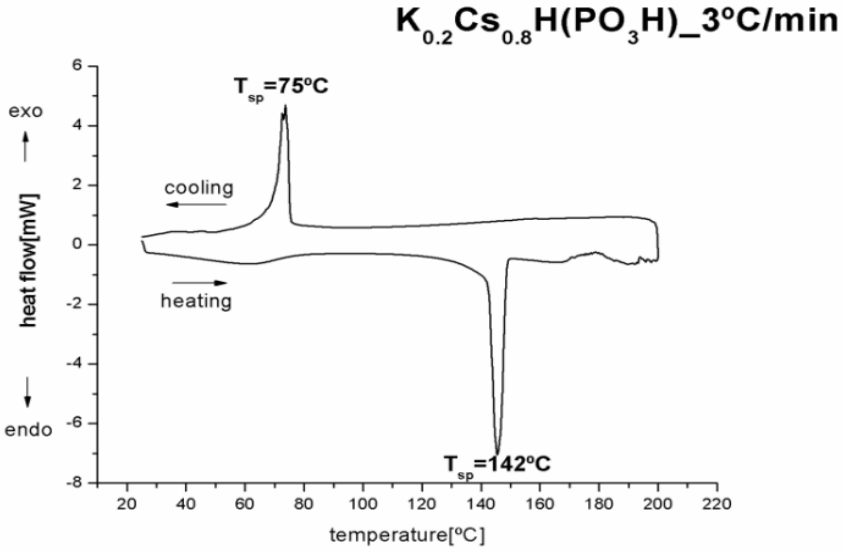

Figure A.2 Thermal behavior of $K_{0.2}Cs_{0.8}H(PO_3H)$ for a heating-cooling cycle
Upon heating; T_{sp}=142 ºC, ΔH= -52 J/g, Upon cooling; T_{sp}=75 ºC
T_{sp} is superprotonic phase transition temperature. Onset temperatures are accepted as transition temperature.

A.1.2 Phase Transition of the solid solutions between x=0.3 ($K_{\%30}Cs_{\%70}$), x=0.4 ($K_{\%40}Cs_{\%60}$), x=0.5 ($K_{\%50}Cs_{\%50}$) and x=0.6 ($K_{\%60}Cs_{\%40}$)

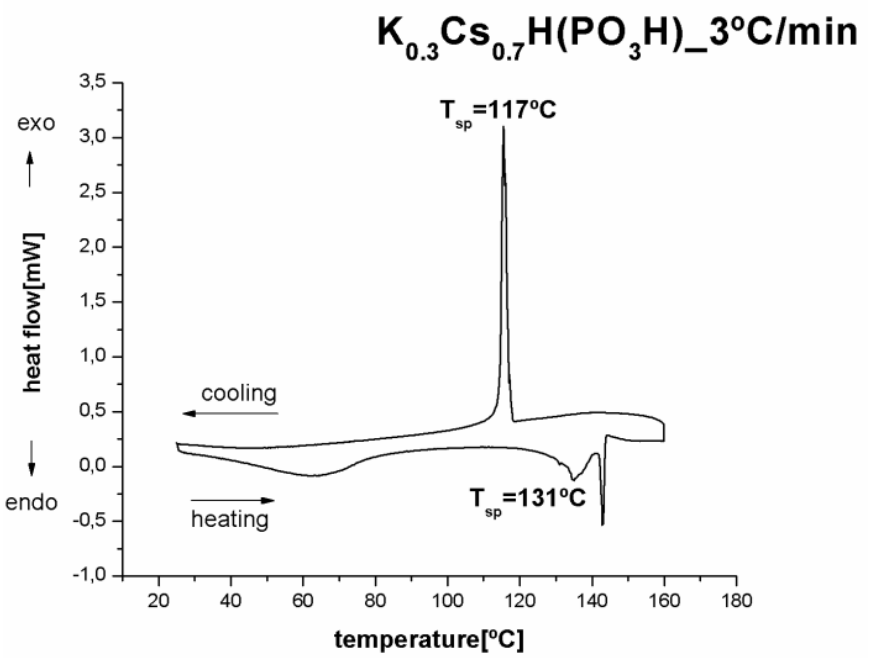

Figure A.3 Thermal behavior of $K_{0.3}Cs_{0.7}$ $H(PO_3H)$ for a heating-cooling cycle
Upon heating; T_{sp}= 131 ºC , ΔH= -9 J/g, Upon cooling; T_{sp}=117 ºC
T_{sp} is superprotonic phase transition temperature. Onset temperatures are accepted as transition temperature. Second peak at 142 ºC is due to decomposition.

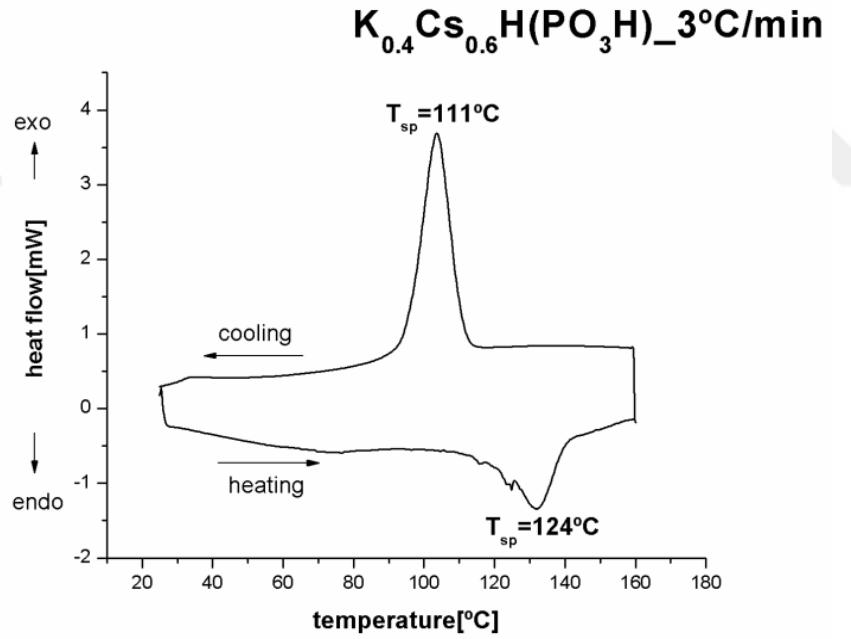

Figure A.4 Thermal behavior of $K_{0.4}Cs_{0.6}$ $H(PO_3H)$ for a heating-cooling cycle
Upon heating; T_{sp}= 124 ºC , ΔH= -7 J/g, Upon cooling; T_{sp}= 111 ºC
T_{sp} is superprotonic phase transition temperature. Onset temperatures are accepted as transition temperature.

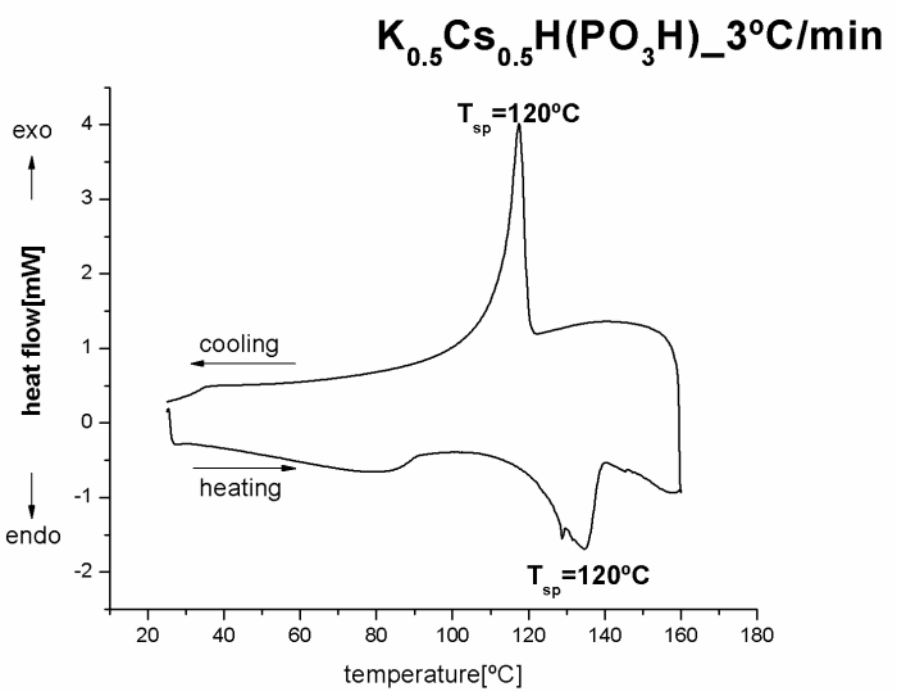

Figure A.5 Thermal behavior of $K_{0.5}Cs_{0.5}H(PO_3H)$ for a heating-cooling cycle

Upon heating; T_{sp}= 120 ºC , ΔH= -7 J/g, Upon cooling; T_{sp}= 120 ºC

T_{sp} is superprotonic phase transition temperature. Onset temperatures are accepted as transition temperature.

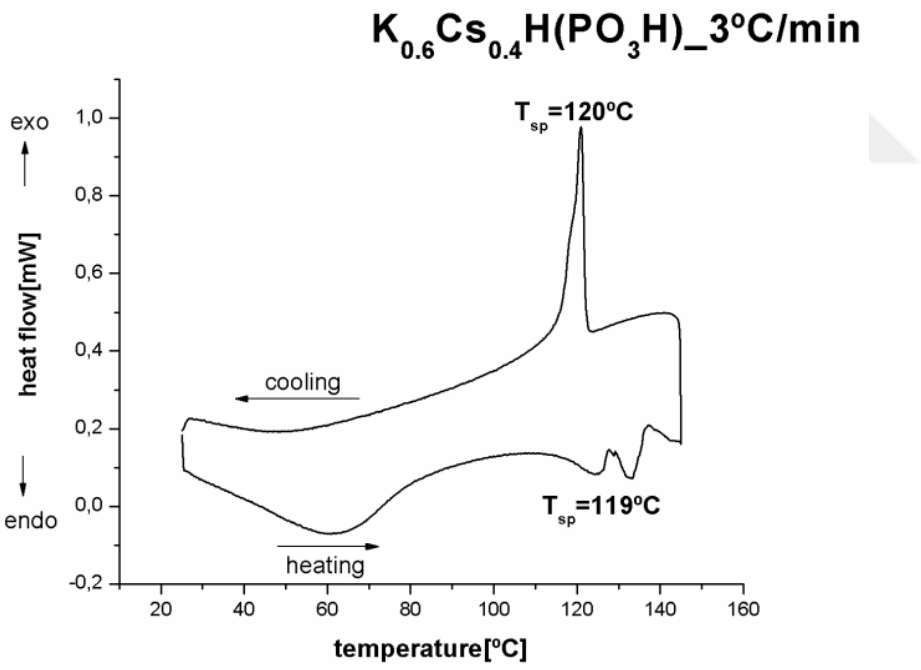

Figure A.6 Thermal behavior of $K_{0.6}Cs_{0.4}H(PO_3H)$ for a heating-cooling cycle

Upon heating; T_{sp}= 122 ºC, ΔH= -7 J/g, Upon cooling; T_{sp}= 111 ºC

T_{sp} is superprotonic phase transition temperature. Onset temperatures are accepted as transition temperature.

A.1.3 Phase Transition of the solid solutions between x=0.7 ($K_{\%70}Cs_{\%30}$), x=0.8 ($K_{\%80}Cs_{\%20}$) and x=0.9 ($K_{\%90}Cs_{\%10}$)

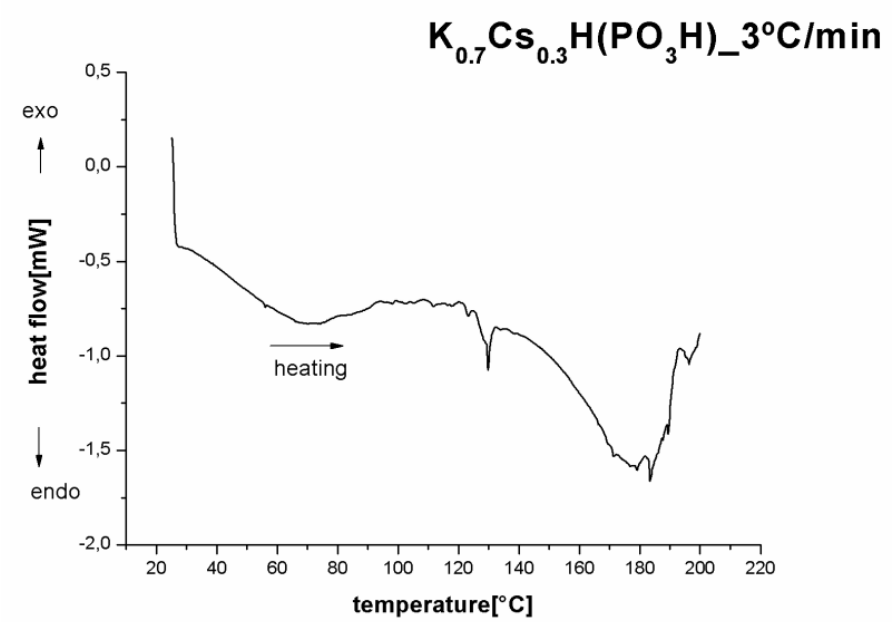

Figure A.7 Thermal behavior of $K_{0.7}Cs_{0.3}H(PO_3H)$ for a heating cycle
No phase transition

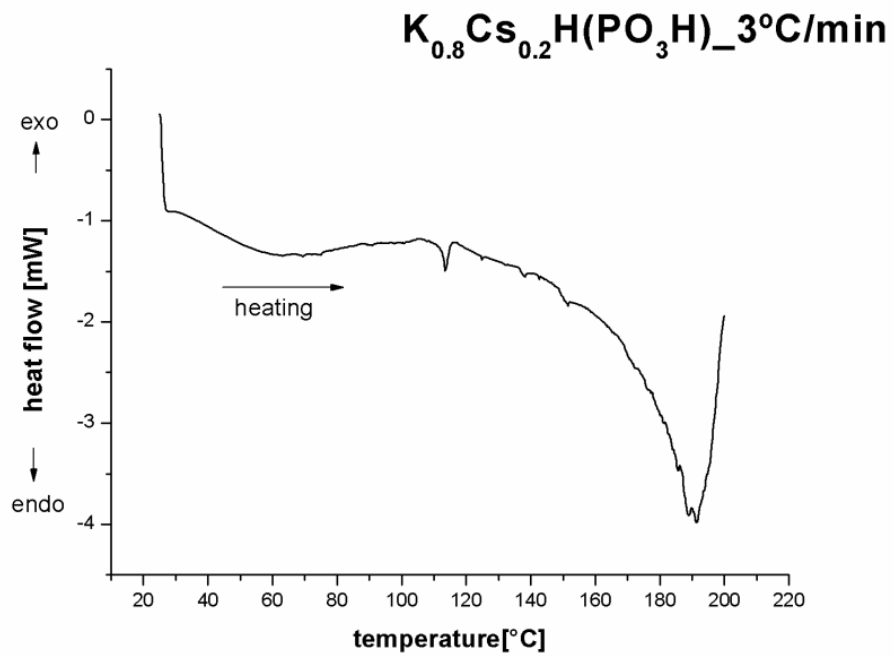

Figure A.8 Thermal behavior of $K_{0.8}Cs_{0.2}H(PO_3H)$ for a heating cycle
No phase transition

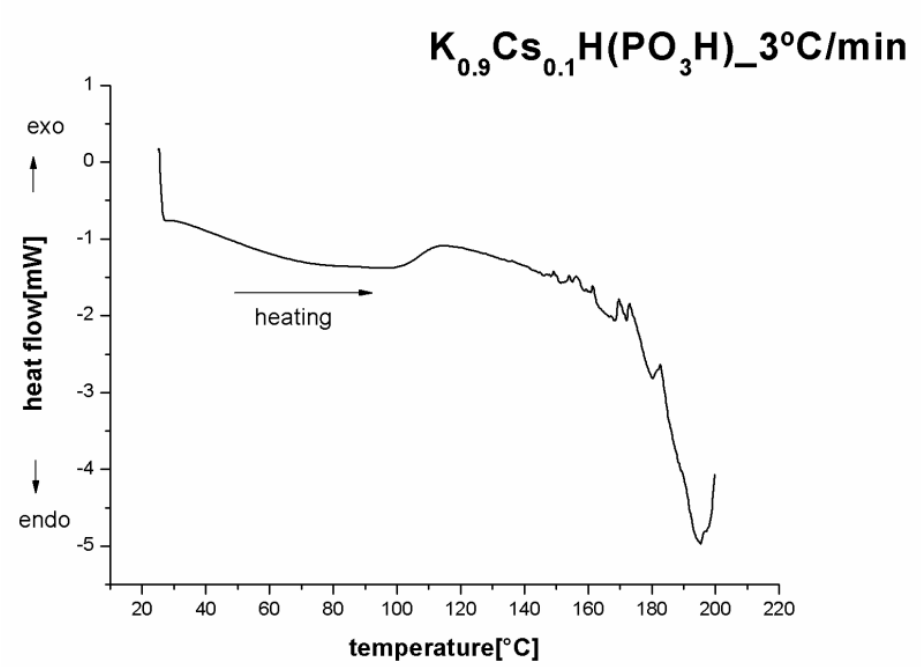

Figure A.9 Thermal behavior of $K_{0.9}Cs_{0.1}H(PO_3H)$ for a heating cycle
No phase transition

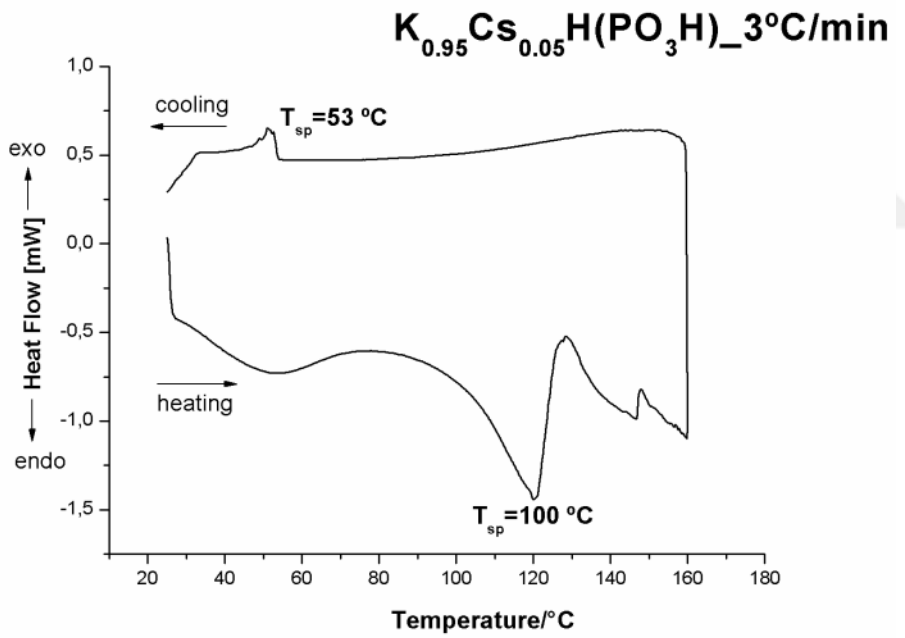

Figure A.10 Thermal behavior of $K_{0.95}Cs_{0.05}H(PO_3H)$ for a heating-cooling cycle
Upon heating; T_{sp}= 100 ºC , ΔH= -31 J/g, Upon cooling; T_{sp}= 53ºC
T_{sp} is superprotonic phase transition temperature. Onset temperatures are accepted as transition temperature.

CONDUCTIVITY RESULTS OF $K_xCs_{(1-x)}H(PO_3H)$ by IMPEDANCE SPECTROSCOPY

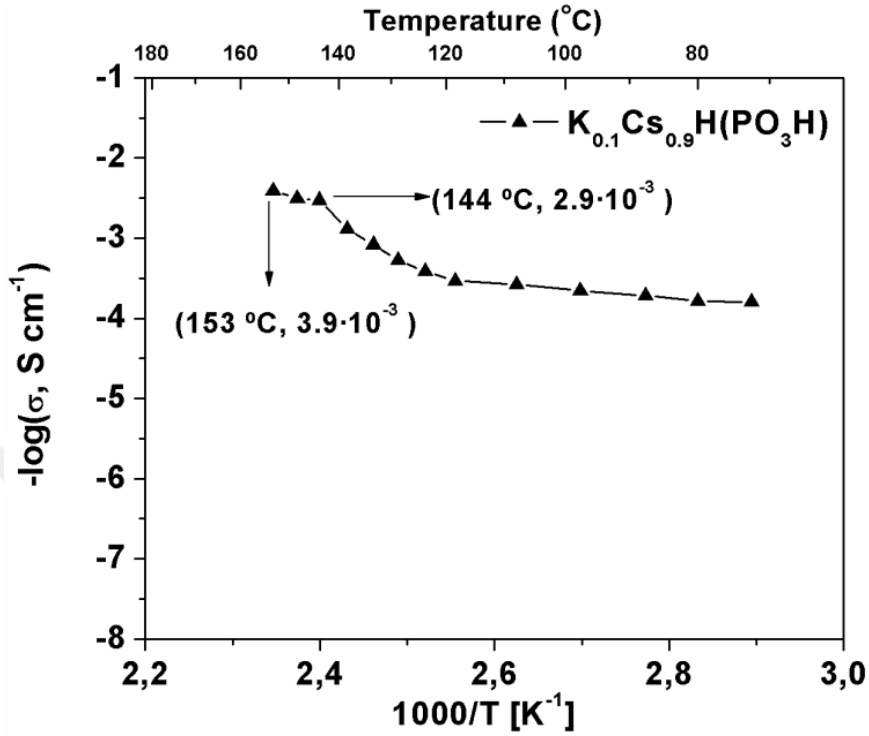

Figure A.13 -log conductivity vs. temperature plot for $K_{0.1}Cs_{0.9}H(PO_3H)$

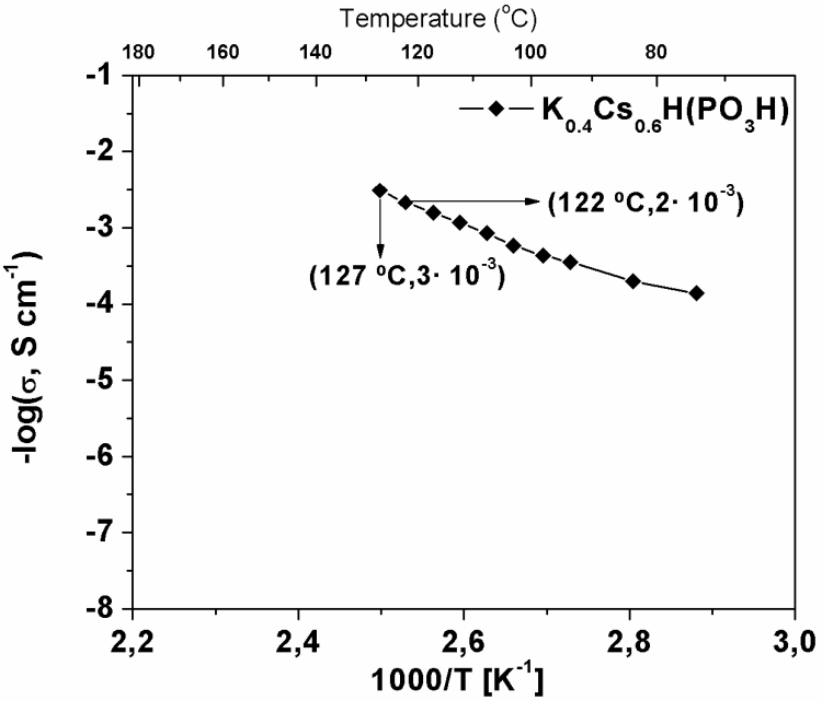

Figure A.14 -log conductivity vs. temperature plot for $K_{0.4}Cs_{0.6}H(PO_3H)$

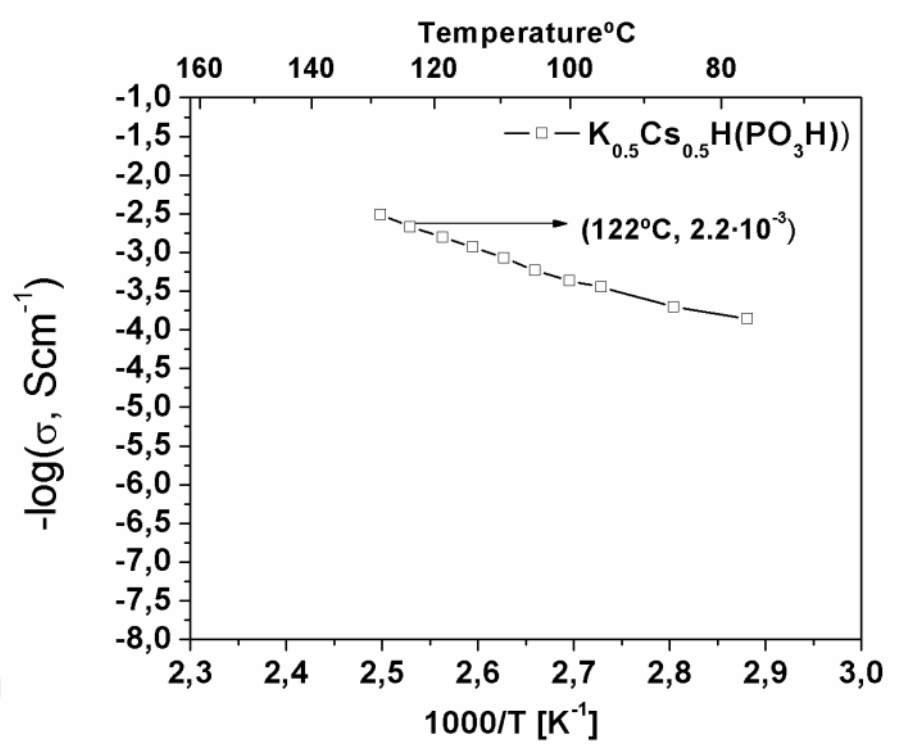

Figure A.15 -log conductivity vs. temperature plot for $K_{0.5}Cs_{0.5}H(PO_3H)$

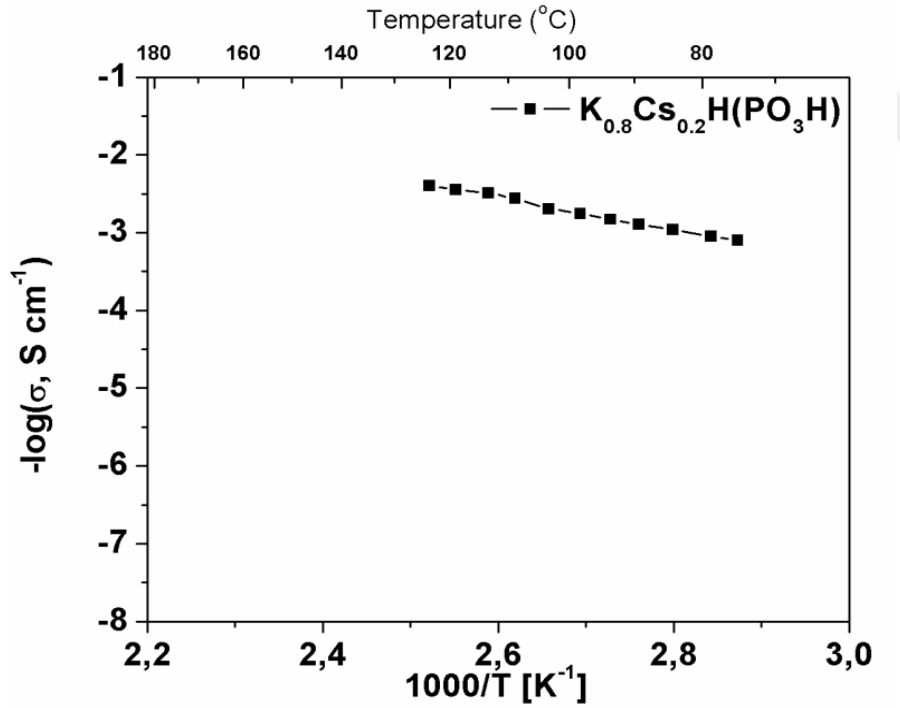

Figure A.16 -log conductivity vs. temperature plot for $K_{0.8}Cs_{0.2}H(PO_3H)$

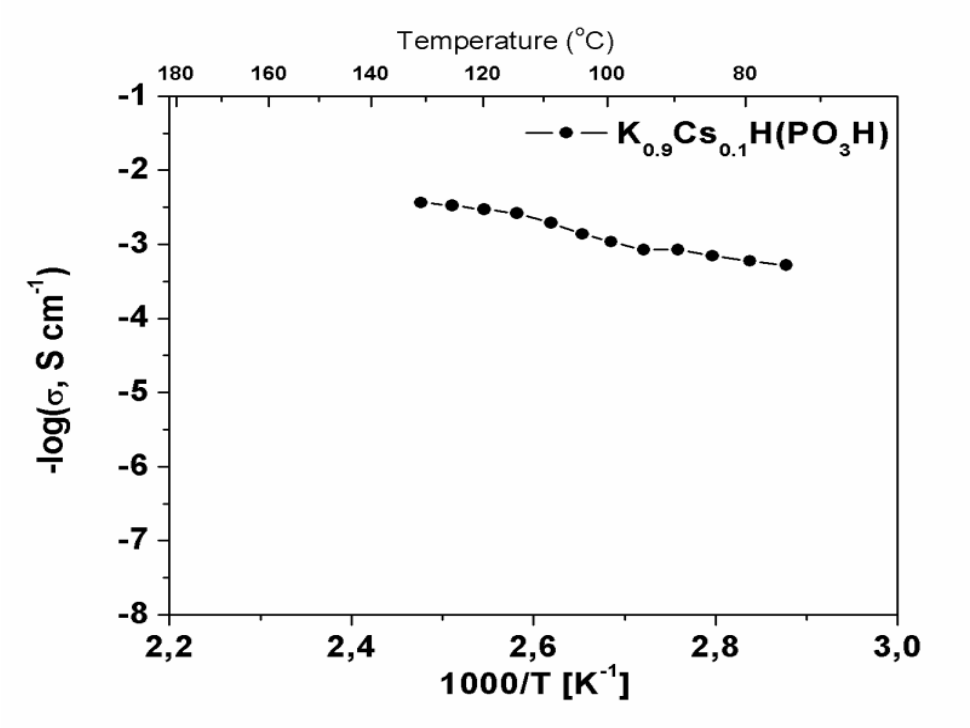

Figure A.17 -log conductivity vs. temperature plot for $K_{0.9}Cs_{0.1}H(PO_3H)$

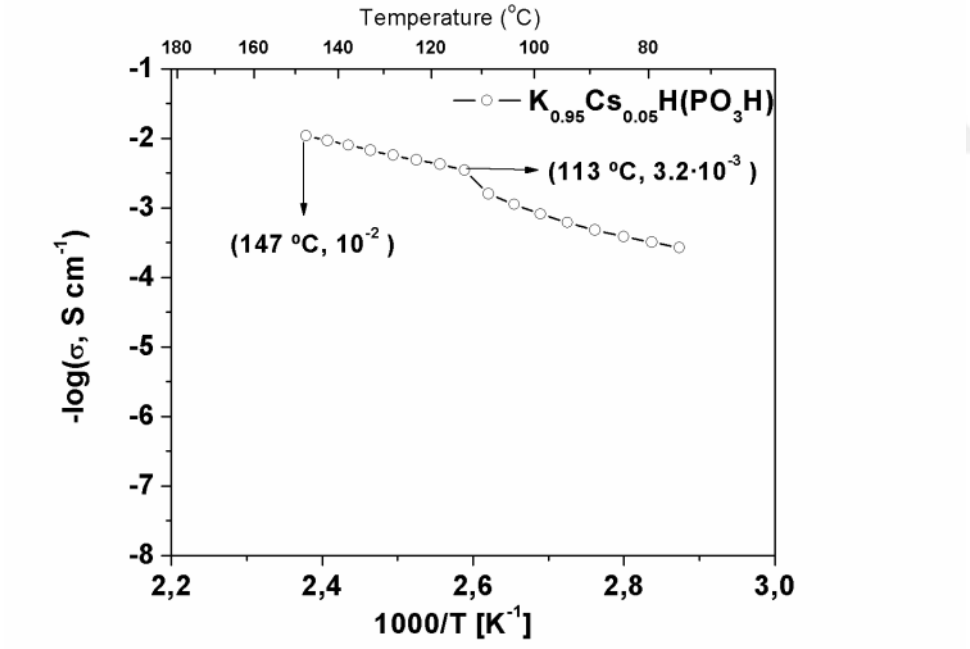

Figure A.18 -log conductivity vs. temperature plot for $K_{0.95}Cs_{0.05}H(PO_3H)$

Bibliography

1. Vielstich, W., A. Lamm, and H.A. Gasteiger, *Handbook of fuel cells: fundamentals, technology, and applications*. 2003, Chichester: Wiley. 4 v.
2. Haile, S.M., *Fuel cell materials and components*, in *Acta Materialia*. 2003: Pasadena.
3. Hogarth, W.H.J., J.C.D.d. Costa, and G.Q.M. Lu, *Solid acid membranes for high temperature (>100 ºC)proton exchange membrane fuel cells.* Journal of Power Sources, 2004.
4. Sossina M. Haile, Dane A. Boysen, and C.R.I. Chisholm, *Solid acids as fuel cell electrolytes.* Letters to Nature, 2001. **410**.
5. Zhou, W., A.S. Bondarenko, and H.J.M. Bouwmeester, *Superprotonic Conductivity in $MH(PO_3H)$ ($M=Li^+$, Na^+, K^+, Na^+, Rb^+, Cs^+, NH_4^+),* . Solid State Ionics, 2008.
6. Löfken, J.O. *Feste Säuren machen kühle Brennstoffzellen effizient*. 2001; Available from: http://www.wissenschaft.de/wissenschaft/news/154260.html.
7. Haile, S.M., et al., *Solid Acid Proton Conductors: from laboratory curiosities to fuel cell electrolytes.* Faraday Discussions, 2006.
8. *Superprotonic Solid Acid Fuel Cells: a Hidden, Cheap, Easy Way to Maintain Power Source*. 2009; Available from: http://www.greenoptimistic.com/2009/01/12/solid-acid-fuel-cell-superprotonic/.
9. Unnikrishnan, S. *Micro-fuel cell based on solid-acid electrolytes*. 2005; Available from: http://tst.ewi.utwente.nl/research/microfluidics/mfc/index.html.
10. *Types of Fuel Cells*. 2009; Available from: http://www1.eere.energy.gov/hydrogenandfuelcells/fuelcells/fc_types.html.
11. Boysen, D.A., *Superprotonic Solid Acids: Structure, Properties and Applications*, in *California Institute of Technology*. 2004.
12. Uda, T. and S.M. Haile, *Thin-Membrane Solid-Acid Fuel Cell.* Electrochemical and Solid-State Letters, 2005.
13. Ladd, M.F.C., *Structure and Bonding in Solid State Chemistry*. 1979.
14. Vinogradov, S.N. and R.H. Linnell, *Hydrogen bonding*. 1971, New York ; London: Van Nostrand Reinhold. xi, 319 p.
15. Chisholm, C.R.I., *Superprotonic Phase Transitions in Solid Acids: Parameters affecting the presence and stability of superprotonic transitions in the MH_nXO_4 family of compounds ($X=S$, Se, P, As; $M=Li$, Na, K, NH_4, Rb, Cs)*, in *California Institute of Technology*. 2002.
16. Lee, H.-S. and M.E. Tuckerman, *The Structure and Proton Transport Mechanism in the Superprotonic Phase of CsH_2PO_4: An Ab Inito Molecular Dynamic Study.* Journal of Physical Chemistry C, 2008.
17. Rao, C.N.R. and K.J. Rao, *Phase transitions in solids : an approach to the study of the chemistry and physics of solids*. 1978, New York ; London: McGraw-Hill. xi, 330.
18. West, A.R., *Solid state chemistry and its applications*. Repr. with corrections ed. 1987, Chichester: Wiley. vii, 734.
19. Colomban, P., *Proton Conductors: solids, membranes, and gel materials and devices*. 1992: Cambridge University Press.
20. Yamane, Y., K. Yamada, and K. Inoue, *Superprotonic solid solutions between $CsHSO_4$ and CsH_2PO_4.* Solid State Ionics, 2008: p. 483.
21. Haile, S.M. *FUEL CELLS Powering Progress in the 21st Century*. 2001; Available from: http://www.eas.caltech.edu/engenious/fall01/haile.html.
22. Taninouchi, Y.-k., T. Uda, and Y. Awakura, *Dehydration of CsH_2PO_4 at Temperatures Higher than 260 °C and the Ionic Conductivity of Liquid Product.* Solid State Ionics, 2007.
23. Chisholm, C.R.I. and S.M. Haile, *Superprotonic behavior of $Cs_2(HSO_4)(H_2PO_4)$-a new solid acid in the $CsHSO_4$-CsH_2PO_4 system.* Solid State Ionics, 2000.
24. Chisholm, C.R.I. and S.M. Haile, *Superprotonic behavior of $Cs_2(HSO_4)(H_2PO_4)$ – a new solid acid in the $CsHSO_4$ –CsH_2PO_4 system.* Solid State Ionics, 2000.
25. Chisholm, C.R.I., D.A. Boysen, and S.M. Haile, *Superprotonic Phase Transition in $Cs(HPO_3H)$.* Chem. Mater, 2002.

26. Bocchetta, P., R. Ferraroa, and F.D. Quartoa, *Advances in Anodic Alumina Membranes thin Film Fuel Cell: CsH2PO4 pore-filler as proton conductor at room temperature.* Journal of Power Sources, 2008. **vol. 187**(issue 1).
27. Bocchetta, P., G. Chiavarotti, and F.D. Quartoa, *Nanoporous alumina membranes filled with solid acid for thin film fuel cells at intermediate temperatures* Electrochemistry Communications, 2004. **vol. 6**(issue 9).
28. Shriver, D.F., P.W. Atkins, and S.H. Strauss, *Inorganic chemistry*. 3rd ed. 1999, Oxford: Oxford University Press. xvii, 767.
29. Lifshin, E., *X-ray characterization of materials*. 1999, Weinheim Chichester: Wiley-VCH. xvi, 261.
30. Nichol, A.C., W. Hayes, and University of Oxford. Mathematical and Physical Sciences Division., *Infrared spectroscopy of solids*. 1990, University of Oxford, 1990. p. 1 v. (various paging.).
31. Baran, J., M.M. Ilczyszyn, and H. Ratajczak, *Polarised vibrational spectra of KH_2PO_3 single crystals.* Journal of Molecular Structure, 2000.
32. Boysen, D.A., T. Uda, and S.M. Haile, *High-performance solid acid fuel cells through humidity stabilization.* www.sciencemag.org, 2004. **303**.
33. Kosterina, E.V., S.I. Troyanov, and L.A. Aslanov, *Synthesis and crystal structure of acid phosphites RbH_2PO_3, CsH_2PO_3, and TlH_2PO_3.* Russian Jornal of Coordination Chemistry, 2000. **27**.
34. Atkins, P.W. and J. De Paula, *Atkins' Physical chemistry*. 8th ed. 2006, Oxford ; New York: Oxford University Press. xxx, 1064 p.
35. Dettmann, P., *Lecture notes of heat and mass transfer* Fachhochschule Münster, 2009.
36. Dettmann, P., *Laboratary guides for the practical training Heat and Mass Transfer.* Laboratory of Chemical Environmental Technology, Fachhochschule Münster, 2009.
37. Dettmann, P., *Laboratory guides for the practical training Advanced Physical Chemistry* Laboratory of Chemical Environmental Technology, Fachhochschule Münster, 2009
38. Bronowska, W., *X-ray study of the high temperature phase transition of CsH_2PO_4 crystals.* Solid State Communications, 1989. **Vol. 76**.
39. Ikedo, Y., J. Sugiyama, and J.S. Lord, *Muon dynamics in superprotonic conductors.* Physica B, 2008.
40. Otomo, J., S. Wang, and H. Nagamoto, *Microstructure development of mesoporous silica thin films with pore channels aligned perpendicularly to electrode surfaces and application to proton conducting composite electrolyte membranes.* Journal of Membrane Science, 2006.
41. Tsuboi, M., *Vibrational spectra of phosphite and hypophosphite anions, and the characteristic frequencies of PO_3^{--} and PO_2^{-} groups.* University of Michigan, 1956.
42. Bocchetta, P., F. Conciauro, and F.D. Quarto, *Nanoscale membrane electrode assemblies based on porous anodic alumina for hydrogen–oxygen fuel cell.* Solid State Electrochem, 2007.
43. Boysen, D.A. and S.M. Haile, *High-Temperature Behavior of CsH_2PO_4 under Both Ambient and High Pressure Conditions.* Chem. Mater, 2002.
44. Norby, T., *The promise of protonics.* Nature 2001. **410**.
45. Chisholm, C.R.I. and S.M. Haile, *X-ray structure refinement of $CsHSO_4$ in phase II.* Materials Research Bulletin, 2000. **Vol. 35**.
46. Baran, J. and M.K. Marchewka, *Vibrational investigation of phase transitions in $CsHSO_4$ crystal.* Journal of Molecular Structure, 2002. **Vol. 614**.
47. Haile, S.M. and Cailiornia Institute of Technology., *Fuel cells powering progress in the 21st century, January 29, 2003 Earnest C. Watson lecture*. 2005, California Institute of Technology,: Pasadena, Calif.
48. Babilo, P., S.M. Haile, and California Institute of Technology. Division of Engineering and Applied Science., *Processing and characterization of proton conducting yttrium doped barium zirconate for solid oxide fuel cell applications*. CIT theses ; 2007. 2007, Pasadena, Calif.: California Institute of Technology. xvii, 152 leaves.
49. Cowan, L., S.M. Haile, and California Institute of Technology. Division of Engineering and Applied Science., *Superprotonic solid acid phase transitions and stability*. CIT theses ; 2007. 2007, Pasadena, Calif.: California Institute of Technology. xxvi, [138] leaves.
50. Kislitsyn, M.N., S.M. Haile, and California Institute of Technology. Division of Engineering and Applied Science., *Materials chemistry of superprotonic solid acids /cMikhail N. Kislitsyn*

; Sossina Haile, committee chair and advisor. CIT theses ; 2009. 2009, Pasadena, Calif.: California Institute of Technology. xxi, [160] leaves.
51. Lai, W., S.M. Haile, and California Institute of Technology. Division of Engineering and Applied Science., *Impedance spectroscopy as a tool for electrochemical study of mixed conducting ceria*. CIT theses ; 2007. 2007, Pasadena, Calif.: California Institute of Technology. xiv, 152 leaves.
52. McDougall, A., *Fuel cells*. Energy alternatives series. 1976, London: Macmillan. xii, 147 p.
53. Breiter, M.W., *Electrochemical processes in fuel cells*. Anorganische und allgemeine Chemie in Einzeldarstellungen. 1969, [New York]: Springer-Verlag New York. xi, 274 p.
54. Boysen-Jensen, P., *Die stoffproduktion der pflanzen*. 1932, Jena,: G. Fischer. vi, 108 p.
55. International Energy Agency., *Prospects for hydrogen and fuel cells*. Energy technology analysis. 2005, Paris, France: International Energy Agency. 253 p.
56. Mackay, K.M. and R.A. Mackay, *Introduction to modern inorganic chemistry*. 4th ed. 1989, Glasgow ; London Englewood Cliffs: Blackie ;Prentice Hall. xiii, 402 p.
57. Cotton, F.A. and G. Wilkinson, *Advanced inorganic chemistry : a comprehensive text*. 4th ed. 1980, New York ; Chichester: Wiley. xvii, 1396 p.
58. George, W.O., et al., *Infrared spectroscopy*. 1987, Chichester [West Sussex] ; New York: Published on behalf of ACOL, London, by Wiley. xx, 537 p.
59. Colthup, N.B., *Introduction to infrared and Raman spectroscopy*. 1964, New York: Academic Press. xii, 511 p.
60. Brügel, W., *An introduction to infrared spectroscopy*. 1962, London New York: Methuen ;Wiley. 419 p.
61. Buerger, M.J., *X-ray crystallography : an introduction to the investigation of crystals by their diffraction of monochromatic X- radiation*. 1942, New York ; London: Wiley. xxii, 531 p. incl. illus., tables.
62. Bacon, G.E., *X-ray and neutron diffraction*. 1st ed ed. Commonwealth and international library. Selected readings in physics. 1966, Oxford: Pergamon. x, 368 p.
63. Klug, H.P. and L.E. Alexander, *X-ray diffraction procedures for polycrystalline and amorphous materials*. 1954, New York London: Wiley ;Chapman & Hall. 716 p.
64. Macdonald, J.R., *Impedance spectroscopy : emphasizing solid materials and systems*. 1987, New York ; Chichester: Wiley. xvi, 346 p.
65. Barsoukov, E. and J.R. Macdonald, *Impedance spectroscopy : theory, experiment, and applications*. 2nd ed. 2005, Hoboken, N.J.: Wiley-Interscience. xvii, 595 p.
66. Bershtein, V.A., et al., *Differential scanning calorimetry of polymers : physics, chemistry, analysis, technology*. Ellis Horwood series in polymer science and technology. 1994, New York ; London: Ellis Horwood. xii, 253 p.
67. MacCallum, J.R. and C.A. Vincent, *Polymer electrolyte reviews*. 1987, London: Elsevier Applied Science.
68. Gottesfeld, S., *Polymer electrolyte fuel cells*. Electrochimica acta ; v. 40, no. 3. 1995, Oxford,. p. 283-375.
69. Gray, F.M. and Royal Society of Chemistry (Great Britain), *Polymer electrolytes*. 1997, Cambridge: Royal Society of Chemistry. xii, 175 p.
70. Kordesch, K. and G. Simader, *Fuel cells and their applications*. 1996, Weinheim ; New York: VCH. xiv, 375 p.
71. Bockris, J.O.M. and S. Srinivasan, *Fuel cells: their electrochemistry*. 1969, New York,: McGraw-Hill. xxiii, 659p.